PROCESSING BY ELECTROSPINNING METHOD AND CHARACTERIZATION OF POLY(LACTIC ACID) AND POLY(LACTIC ACID)-BASED COMPOSITE NANOFIBERS

A THESIS SUBMITTED TO
THE GRADUATE SCHOOL OF NATURAL AND APPLIED SCIENCES
OF
MIDDLE EAST TECHNICAL UNIVERSITY

BY

EMİNE ÜMRAN AŞCI

IN PARTIAL FULFILLMENT OF THE REQUIREMENTS
FOR
THE DEGREE OF MASTER OF SCIENCE
IN
CHEMICAL ENGINEERING

JUNE 2022

Approval of the thesis:

PROCESSING BY ELECTROSPINNING METHOD AND CHARACTERIZATION OF POLY(LACTIC ACID) AND POLY(LACTIC ACID)-BASED COMPOSITE NANOFIBERS

submitted by **EMİNE ÜMRAN AŞCI** in partial fulfillment of the requirements for the degree of **Master of Science** i**n Chemical Engineering, Middle East Technical University** by,

Prof. Dr. Halil Kalıpçılar
Dean, Graduate School of **Natural and Applied Sciences** _____

Prof. Dr. Pınar Çalık
Head of the Department, **Chemical Engineering** _____

Prof. Dr. Göknur Bayram
Supervisor, **Chemical Engineering Dept, METU** _____

Examining Committee Members:

Prof. Dr. Servet Gülüm Şumnu
Food Engineering, METU _____

Prof. Dr. Göknur Bayram
Chemical Engineering, METU _____

Prof. Dr. Necati Özkan
Polymer Science and Technology, METU _____

Assoc. Prof. Dr. Erhan Bat
Chemical Engineering, METU _____

Assoc. Prof. Dr. Özcan Köysüren
Energy Engineering, Ankara University _____

Date: 23.06.2022

I hereby declare that all information in this document has been obtained and presented in accordance with academic rules and ethical conduct. I also declare that, as required by these rules and conduct, I have fully cited and referenced all material and results that are not original to this work.

Name Last name: Emine Ümran Aşcı

Signature:

ABSTRACT

PROCESSING BY ELECTROSPINNING METHOD AND CHARACTERIZATION OF POLY(LACTIC ACID) AND POLY(LACTIC ACID)-BASED COMPOSITE NANOFIBERS

Aşcı, Emine Ümran
Master of Science, Chemical Engineering
Supervisor: Prof. Dr. Göknur Bayram

June 2022, 138 pages

Electrospinning method is a versatile, cost-effective and viable technique to produce nanofibers with high ratios of surface area to the volume. The ability to obtain characteristics of the nanofibers via electrospinning, i.e., small pore size, high porosity and surface area/volume ratio, are some of the significant reasons why this method has eventually become a widespread technique for developing continuous and long fibers with nanometer-scale diameters. Furthermore, these advantages enable the produced nanofibers to be a class of nanomaterials suitable for various applications in industry and academic research.

In this study, it is aimed to optimize the electrospinning process parameters (i.e., solution feed rate, tip-to-collector distance and applied voltage) and solution properties by changing the solvent ratio and solution concentration for the neat polylactic acid (PLA) nanofiber production. Furthermore, the effect of polyethylene glycol (PEG) and halloysite nanotubes (HNTs) addition on the performance of nanofibers was also investigated by generating PLA/PEG and PLA/HNT nanofibers. Also, the influence of solution preparation methods on properties of PLA/PEG/HNT nanofibers were studied. All the prepared mats were characterized in terms of their

morphology, thermal and mechanical properties. In addition, water contact angle measurements were performed on the generated nanofibrous mats.

The obtained results indicated that 13 wt.% of polymer solution concentration, 1 ml/h of feed rate, 20 cm of tip-to-collector distance, 20 kV of applied voltage and 80/20 v/v chloroform (CHL)/dimethylformamide (DMF) solvent ratio were the optimum parameter values for the electrospinning of neat PLA. Moreover, inclusion of 15 wt.% PEG and 0.5 wt.% HNT resulted in enhanced mechanical properties of the nanofibrous PLA/PEG and PLA/HNT mats, respectively. The results revealed that the tensile strength value of PLA/PEG and PLA/HNT nanofibers increased by 80% and 13%, respectively compared to the neat PLA nanofibrous mat at the optimum conditions. Also, degree of crystallinity was found to be 38% and 22% for PLA/PEG and PLA/HNT mats, respectively while it was calculated as 15% for the neat PLA sample. For the electrospinning of PLA/PEG/HNT nanofibers, the solution preparation method in which suspension of HNTs was sonicated for 30 mins before adding PLA and PEG to the solution and magnetically stirred for 4 hours, led to enhanced performance of the nanofibers. The tensile test results indicated that the tensile strength and tensile modulus increased by 95% and 27% for PLA/PEG/HNT samples, respectively compared to neat PLA nanofibers. The decomposition temperature of the nanofibrous mats did not significantly change with the parameters of the study.

Keywords: Composite Nanofibers, Electrospinning, Polylactic Acid, Polyethylene Glycol, Halloysite Nanotubes

ÖZ

POLİ(LAKTİK ASİT) VE POLİ(LAKTİK ASİT) BAZLI KOMPOZİT NANOFİBERLERİN ELEKTROEĞİRME METODU İLE PROSESİ VE KARAKTERİZASYONU

Aşcı, Emine Ümran
Yüksek Lisans, Kimya Mühendisliği
Tez Yöneticisi: Prof. Dr. Göknur Bayram

Haziran 2022, 138 sayfa

Elektroeğirme yöntemi yüksek yüzey alanı/hacim oranına sahip nanofiberlerin üretiminde çok yönlü, uygun maaliyetli ve elverişli bir tekniktir. Elektroeğirme ile nanofiberlerin yüksek gözeneklilik, küçük gözenek boyutu ve yüksek yüzey alanı/hacim oranı gibi özelliklerinin elde edilebilirliği, bu yöntemin aralıksız, uzun ve nanometre ölçekli çapa sahip fiberler geliştirmek için nihayetinde yaygın bir teknik haline gelmesinin önemli nedenlerinden bazılarıdır. Ayrıca bu avantajlar üretilen nanofiberlerin endüstride ve akademik araştırmalarda çeşitli uygulamalar için uygun bir nanomalzeme sınıfı olmasını sağlamaktadır.

Bu çalışmada, saf polilaktik asit (PLA) nanofiberlerinin üretimi için elektroeğirme proses parametrelerinin (çözelti besleme hızı, toplama uzaklığı ve voltaj), ve çözücü oranı ile çözelti konsantrasyonu değiştirilerek çözelti özelliklerinin optimize edilmesi amaçlanmıştır. Buna ek olarak, polietilen glikol (PEG) ve halloysit nanotüplerin (HNT'ler) eklenmesinin nanofiberlerin performansına etkisi de PLA/PEG ve PLA/HNT nanofiberleri üretilerek incelenmiştir. Ayrıca, çözelti hazırlama yöntemlerinin, PLA/PEG/HNT nanofiberlerin özellikleri üzerindeki etkisi çalışılmıştır. Elde edilen tüm dokumalar morfolojileri, mekanik ve termal özellikleri

açısından karakterize edilmiştir. Ek olarak oluşturulan nanofiber dokumalar üzerinde su temas açısı ölçümleri yapılmıştır.

Elde edilen sonuçlar, ağırlıkça %13 polimer solüsyonu konsantrasyonu, 1 ml/saat çözelti besleme hızı, 20 cm toplama uzaklığı, 20 kV voltaj ve hacimce 80/20 oranında kloroform (CHL)/dimetilformamid (DMF) çözücü sisteminin saf PLA'nın elektroeğirme işlemi için optimum parameter değerleri olduğunu göstermiştir. Ek olarak ağırlıkça %15 PEG ve ağırlıkça %0.5 HNT ilavesi sırasıyla PLA/PEG ve PLA/HNT nanofiber dokumaları için gelişmiş mekanik özelliklerle sonuçlanmıştır. Sonuçlar, PLA/PEG ve PLA/HNT nanofiberlerinin çekme mukavemet değerlerinin optimum koşullarda saf PLA nanofiber dokumasına kıyasla sırasıyla %80 ve %13 arttığını ortaya çıkarmıştır. Ayrıca, PLA/PEG ve PLA/HNT dokumaları için kristallik derecesi sırasıyla %38 ve %22 olarak bulunurken, saf PLA numunesi için %15 olarak hesaplanmıştır. PLA/PEG/HNT nanofiberlerinin elektroeğirmesi için, HNT'lerin süspansiyonunun, PLA ve PEG eklenmeden önce 30 dakika boyunca sonikasyona tabi tutulduğu ve çözeltinin 4 saat boyunca manyetik karıştırıcı ile karıştırıldığı çözelti hazırlama yöntemi, nanofiberlerin performansının artmasını sağlamıştır. Çekme testi sonuçları saf PLA nanofiberlerine kıyasla PLA/PEG/HNT numuneleri için gerilme mukavemeti ve gerilme modülünün sırasıyla %95 ve %27 arttığını göstermiştir. Nanofiber dokumalarının bozunma sıcaklığı bu çalışmada yer alan parametrelerle önemli ölçüde değişmemiştir.

Anahtar Kelimeler: Kompozit Nanofiberler, Elektroeğirme, Polilaktik Asit, Polietilen Glikol, Halloysit Nanotüpler

To my beloved family…

ACKNOWLEDGMENTS

I would like to express my deepest gratitude, appreciation, and respect to my supervisor Prof. Dr. Göknur Bayram, for her valuable guidance, ceaseless support, understanding, encouragement, and insight throughout the research. It was a great honor and tremendous chance for me to work with her. I sincerely appreciate her being closely interested in every phase of my thesis work. I am thankful for her guidance during writing of my thesis and providing invaluable comments and revisions. Her strong scientific knowledge, as well as her compassion have been a major factor to pursue my academic career in the same field. I am also grateful for the time and effort she has taken and her counsel contributing to my academic and personal life.

This work was supported by the Scientific Research Projects Coordination of the Middle East Technical University [Grant Number: TEZ-YL-304-2020-10205].

I would thank to my kindhearted friends, Dr. Berrak Erkmen and Refik Barış Yılmaz in Polymer Engineering Laboratory for sharing their experiences. This thesis would not have been accomplished without their never-ending support, friendship, and great help in research and experiments.

I am so thankful for the support and love of my sweet roommates. I want to express my most profound appreciation to Azra Rafiq, Buket Altınçelep and Sonum Bandesha for their kindness and continuous effort for creating a happy, peaceful, and warm atmosphere in our room in dormitory. I would like to mention my warmest appreciation to my dearest friends Selin Cansu Gölboylu Aslınur Erdemoğlu, Meltem Başbay, Buse Onay, Özge Demirdoğan, Arda Uslu and Sema Zabcı for their friendship and support throughout this study.

I would like to express my gratitude to my director Eray Sarıbaş, my manager Mehmet Kaptan and PETKİM Production Scheduling Supervisor Cihan Onur Çelik in SOCAR Turkey, for their tolerance and support. I want to acknowledge my lovely co-workers, Yekta Işıl Dikbaş, Vusal Guluyev, Orhun Uzun, Ceren Kantar, Elif Gökçe Uzunpınar for their endless support and kind friendship.

Last but not least, I would like to sincerely thank my beloved family, who always be there for me. A special thanks to my precious parents Gülümser Aşcı and Mehmet Saim Aşcı, and my lovely brother Mehmet Enes Aşcı for always encouraging and comforting me. This thesis would have been almost impossible without their endless love, trust, and support in all parts of my life. Without them, I could not become a person who I am now. I appreciate them for being my biggest chance, without their encouragement, love, and affection my success would not have been possible.

TABLE OF CONTENTS

LIST OF TABLES

TABLES

LIST OF FIGURES

FIGURES

LIST OF ABBREVIATIONS

AV	Applied Voltage, kV
CS	Crosshead Speed, mm/min
CT	Collector Type
d	Days
DSC	Differential Scanning Calorimetry
ED	Electrospinning Duration, sec, min or h
h	Hours
on	Overnight
RS	Rotational Speed, rpm
SC	Solution Concentration, wt. % or wt./v %
SD	Sample Dimensions, mm x mm or cm x cm
SDD	Sample Drying Duration, overnight or day
SGL	Sample Gauge Length, mm or cm
SR	Solvent Ratio, v/v
ST	Sample Thickess, μm
SEM	Scanning Electron Microscopy
SFR	Solution Feed Rates, ml/h
TCD	Tip-to-Collector Distance, cm
TGA	Thermal Gravimetric Analysis
WCA	Water Contact Angle, ^{0}
wt.	Weight

CHAPTER 1

INTRODUCTION

Electrospinning is a method of generating nanofibers by including an electrohydrodynamic process that utilizes the electrostatic forces. This technique is applied in order to obtain fibrous morphologies from polymeric melts or solutions containing synthetic and natural polymers. The electrospinning method is superior to other nanofiber generation techniques including template synthesis, phase separation, drawing, and self-assembly due to its ability of simply producing long and continuous nanofibers, cost-effectivity, and versatility [1]. Therefore, all of these advantages enable the produced nanofibers to be a class of nanomaterials suitable for various applications, including their usage as filtration membranes, smart mats, catalytic supports, energy support components, photonic and electronic devices as well as biomedical scaffolds [2].

During the electrospinning process, a liquid droplet is electrified to generate a polymer jet, which is followed by stretching and elongation to produce fibers. In this process, the formation of the polymer jet is provided by the potential difference between the collector and the tip of the nozzle [1]. Generally, the electrospinning method with a polymer solution has four main steps. The first step is the charging of the liquid droplet and Taylor cone formation (or cone-shaped polymer jet). This is followed by the extension of the charged polymer jet along a straight line. As the third step, thinning of the jet under an electric field and growth of the whipping instability (which is also known as the electrical bending instability) occur. Finally, the solvent evaporates and the polymer jet as the solid fibers are collected on the surface of the collector [2].

Nowadays, a variety of polymers are used in the electrospinning process to obtain fine nanofibers for diverse applications. Nanofibers produced from these electrospun

polymer solutions via the electrospinning process have been extensively used in various applications including tissue engineering scaffolds, biomedical applications, protective clothing, optical and chemical sensors, filtration, and nanocomposite production [3]. Polylactic acid (PLA) is one of the polymers used in electrospinning process, and it is one of the most investigated polymers among the commercially available biodegradable thermoplastic polymers. Biodegradable polymers can be an alternative solution to solve the problem of solid waste related to decrease in the availability of landfills, global warming due to the increase in the amount of CO_2 in the atmosphere, and initiatives to find renewable or sustainable raw material sources [4]. Since PLA has a low production cost, it is economically competitive with commercial polymers that are petroleum-based [5].

PLA can be synthesized by ring opening polymerization of cyclic lactide as diester of lactic acid or by lactic acid condensation. In order to obtain high molecular weight polylactide in a large scale, ring opening polymerization is applied. In this synthesis method, as the first step, a condensation reaction occurs in order to prepolymerize lactic acid. As a result, low molecular weight polylactic acid is formed as the intermediate product which is depolymerized to cyclic lactide. Generally, this method has purification steps since lactide has impurities due to the acids or oligomers. Purification processes are significant in terms of avoiding the impact of contaminations on the polymerization rate or polylactic acid molecular weight. After the purification steps are completed, high molecular weight polylactic acid is obtained by the ring opening polymerization reaction of lactide [6-8]. For the last step, catalysts like N-heterocyclic carbine, 4-dimethylaminopyridine and stannous octoate are used. Since it has high catalytic activity and easier controllability, stannous octoate is the most common used catalyst [9-11].

In general, in order to produce low molecular weight polylactic acid condensation of lactic acid is applied. In this synthesis method, an esterification reaction occurs between the hydoxyl groups and carboxylic groups of the monomers [11]. Since this reaction is reversible, transesterification, which forms cyclic lactides, can occur. In order to produce high molecular weight polylactic acid with high conversion and

avoid transesterification reactions, the formed water in the reaction should be removed from the system. However, water removing process is difficult since the viscosity increases with the increasing conversion. In the literature, inclusion of catalysts, usage of vacuum in the system and azeotropic distillation process application are recommended to handle this problem [11-13].

Electrospun nanofibers are reported to be produced from numerous natural polymers, synthetic polymers, or by blending the both types of polymers. In recent years, polyethylene glycol (PEG) has become one of the synthetic polymers that have been widely used in electrospinning applications. PEG is one of the plasticizers used for polymers. In order to enhance ductility, flexibility and processability, plasticizers are extensively used in the industry. For the semicrystalline polymers like PLA, plasticizers are efficient not only for lowering the glass transition of amorphous parts but also for decreasing the melting point of the crystalline parts [14]. Moreover, PEG is bio-compatible, electrically and thermally stable, and has a lack of toxicity. In addition to these advantageous properties, being a polyol enables PEG to be used in various areas including pharmaceuticals, toothpaste, medicines, or skin creams since its has a propery of being biologically inert. In addition to all of this, halloysite nanotubes (HNTs) are inorganic nanoclay materials that are naturally occurring and consist of Silisium (Si), Aluminum (Al), and Oxygen (O) elements. They may have different morphologies like tubular, spherical, or platy forms. The nanostructure and unique morphology enable HNTs to have high surface areas which results in many possible application areas, such as catalysis and drug release. Moreover, HNTs have been widely used as polymer additives since they are biocompatible, harmless, inexpensive, and have unique thermal properties and morphologies [15, 16].

In addition to plasticizing effect of PEG which improves the strain at break, it can also perform as a compatibilizer between the polymer matrix and filler in the composites. Nonetheless, having plasticizers like PEG may decrease the mechanical and thermal stability of the polymer matrix. In order to balance these stability decreases and overcome these problems, the addition of nanoparticles can be considered [17]. Sharma et al. [18] investigated the effect of PEG and HNT addition

on mechanical and thermal properties of nanocomposite films produced by solvent casting method. It was found that addition of PEG increased elongation at break and toughness but decreased elastic modulus and tensile strength. The addition of HNT in PLA/PEG compensated the reduction in the mechanical stability. Moreover, it was seen that the thermal stability of PLA/PEG/HNT nanocomposite films was greater than the PLA and PLA/PEG films.

In the literature, various number of studies have been carried out to produce neat PLA nanofibers by using the electrospinning process. However, there is a lack of research on the use of PLA with PEG and HNTs in the electrospinning method. PEG has the potential of acting as a compatibilizer between PLA and HNTs. Furthermore, HNTs have the potential to improve the thermal and mechanical properties of the polymer matrix. In addition, it has been detected that there is a research gap in investigating the effect of polymer solution preparation methods on the nanofiber morphology, mechanical and thermal properties. In this study, an elaborate optimization study including the generation of neat PLA fibers with the optimum conditions was performed. Moreover, the effect of process parameters on the nanofiber morphology was investigated. After the parameter optimization step, in order to observe the influence of PEG on the nanofiber structure, PLA/PEG nanofibrous mats were generated at different PEG concentrations. After completing this step, HNTs-added PLA composite nanofibers were generated with the aim of investigating the influence of HNTs concentration and PLA/HNT suspension preparation methods on the nanofiber morphology. As the final step, PLA/PEG/HNT nanofibers were produced by applying different polymer solution preparation methods. All the prepared mats were characterized in terms of their morphology, mechanical and thermal properties. Furthermore, water contact angle measurements were performed on the samples.

CHAPTER 2

BACKGROUND

2.1 Nanotechnology

Nanotechnology is an advancing field covering studies and applications at the nanoscale (with a size range of 0.1 to 100 nm) and it has implementations in various fields. This technology is basically built on the progression of individual atoms, molecules, and compounds to some structures in order to have different materials with advanced properties. In addition, nanotechnology has an interest in the size reduction of large particles and converting them to the smallest structures. Materials at the nanoscale have different properties than materials at a larger scale. By nanotechnological applications, material properties like electrical conductivity, physical strength and chemical reactivity can be adjusted [19].

Electrospinning is an excellent method for nanotechnological applications. With the recent developments in nanotechnology, electrospinning made a mark as a technique for the fabrication of nanofibers. By this method, nanofibers can be efficiently generated with the desired morphologies [20]. Fibers are one-dimensional structures with high ratios of surface area to volume that can be generated naturally and synthetically. Nowadays, nanofibers obtained from polymers have been used in various fields like filtration, sensors, composite production, surface applications and tissue engineering [21].

2.2 Electrospinning

Among the other methods (i.e., phase separation, template synthesis, drawing, and self-assembly), electrospinning is a unique nanofiber production approach. This spinning technique has been drawing attention since the 1990s due to cost efficiency,

versatility, simplicity and ability to produce continuous fibers. In the electrospinning technique, fine fibers are produced from the polymer melts or solutions by using electrostatic forces. As a result, obtained fibers have a smaller diameter (from nanometer to micrometer scale) and a larger surface area than the fibers generated by the conventional methods. The electrospinning process is mainly built on the principle of the repulsive electrical forces overcoming the surface tension on the charged polymer liquid surface. Hence, a DC voltage is necessary for this process [3].

A general electrospinning setup consists of the following components: a syringe where the polymer solution is kept, a spinneret in which the solution is fed to the system, a pump for controlling the solution feed rate, a high voltage power supply to inject charge of a specific polarity to the polymer solution, and a collector that is either a metal plate or a rotating drum. According to the spinning direction, there have been three standard electrospinning setups in the literature which are vertical, bottom-up and horizontal [22]. The schematic representation of each electrospinning setup can be seen in Figure 2.1.

In the bottom-up electrospinning setup, four different types of force are exerted on the polymer solution. Electrostatic forces act on the polymer solution in the same direction with the electrical potential difference and stretch the solution. On the other hand, surface tension, gravitational and viscoelastic forces act in the opposite direction and hinder the stretching of the polymer solution. As the applied electrostatic force reaches the critical value, surface tension is overcome, gravitational and viscoelastic forces [3]. Thus, the electrospinning process initiates with the formation of the Taylor Cone from the polymer solution and eventually, a charged polymer jet is ejected from the tip of the Taylor Cone. The formed jet stretches and moves towards the collector. Between the spinneret tip and the collector, the polymer jet bends and develops a spiral movement called whipping, which leads to solvent evaporation. Solvent evaporation occurs to such an extent that the intermolecular forces between the polymer molecules become more robust so that the polymer jet stretching stops and fiber formation is completed [23].

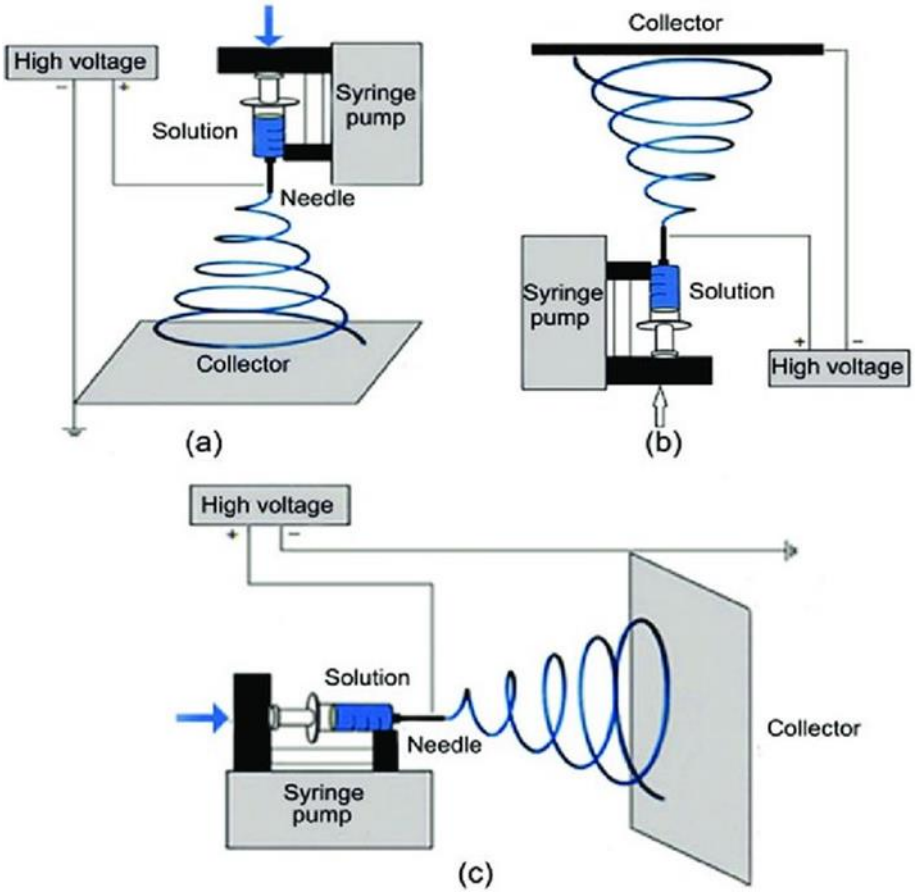

Figure 2.1 A schematic view of the different electrospinning setups (a) vertical (b) bottom-up (c) horizontal [22].

2.3 Parameters Affecting Electrospinning Process

Parameters that have an essential effect on the electrospinning process can be divided into three main groups. These are; solution parameters, process parameters, and ambient parameters. Each of these main parameter groups significantly influences the morphology of the fibers obtained by the electrospinning process. By suitably manipulating these three main parameter groups, nanofibers with desired morphology and diameters can be obtained.

2.3.1 Solution Parameters

Viscosity, solution concentration, molecular weight, conductivity, and the surface tension of the polymer solution are the solution parameters that influence the morphology of the sample generated by electrospinning process.

2.3.1.1 Viscosity

The viscosity of the solution is a significant parameter that affects the fiber size and the fiber morphology during the electrospinning of the polymeric materials. At low viscosity values, there is no continuous fiber formation. Therefore, at low viscosities, fibers with a beaded structure are obtained. The beaded structure obtained via the electrospinning process can also be explained by the inadequate surface tension. Since the surface tension is insufficient, droplets are formed to diminish the surface area in the polymer jet. On the other hand, there is an adversity in the ejection of jets from the polymer solutions at high viscosity values. Since the viscoelastic forces are strong at high viscosities, the axial stretching is going to be inadequate. This would result in obtaining thick fibers [24]. Therefore, an optimal viscosity range is required for the electrospinning process.

Viscosity, molecular weight of the polymer, and polymer concentration have a relation with each other. The solution viscosity is directly proportional to the concentration of the solution and the molecular weight of the polymer. As the solution viscosity (or the polymer concentration) increases, more uniform fibers with larger diameters are obtained.

According to Doshi and Reneker [25], viscosity of the solution has a vital role while determining the range of the concentrations in order to obtain continuous fibers. For the solutions with low viscosity values, the dominant factor is the surface tension. Hence, just beads or beaded fibers are formed at low viscosities. On the contrary, a continuous fibrous structure is obtained above the critical concentration, and the concentration of the solution affects its morphology. It can be concluded that a

polymer-specific, optimal viscosity value exists for the electrospinning process, and this property has a conspicuous influence on the fiber morphologies.

2.3.1.2 Solution Concentration

The solution concentration is another important parameter that affects the fiber production and morphology. In the electrospinning process, a minimum solution concentration value is essential to obtain fiber formation. In this process, the stretching of the polymer jet is required to produce nanofibers. Solution concentration has a significant impact on this stretching. At low concentrations, due to the stretching and the surface tension, the entangled polymer chains break into smaller pieces before reaching the collector [26]. As a result, at low concentrations, a mixture of fibers and beads is obtained. In addition, as the solution concentration increases, the viscosity and the chain entanglements are also increasing. At high solution concentrations, chain entanglements can overcome the surface tension. Therefore, the shape of the beads starts to change from spherical form to spindle-like and finally, uniform fibers without any beads can be produced [3].

In the electrospinning process, there should be an optimum concentration value. When the solution concentration exceeds this value, the formation of continuous and smooth fibers is prohibited due to the needle-tip blocking caused by the rapid evaporation of the solvent during the process. This situation may result in the formation of defective fibers [26]. If the solution concentration is too high, the formation of thicker fibers is observed due to the higher viscosity resistance at higher polymer concentrations [3]. Ki et al. [27] stated that a power-law relationship exists between the solution concentration and fiber diameter in which the fiber diameter increases with the increasing concentration.

2.3.1.3 Molecular Weight

The molecular weight of the solution is another property that has an essential effect on rheological properties, such as viscosity, and also on surface tension. It also affects electrical properties like conductivity and dielectric strength. The molecular weight of the polymer indicates the number of chain entanglements in the polymer structure. Chain entanglements play a vital role in the electrospinning process and thus in the electrospun fiber morphology. At a constant solution concentration, the number of beads and droplets increases with decreasing molecular weight. As the molecular weight of the polymer is increased, the desired viscosity value for the fiber formation is obtained, and fibers with larger diameters are produced [3]. In order to have uniform and defect-free electrospun nanofibers, a sufficient level of intermolecular interaction is required. If the intermolecular interaction is obtained by an oligomer, then the effect of molecular weight on the morphology will not be extremely essential [28].

Tan et al. [29] reported that low concentrations of high molecular weight poly-L-lactic acid (HM-PLLA) could provide a sufficient number of chain entanglements. Therefore, an adequate level of solution viscosity for generating a uniform jet during the electrospinning process was obtained. Moreover, the effect of surface tension that has an essential role in bead formation was restrained. According to Koski et al. [30] increasing the molecular weight has resulted in fiber diameter increment. At low molecular weights, fibers with circular cross-sections were produced. As the solution concentration is increased, the fiber diameter has also increased, and the fibers have changed their forms from circular cross-sections to ribbon-shaped fibers.

2.3.1.4 Conductivity

The conductivity of the solution depends on the solvents used, polymer type and the availability of ionizable salts. Repulsion of charges on the polymer jet surface causes stretching to occur. Since the polymer jet carries more charge, the stretching will be

more in high conductive solutions. As the electrical conductivity of the solution increases, the diameter of electrospun fibers significantly decreases. In addition, solutions with low conductivity have inadequate polymer jet stretching during the electrospinning process. Hence, beaded morphologies may be observed. On the other hand, solutions with very high conductivity are extremely unstable. This instability inhibits the continuous electrospinning process [3]. Zong et al. [31] investigated the effect of ions on the morphology and the fiber diameter by adding ionic salt. The presence of the ionic salts (KH_2PO_4, NaCl and NaH_2PO_4) increased the conductivity and enabled the generation of smooth fibers with smaller diameters.

Yang et al. [32] produced Polyvinylpyrrolidone (PVP) nanofibers via the electrospinning method and investigated the effect of different solvents on fiber morphology and diameter. For this purpose, polymer solutions were prepared with various solvents, including N,N-dimethylformamide (DMF), ethanol, dichloromethane, and their electrical conductivity values were compared. It has been found that fiber diameter decreases with the increase of the solution electrical conductivity. Fibrous structures with small diameters have the potential to be used in different fields such as composite production, tissue engineering, composite production and filtration.

2.3.1.5 Surface Tension

Due to the surface tension, the polymer solution accumulates on the tip of the nozzle. During the electrospinning process, when the surface tension is balanced with the electrical forces, the polymer droplet is elongated in order to develop a Taylor Cone. As the electrical forces start to exceed the surface tension, a polymer jet is created, and it has a movement through the collector [31]. Surface tension is more likely a function of solvent compositions in the solution and it plays a vital role during the electrospinning process. Smooth and beadless fibers can be achieved by decreasing the solution surface tension. Different solvents can contribute to different solution surface tension values. The electrospinning process is constrained by the high surface

tension of the solution due to the unstable jets and sprayed droplets generation [3]. At low solution concentrations, solvent molecules interact less with polymer molecules. Therefore, solvent molecules tend to take the form of droplets due to the surface tension. As the solution concentration increases, the interaction between the solvent and the polymer molecules improves. Hence, the tendency to form a spherical shape for solvent molecules is reduced [1]. Consequently, diminishing the surface tension by changing the solvent type avoids the beaded morphology at the constant solution concentration [28]. Essentially, surface tension is important while determining the upper and lower limits of electrospinning frame if all of the other variables remain constant [3].

Pant et al. [33] studied the effect of different solvent systems on fiber morphology and diameter. Polyamide-6 (PA6) nanofibers were generated with varying solvent systems and compared at a constant concentration value. According to this study, fibers obtained from solutions with lower surface tension had fewer beads, and with the increasing surface tension, the polymer jet became unstable. Therefore, more beads appeared on the nanofibrous mats.

2.3.2 Process Parameters

Voltage, tip-to-collector distance, and feed rate of the polymer solution are the process parameters that are crucial for the electrospinning process due to their effect on the polymer jet.

2.3.2.1 Voltage

The applied voltage is another essential factor in the electrospinning process. The fiber formation occurs after a particular value of applied voltage is exceeded. This specific value varies according to the polymer solutions, and it should be adequate to overcome the surface tension so that the electrospinning process can be initiated [3]. As the applied voltage value gets larger than the threshold value, the polymer jet

accelerates, resulting in an increase in the amount of the polymer solution turning into fibers. When higher voltages are applied, more polymer solution is fed to the nozzle and ejected by the higher electrical forces. This facilitates the formation of an unstable and smaller Taylor Cone [31].

In many cases, the higher applied voltage leads to a diminution in the fiber diameter by increasing the stretching of the polymer solution and accelerating the polymer jet due to the greater electrical field. This strong electrical field also provides rapid evaporation of the solvent from the fibers and faster pulling of fibers. The electrostatic repulsive forces, thus the electrical potential increase on the polymer jet with the increasing applied voltage, which favors reducing the fiber diameter [3].

The flight time of the polymer jet is another parameter that influences the fiber diameter. Longer flight times enable the solvent to have more time for evaporation. Therefore, fibers with smaller diameters are obtained. Consequently, the fiber diameter may rise up to a particular voltage value and then decline. Thus, adjusting the applied voltage to an optimum value makes it possible to have smooth fibers [34].

In a study of Uchko et al. [34] the effect of process parameters including applied voltage on fiber morphology was investigated. It has been observed that increasing the applied voltage resulted in the reduction of fiber diameter. Furthermore, electrical potential and hence applied voltage have an effect on bead formation. Deitzel et al. [35] reported the impact of solution concentration and electrical potential on morphology of fibers. According to this study, the shape of the polymer jet surface changed, and stability decreased with the increasing applied voltage. As a result, bead formation was observed. It is found that the solution concentration is the most important electrospinning parameter that affects the fiber diameter. Yördem et al. [36] state that voltage has an impact on fiber diameter. However, the level of significance differs with the tip-to-collector distance and the solution concentration. In other words, electrical potential is a process parameter that depends on the tip-to-collector distance and polymer solution concentration.

2.3.2.2 Tip to Collector Distance

As another approach to obtain smooth fiber morphologies, distance between the tip and the collector has been investigated. There should be an optimum tip to collector distance that provides adequate flight time and magnitude of stretching. Therefore, with an optimum tip to collector distance, the required flight time for solvent evaporation from the polymer jet can be provided and uniform fibers are produced. If the optimum tip to collector distance is not provided, beaded fibers are observed whether at too far or too close distances [3].

The time spent for fibers to dry before reaching the collector reduces with the decreasing tip to collector distance. Moreover, the electric field strength is inversely proportional to the distance. Hence, the electric field will get stronger, and the polymer jet will be accelerated as the distance between tip to collector decreases. Consequently, the polymer jet instabilities occur due to the inadequate solvent evaporation time and high voltage [28]. In addition, flatter and shorter fibers have been generated at the small tip to collector distance values and with the increase in the distance, rounder fibers have been obtained [3].

Mazoochi et al. [37] investigated the effect of electrospinning parameters, that were applied voltage and tip-to-collector distance, on the polysulfone (PSf) nanofiber morphology. As a result of this study, it was found that the fiber diameter increased as the applied voltage was increased from 10kV to 15kV. When the applied voltage was increased to 20kV, a reduction in the fiber diameter was observed. In addition, increasing the applied voltage has increased the surface charge of the polymer jet. As a result, the frequency of bead formation was reduced. The time of complete evaporation was adjusted by the distance between the tip and the collector. Collecting distance values of 5, 10 and 15 cm were selected to find the optimum process conditions by keeping other electrospinning parameters constant. It was found that the tip-to-collector distance directly affects the polymer jet flight time and electric field strength. Thus, spinnability and fiber diameter were directly affected by the collecting distance. Due to the electrospraying, droplets were obtained at very

short distances. Increasing the distance between tip-to-collector resulted in a decrease in the fiber diameter.

2.3.2.3 Feed Rate

In the electrospinning process, the feed rate of the polymer solution is a significant process parameter since it affects the material transfer rate and the polymer jet velocity. Low feed rates are more desirable in order to have adequate time for solvent evaporation and polarization of the polymer solution. High flow rates result in beaded fibers with larger diameters due to insufficient solvent evaporation time and volume increase [3].

Zuo et al. [38] studied the effect of solution feed rate and applied voltage. SEM images were analyzed to figure out the influence of these process parameters on the fiber morphology. It has been found that higher applied voltages and feed rates favored the formation of beaded fibers. In addition, increasing feed rate did not cause any statistically significant change in average fiber diameter.

2.3.3 Ambient Parameters

Apart from process and solution parameters, the fiber morphology is also influenced by ambient parameters. These parameters are humidity and temperature. In this section, conducted studies and their results to examine the effect of the ambient parameters on the electrospinning process are presented.

2.3.3.1 Humidity

Humidity is one of the factors that influence the pore formation on the fiber surface. In a study by Casper et al. [39], the effect of humidity and molecular weight in the electrospinning process were studied. For this purpose, polystyrene (PS) with four different molecular weights were used in the electrospinning process. It was found

that electrospinning in an atmosphere with a humidity level of less than 25% resulted in smooth fibers without any surface features. When the humidity level was increased to 30%, pores began to form on the fiber surface. The number of pores on the fiber surface, the pore size distribution, and the pore diameter increased with the increasing humidity level. In the electrospinning process, fibers with larger pores that are less uniform in both shape and size were obtained by using solutions with higher polymer molecular weight. Similarly, Natajaran et al. [40] produced PLA nanofibers at different relative humidity values. According to the obtained results, at relatively low humidity levels (around 25%), fibers did not show any porous surface morphology. The generated nanofibers had a uniform diameter distribution at low humidity levels due to the less charge dissipation during the spinning. The level of porosity increased with the increasing relative humidity.

2.3.3.2 Temperature

The solvent evaporation rate and the polymer solution viscosity are dependent on temperature. The rate of solvent evaporation shows an exponential decrease with decreasing temperature. Therefore, it takes a longer time for the solvent to evaporate, continuing the stretching of the polymer jet. On the other hand, the temperature has an opposing effect on the polymer viscosity. The polymer chains have less freedom to move and more rigidity at lower temperatures. This results in higher solution viscosity with the decreasing temperature. Lower stretching rate can be obtained by the higher solution viscosity due to a lower temperature. As a result, thicker fibers are generated [41].

In a study of De Vrieze et al. [42], PVP nanofibers were generated at different ambient temperatures. This study was conducted to investigate the dependency of two major solution properties, which are solvent evaporation rate and polymer solution viscosity, on temperature. For this purpose, temperatures of 283, 293 and 303 K were tried by keeping the other electrospinning parameters constant. The evaporation rate of the solvent and the viscosity of the solution have an influence on

the average fiber diameter, and they have two opposing mechanisms. It was found that at 283 and 303 K, the fiber diameter was smaller than the diameter at 293 K. At 283 K, the temperature effect on solvent evaporation rate was dominant over the effect on solution viscosity due to the exponential change of the evaporation rate of solvent with the temperature. On the other hand, at 303 K, the temperature effect on viscosity was dominant over the effect on the solvent evaporation rate due to the exponential diminishment of the viscosity as a function of increasing temperature. Both effects resulted in a reduction in the fiber diameter. Therefore, at low temperatures, a smaller fiber diameter was obtained due to the effect of temperature on the solvent evaporation rate. Moreover, fibers with smaller diameters were also obtained at high temperatures due to the temperature effect on the solution viscosity. At intermediate temperature levels, the fiber diameter reached the maximum value.

2.4 Solvents Used in the Electrospinning Process

Since the solution preparation is the first and foremost step of the electrospinning process, selecting a suitable solvent system has an essential effect on the spinnability. Fundamentally, solvents have two critical roles in the electrospinning process; to dissolve the polymer molecules for polymer jet formation and transport dissolved polymer molecules towards the collector. In order to have a successful electrospinning, solvents with the properties like sufficient volatility, conductivity, boiling point and vapor pressure should be selected. Depending on the solvent type, the intermolecular interaction between the polymer and solvent is either repulsive or attractive. Therefore, the chosen solvent system should conserve the polymer solution integrity.

During the electrospinning process, solvent evaporation and phase separation occur due to the polymer jet thinning. The vapor pressure and boiling point of the solvent perform a significant role in specifying the evaporation rate and thus the drying time. Moreover, solvent volatility has a crucial role in nanofiber formation because it affects the phase separation in the electrospinning process. The morphology and

diameter of the fibers are dependent on solution parameters such as surface tension [3]. The surface tension of the is dependent to both on polymer and solvent and can be adjusted by changing the solvent type.

Yang et al. [32] studied the effects of different solvents on PVP nanofibers generation by keeping the solution concentration constant. It was found that different solvents contributed to different surface tension values. By reducing the surface tension, bead formation was reduced, and smooth fibers were produced. Casasola et al. [43] studied the effect of different solvent systems on PLA fiber morphology and diameter. For this purpose, polymer solutions were prepared with various single and binary solvent systems. For the single solvent systems, only solutions prepared with solvents having high conductivity, high dielectric constant and low surface tension produced adequate amount of fibers to form a nanofibrous mat. Since the polymer jet did not have sufficient time to complete drying before reaching the collector, solutions prepared with solvents having high boiling points could not generate nanofibers. For the binary solvent system, as the electrical conductivity increased, defect-free nanofibers were obtained. In addition, it was found that the average diameter of nanofibers decreased when a solvent with a higher boiling point was chosen as the second solvent in the binary solvent system.

2.5 Characterization Methods

2.5.1 Thermal Analysis

Thermal analysis is highly crucial in terms of determine the relation between various physical properties of the material and temperature. In order to observe the behavior of the polymeric materials under controlled temperature programs in certain atmosphere, several methods are carried out. Differential Scanning Calorimetry (DSC), Thermogravimetric Analysis (TGA), Thermomechanical Analysis (TMA), Thermodilatometry (TD), Dynamic Mechanical Analysis (DMA) and Dielectric Analysis (DEA) are the techniques applied to the polymers for the thermal

characterization. Thermal analysis also enables one to have an idea about other parameters such as ageing, thermal transitions, the influence of additives and the effect of different environmental conditions on the polymeric material. While conducting the thermal analysis of the polymeric materials, DSC and TGA are extensively used methods, which were also performed in this study for the thermal characterizations [44].

DSC is an effective way to measure the amount of energy released or absorbed by a sample and the heat capacity of the material. DSC has two small sample pans; one is for the sample of polymeric material and the other is for the reference sample. Each pan is located on the top of a heater which is used to heat the two pans with a predetermined heat rate. The same temperature program is applied to both sample pans throughout the analysis and heat flow as a function of temperature or time is recorded. Moreover, by applying the DSC method, thermal properties (i.e., glass transition temperature, melting point, heat of fusion, degree of crystallinity and curing kinetics) can be analyzed. In order to obtain an efficient heat transfer, samples should have good contact with the sample pan and likewise, sample pans should make good contact with the heater surface [45, 46].

TGA is a technique in which a constant heat rate is applied to the samples and the weight change is measured as a function of temperature or time. Throughout the TGA analysis, as the samples are heated, the components of the polymeric material decompose or evaporate at specific temperatures which results in a series of weight loss steps in the obtained TGA curve. This method can yield significant properties of polymeric material including volatile content, plasticizer content, effectiveness of inorganic filler or additive content, carbon content, decomposition kinetics and oxidative stability [45, 46].

In the literature, a lot of studies have been conducted in order to investigate the effect of electrospinning process and electrospinning parameters on the degree of the crystallinity. Zong et al. [31] claimed that electrospun PLA fibers had lower degree of crystallinity values than that of pristine PLA resin, since during the

electrospinning process, the stretched polymer chains solidified rapidly. Similarly, Ramdhanie et al. [47] observed that PLA fibers showed lower degree of crystallinity levels compared to the one of as received PLA pellets. Moreover, Zhao et al. [48] investigated the impact of applied voltage on degree of crystallinity of ethyl-cyanoethyl cellulose fibers. It was reported that the travel time of the polymer jet from needle tip to collector and molecular orientation were significantly affected by the electrostatic field and thus the applied voltage. As a result, it was concluded that up to an optimum applied voltage, the degree of crystallization value reached a peak value and then declined as the applied voltage increased.

Ero-Phillips et al. [49] conducted an elaborate study on the influence of electrospinning parameters on thermal properties. It was seen that the glass transition temperature of the fibers generated at any electrospinning parameter value had lower value than that of pristine PLA granules. This result was contributed the reduction in the amount of chain entanglements and higher surface area within polymer chains in fibers compared to pellets. On the other hand, glass transition temperature increased with the increasing polymer concentration since the polymer chain interactions increased. In addition, at low polymer concentration solutions lower degree of crystallization was obtained due to the smaller chain entanglements and slower solidification of polymer fibers during the electrospinning process.

Ero-Phillips et al. [49] also observed that the degree of crystallization increased as the applied voltage was increased to an optimum value and increasing voltage beyond this optimum value the degree of crystallization showed a diminution trend. The increase in the degree of crystallization before the optimum applied voltage was caused by the increase in the polymer chain alignment and molecular orientation. As the applied voltage was increased, an increase of number of charges in the polymer solution occurred and this resulted in an increment in the polymer jet stretching. Therefore, an increase in the degree of crystallization was observed. On the other hand, it was seen that degree of crystallization was also affected by the polymer jet flight time during the electrospinning process. At higher applied voltage values than the optimum voltage, the flight time was pretty inadequate. Since the flight time of

the polymer jet decreased, the jet has a greater acceleration. As a result, degree of crystallization showed a decreasing trend. When the influence of tip-to-collector distance on the thermal properties was investigated, it was seen that changing collection distance did not have a crucial effect on the degree of crystallinity when the applied voltage values are at or close to the optimum. This was attributed to the fact that the varying tip-to-collector distance might not have a significant impact on the polymer jet flight time since jet has a complicated three dimensional whipping trajectory. Therefore, this might indicate that varying applied voltage has a more significant role in the jet trajectory than the tip-to-collector distance. In addition, increasing applied voltage and tip-to-collector distance values did not cause a change in the glass transition temperature of the electrospun mats.

Kim et al. [50] investigated the influence of the propolis concentration on the thermal properties of the electrospun polyurethane (PU) fibers. The study reported that the increase in the propolis concentration resulted in a decrease in the degree of crystallization since the polymer chain orientation was influenced by the inclusion of the propolis. In addition, it was observed that each sample showed a single step degradation, and as the propolis concentration increased a gradual decrease in the thermal decomposition temperature was obtained. Since the propolis has a lower thermal stability, the addition of propolis in polymer matrix caused a decrease in the thermal stability of the nanofibrous mats.

2.5.2 Mechanical Analysis

Mechanical characterization is highly crucial to predict the performance of the material. Determination of the material behavior under forms of loading is essential to compare and develop materials and processes. Tensile, impact, compression, shear, hardness, tear resistance, bending, abrasion, fatigue, and torsion are the tests applied to the polymers for the mechanical characterization. In this study, tensile test was conducted as the mechanical characterization.

Tensile test is an effective and most informative standard characterization method. This test is conducted by applying loading to the material sample extensionally. The exerted force is measured while the sample elongates at a constant extension rate. After the test, the stress-strain curve is plotted. From this graph, tensile strength, tensile modulus, elongation at break, and yield strength values can be extracted. Polymers are viscoelastic materials. Since polymers are dependent on test speed, it is an essential parameter for the tensile test. There are many morphological parameters that can strongly influence the mechanical performance of the nanofibrous mats, such as the entanglements between the fibers, fiber diameter, porosity, and the orientation of the fibers [51]. Moreover, there is no standard method for conducting the tensile test of the electrospun materials in the literature. Different techniques and process parameters have been applied to obtain the mechanical properties of the electrospun samples. In addition to fiber morphology, mechanical properties of the fibrous mats are severely dependent on the measurement method and processing parameters of the fiber generation [52]. This section presents various examples of tensile test applications on electrospun PLA mats and their results.

Scaffaro et al. [53] conducted a comparative study between aligned and randomly oriented electrospun fibers of neat PLA and PLA/graphene nanopellets (GnP). For the electrospinning process, solutions with a total solution concentration (SC) of 10 wt. % were prepared with a solvent system ratio (SR) of 2:1 v/v chloroform/acetone (CHL / AC). Electrospinning conditions were chosen as solution feed rate (SFR) of 1 ml/h, tip-to-collector distance (TCD) of 13 cm, and applied voltage (AV) of 17 kV. Load cell (LC) value of 1 kN was determined as one of the tensile stress parameters. Since samples have high elongation, two different crosshead speed (CS) values were applied as the following: 1 mm/min for 2 minutes and then 50 mm/min for the rest of the test. All the samples have the sample dimension (SD) of 10mm x 30mm. The sample thickness (ST) for each sample was measured before performing the test. It was found that the tensile modulus value for the randomly oriented neat PLA electrospun fibers was 62.46 ± 3.64 MPa. However, for the aligned neat PLA electrospun fibers, elastic modulus was found to be more than three times higher

compared to the value which belongs to randomly oriented neat PLA fibers and it reached 328 ± 17.4 MPa. In addition, for the aligned neat PLA fibers, tensile strength and elongation at break was found as 6.69 ± 0.56 MPa and 30.88 ± 6.18 %, respectively. Tensile strength of the randomly oriented neat PLA fibers was found more diminutive than aligned fibers with a value of 1.80 ± 0.07 MPa. On the other hand, randomly oriented pristine PLA fibers had a greater elongation at break value than aligned fibers, and it was obtained as 141 ± 7.6 %. By this study, it can be concluded that the orientation of the fibers has a vital influence on the mechanical behavior of the nanofibrous mats. Other specifications of tensile tests applied in the literature and the values of the tensile properties are given in Table 2.1.

Table 2.1 Literature Summary of Electrospinning Parameters and Mechanical Analysis Data.

References	SR	SC (wt.%)	SFR (ml/h)	TCD (cm)	AV (kV)	CS (mm/min)	SD (mm x mm)	LC (kN)	ST (µm)	SGL (mm)	Tensile Strength (MPa)	Tensile Modulus (MPa)	Elongation at Break (%)
Toncheva et al. [54]	DCM	9	5	19	17	25	20 x 60	2.5	100	40	3.9±0.03	94±8	56±7
Apalangya et al. [55]	CHL	10	1.5	20	12.5	50	10 x 60	0.02	20-30	-	1.15 (max)	3.8	18.50
Cai et al. [56]	CHL/DMF (6:1 wt./wt.)	15	1.5	15	18	10	60 x 5	0.2	200	-	0.3±0.02	4.1±0.66	23.02±1.23
Lins et al. [57]	CHL/DMF (4:1 v/v)	15	1	15	25	5	4 x 10	-	Tens of micron	-	4.3±0.8	38±3.4	12.9±2.7
Rodriguez et al. [58]	TFE	15	1.5	25	25	1	50 x 12.5	0.05	577	-	7.1±0.5	13.9±1.0	-
Alharbi et al. [59]	CHL/DMF (4:1 v/v)	8	0.1	15	19	0.5	ISO 527-1:2012 standards	-	2000	10	4.2±0.15	-	40

2.5.3 Water Contact Angle Measurements

When a liquid droplet is dropped on a solid surface, contact angle is formed at the three-phase boundary where solid, liquid, and gas phases have a thermodynamic equilibrium, as in Figure 2.2. Contact angle is a significant parameter to determine the characteristics of wettability, and it is a relatively low-cost, simple and popular technique in polymer surface characterization methods [60].

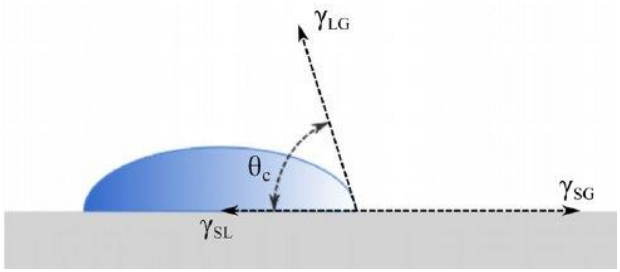

Figure 2.2 Equilibrium contact angle [61].

The interaction between the liquid droplet and solid surface influences the contact angle and thus the wetting behavior. As it can be seen in Figure 2.3, at the contact angles smaller than 90°, the liquid wets the solid surface. In addition, with the contact angles of 180° and above, no wetting occurs on the surface.

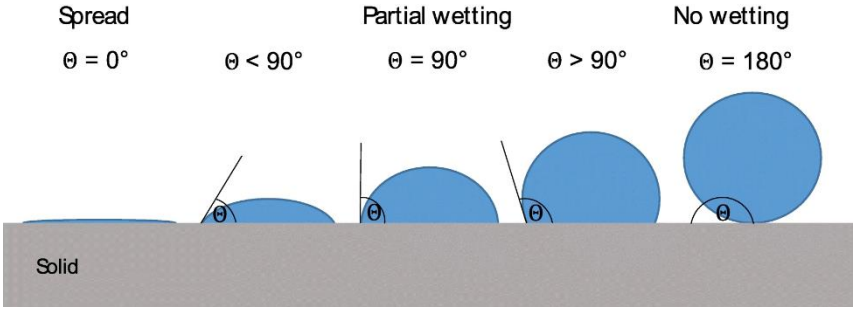

Figure 2.3 Contact angles at different wetting behaviors [62].

Wettability is a significant property of a solid surface for industrial and research applications. The wettability of the surface is determined by two dominant factors: surface energy and surface roughness. Since thin fibers can be generated by electrospinning process, electrospun fibers intrinsically contribute by one degree of

roughness to hydrophobicity [65]. In addition, according to the previous studies the electrospinning parameters indirectly influences the hydrophobicity.

Singh et al. [66] investigated the effect of the polymer solution concentration on the contact angle measurements. Therefore, nanofibrous mats of poly[bis(2,2,2-trifluoroethoxy)phosphazene] were generated at different polymer solution concentrations of 25, 5 and 0.5 wt./v.%. The water contact angle of the samples showed a decrease with the increasing polymer solution concentration. As the polymer solution concentration increased the fiber diameter also increased and thicker fibers were obtained. Since changing polymer solution concentration affected the surface morphology of the nanofibrous mats, it has an indirect influence on the water contact angle. As a result, water contact angle was decreased from 159° to 135° when the polymer solution concentration was increased from 0.5 wt.%v. to 25 wt./v.%.

Kang et al. [67] studied the influence of the solvent type used to prepare electrospinning solution on the contact angle measurements. Therefore, polystyrene (PS) nanofibrous samples were generated by using chloroform (CHL), tetrahydrofuran (THF) and N, N-dimethylformamide (DMF) as the solvent. It was found that the water contact angle for the samples prepared with CHL and THF was evaluated as 138.8 ± 0.5° and 138.1 ± 0.7°, respectively. Since CHL and THS are volatile solvents, they have high evaporation rates which resulted in nanofibrous mats with porous morphology. Hydrophobicity is dependent on surface morphology, hence rougher surfaces resulted in high water contact angle. In addition, the water contact angle was found as 154.2 ± 0.7°. DMF is a non-volatile solvent that has a low evaporation rate. Hence, nanofibrous mats contains residual solvent as nanosized bubbles entrapped in the fibers due to the low evaporation rate of DMF. As a result, higher water contact angle value was obtained since nanosized bubbles acted as a secondary surface with protuberances.

Scaffaro et al. [68] investigated the effect of plasma modification on the wettability and surface energy of electrospun PLA nanofibers and films obtained by solvent

casting method. In order to do that, static contact angles were measured by dropping water (as the polar liquid) and diiodomethane (as the dispersion liquid) droplets on the samples and the images of the droplets were taken for the contact angle analysis. According to the results, since the plasma modification caused a change in the surface chemical composition of PLA and surface roughness, the water contact angle of plasma modified PLA films was lower than that of the neat PLA films. In addition, plasma surface modification of PLA films increased the diiodomethane contact angle when it was compared to the neat PLA films. Moreover, an increase in the surface energy of the films caused by the plasma treatment was observed. On the other hand, the influence of plasma surface modification was seen stronger in the electrospun PLA mats than films. Electrospun neat PLA samples had greater water contact angle values ($115.9 \pm 1.1°$) than that of plasma treated PLA nanofibrous mats ($41.3 \pm 1.7°$). This result was attributed to the high porosity of the sample which enabled to entrap air when the surface was submerged in water. Therefore, air pockets were formed between the solid and water surface boundary which caused the surface to stay hydrophobic. In addition, the contact angle of diiodomethane for both neat and plasma treated sample were evaluated as zero since the surface energy of the fluid was low.

2.6 Composite Nanofibers

Although nanofiber morphology provides enhanced properties, nanocomposites are one of the research areas that have been highly interested due to their advanced mechanical properties, electrical conductivity, thermal stability, and dimensional stability. Generally, nanocomposites consist of two or more different components, with at least one of the compounds should have dimensions in nanoscale [69]. Polymer composite nanofibers are engineered materials, and electrospinning is one of the extensively used methods to produce them. Various examples of polymer composite nanofiber generation via the electrospinning process can be seen in the literature. To this end, assorted types of organic and inorganic nanofillers, e.g.,

carbon nanotubes (CNTs), HNTs, nanoclays, and graphene, have been used for electrospinning studies [70].

2.6.1 Composite Nanofibers with Two Components

In a study of Marsi et al. [71] composite nanofibers were produced by using PLA and titanium dioxide (TiO_2). It was seen that none of the nanofibrous mats showed a beaded structure. As the concentration of TiO_2 was increased from 10% to 35% by weight, the mean fiber diameter increased slightly. A significant decrease occurred in the crystallinity due to the addition of TiO_2. With the increasing amount of TiO_2 on the PLA matrix, a substantial increase in the degradation temperature was observed. Moreover, glass transition temperature increased with increasing TiO_2 concentration.

Touny et al. [72] focused on the influence of halloysite nanotube (HNTs) addition and its concentration on nanofiber morphology. For this purpose, they generated PLA/HNT nanocomposite fibers by using the electrospinning technique. According to this study, it was found that PLA crystallization was affected by the HNT dispersion. The degree of crystallinity of the nanocomposite fibers increased with the increasing HNT concentration in the solution. Furthermore, adding inorganic clay caused an increase in the electrical conductivity of the solution. Therefore, the average fiber diameter decreased to the nanoscale with the addition of HNT. At low HNT concentrations, a few fibers with beaded structure were produced. As the HNT concentration increased, fewer beads and aligned fibers were obtained.

Dong et al. [70] investigated the effect of the HNT concentration and its modification (using BYK-9076, dispersant solution) by several characterization methods. For this aim, PLA/HNT nanofibers with different HNT concentrations (0, 1, 5, and 10wt./v) were produced via the electrospinning process. As a result, the average fiber diameter of nanofibrous PLA/unmodified-HNT composite mats moderately increased due to the increase in the solution viscosity with the rise of unmodified-HNT concentration.

On the other hand, dispersant usage for HNT modification helped to have fine HNT dispersion so that the clogging during the electrospinning process caused by the HNT agglomeration was reduced. Hence, nanofibrous PLA/modified-HNT composite mats with smaller average fiber diameters were generated. The reinforcement effect of HNTs resulted in an increment in the tensile strength and tensile modulus values. In addition, HNT modification had a more outstanding contribution to the improvement of mechanical properties. Thermal analyses showed that as the HNT content increased, an acceleration in the cold crystallization of PLA fiber matrix and improvement in the thermal stability of nanofibrous composite mats were obtained.

The study of Magiera et al. [73] was aimed to analyze and compare the degradation behavior of electrospun neat PLA and PLA/modified-CNT nanofibers in an aqueous environment. Polymer solutions were prepared with PLA and CNT concentrations of 15 wt./v % and 1 wt. %, respectively. Electrical conductivity of the polymer solution increased with the addition of CNT to the system. This increment resulted in convenient jet splitting under an electrical field during the electrospinning process. Water contact angle measurements of nanofibrous mats were conducted in order to determine the chemical nature of the mat surfaces. While electrospun neat PLA mat showed a typical hydrophobic material behavior, electrospun PLA/modified-CNT mats had a slight decrease in the water contact angle values. CNTs had a good dispersion in the polymer solution. Hence, preferable interphase attractive interactions between CNTs and the polymer matrix were obtained. CNT addition gave rise to improvements in the mechanical properties of the nanofibrous mats. All of the nanofibrous samples swelled and had deformation after 14 days of incubation in an aqueous environment.

2.6.2 Composite Nanofibers with Three Components

Özdemir and Hacaloğlu [74] studied the influence of an organically modified montmorillonite (Closite 30B) on the PLA/PEG nanofibers. A twin-screw extruder is used for the melt mixing of the polymers. Nevertheless, throughout the

electrospinning, phase separation was observed. This problem was prevented by introducing the nanoclay additive to the system. As a result of nanoclay addition, the diffusion of PLA and PEG into the silicate layers of nanoclay occurred, and this improved the molecular interactions between the polymeric substances. Moreover, the electrical conductivity of the mixture for the melt electrospinning is enhanced by including quaternary ammonium salts with the nanoclay additive. Therefore, fibers with smaller diameter distribution were obtained.

Liu et al. [75] studied the effect of multiwall carbon nanotubes (MWCNTs) and polyethylene oxide (PEO) on fiber morphology, structure, crystallization behavior, thermal and mechanical properties. For this purpose, PLA, PLA/MWCNT, PLA/PEO, and PLA/PEO/MWCNTs nanofibers with two different concentrations of MWCNTs (0.2 wt.% and 1.3 wt.%) were generated via electrospinning technique. It was seen that the neat PLA nanofibers have shown defect-free morphology. By adding MWCNTs as the hard component, the nanofibers became rougher, and necking occurred in the fiber morphology. Since MWCNTs increased the conductivity of the polymer solution, at the MWCNTs concentration of 0.2 wt.% thinner nanofibers were obtained. On the contrary, for the polymer solution with 1.3 wt.% MWCNTs, the average fiber diameter increased due to the MWCNTs agglomeration, increasing the solution viscosity and decreasing the conductivity. The addition of PEO significantly increased the average fiber diameter of PLA/PEO nanofibers. Moreover, nanofibers obtained from PLA/PEO/MWCNTs system showed smoother morphology with a uniform thickness. Although the mechanical properties were affected strongly by the addition of MWCNTs, these particles did not have an important influence on the molecular orientation, crystallinity, and crystallization behavior of the nanofibers. Moreover, an improvement has been observed in the crystallization behavior, crystallinity and the elongation at break of the nanofibers with the PEO addition as the soft component. Thermal analysis results showed that PEO had a plasticizer effect on PLA and this resulted in a relaxation of PLA chains in addition to the reduction in the crystallization.

The study of Haroosh et al. [76] focused on the influence of polycaprolactone (PCL), unmodified and modified HNT with 3-aminopropyltriethoxysilane (ASP) on the fiber morphology, degree of crystallinity, and thermal properties of PLA. In order to achieve that objective, PLA/PCL and PLA/PCL/HNT nanofibers were generated with two different PCL (9 wt./v. % and 15 wt./v. %) and HNT (1 wt./v. % and 2 wt./v. %) concentrations. It was found that with the increasing concentration of PCL and HNT, the polymer solution viscosity increased. This increment resulted in a rise in average fiber diameter. On the other hand, PLA/PCL/unmodified-HNT had a larger average fiber diameter than PLA/PCL/modified-HNT. This situation was explained by the agglomeration of unmodified-HNTs caused by the weak van der Waals forces between the HNT particles led to a greater increase in viscosity. HNT modification enabled the polymer solution to have a better dispersion in PLA/PCL polymer matrix. A moderate reduction in the degree of crystallinity, crystallization temperature of PLA, melting temperature of PLA, and glass transition temperature of PCL were obtained with the better dispersion of modified HNT. As the PCL concentration increased, the crystallinity level and glass transition temperature of PCL increased.

Yang et al. [77] investigated the effect of two different nanofiller materials on the fiber morphology, thermal stability, and crystal structure of the nanofibrous material. To this end, pristine PLA, PLA/graphene (G), PLA/MWCNTs and PLA/G/MWCNTs nanofibers with various composition ratios were produced by the electrospinning method. For this technique, the polymer solution was prepared by a type of solution-blending method, in which the nanofillers were dispersed in a solvent, and PLA was dissolved in another solvent. These two solutions were added into each other and in order to obtain the final polymer solution, the blended solution was magnetically stirred. PLA/G/MWCNTs composite nanofibers showed a uniform morphology. Moreover, it was observed that graphene and MWCNTs dispersed randomly into the PLA nanofibers. On the other hand, the addition of graphene and MWCNTs did not have a significant influence on the crystal structure of PLA. In addition, the thermal stability of nanofibers reinforced by graphene and MWCNTs

was improved. According to this study, it can be concluded that the addition of graphene and MWCNTs as nanofillers had an essential role on the thermal properties of the composite nanofibers.

2.7 The Scope of the Thesis

Electrospinning is a versatile, efficient, and cost-effective method to fabricate nanofibrous mats compared to other nanofiber production techniques including phase separation, template synthesis, drawing, and self-assembly. By applying this method, nanofibers can be generated with distinguished properties such as high surface area/volume ratio, high porosity, and enhanced mechanical and thermal properties.

PLA is one of the biodegradable thermoplastics used in the electrospinning process, which has a high fiber-forming ability. PLA has a low production cost; therefore, it is economically competitive with commercial polymers that are petroleum-based. On the other hand, PEG is known for being biocompatible, electrically and thermally stable, and having a lack of toxicity. HNTs are very attractive, low cost, inorganic and natural nanomaterials with a nanotube structure. Due to their structures, they are frequently used to prepare thermally stable composite nanofibrous materials with high performance.

As a result of the literature survey, it has been seen that there is a research gap in the use of PLA, PEG and HNTs together as the components of the composite nanofibers generated using the electrospinning technique. It has been thought that PLA/PEG/HNTs composite nanofibers are an appealing field for research purposes since PEG has the potential of performing as a compatibilizer between PLA and HNTs. Moreover, HNTs have the potential to improve the thermal and mechanical properties of the polymer matrix. Moreover, it has been detected that there is a lack of studies investigating the effect of polymer solution preparation methods, electrospinning process duration and drying duration of the samples on the nanofiber

morphology, mechanical and thermal properties of neat PLA and PLA/PEG/HNTs electrospun fibers.

In this thesis, an elaborate optimization study including the generation of neat PLA fibers with the optimum conditions was performed. Moreover, the effect of process parameters on the nanofiber morphology was investigated. After the parameter optimization step, in order to observe the influence of PEG on the nanofiber structure, PLA/PEG nanofibrous mats were generated at different PEG concentrations. Then, HNTs-added PLA composite nanofibers were generated in the scope of investigating the impact of HNTs concentration and PLA/HNT suspension preparation methods on the nanofiber morphology. Finally, PLA/PEG/HNT nanofibers were produced by applying different polymer solution preparation methods. All the prepared mats were characterized in terms of their morphology, mechanical and thermal properties. Furthermore, water contact angle measurements were performed on the samples.

CHAPTER 3

EXPERIMENTAL

3.1 Materials

3.1.1 Polylactic Acid

A transparent injection grade of polylactic acid (PLA) with 5 % D-lactide stereoisomer content was obtained from NaturePlast, France. The weight average molecular weight ($\overline{M}_w$) and the polydispersity ($\overline{M}_w/\overline{M}_n$) of PLA are 278000 and 1.78, respectively [78]. The specifications of PLA provided by the manufacturer are given below in Table 3.1. The chemical formula of PLA is also shown in Figure 3.1.

Table 3.1 Properties of PLA (NaturePlast PLI-005) [79, 117].

Physical Properties	**Method**	**Unit**	**Value**
Density	ISO 1183	g/cm^3	1.25 (±0.05)
Melt Index	ISO 1183	g/10 min	10-30
Melt Temperature	-	°C	144-155
Degradation Temperature	-	°C	240-250
Solubility Parameter, δ	-	$(MPa)^{1/2}$	23.1

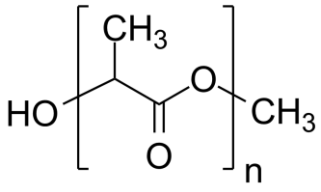

Figure 3.1 Chemical Structure of PLA.

3.1.2 Polyethylene Glycol

Molecular biology grade polyethylene glycol (PEG) (M_n: 6000 g/mol) was procured from Merck. The physical properties of the material are given in Table 3.2. The chemical formula of PEG is also shown in Figure 3.2.

Table 3.2 The Properties of PEG 6000 [80, 118].

Physical Properties	Unit	Value
Density	g/cm^3	1.2
Melting Temperature	°C	60-65
Color	-	White
Solubility Parameter, δ	$(MPa)^{1/2}$	20.2

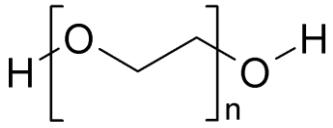

Figure 3.2 Chemical structure of PEG.

3.1.3 Halloysite Nanotubes

Halloysite nanotubes (HNTs) with chemical formula of $Al_2Si_2O_5(OH)_4.2H_2O$ were procured from Sigma-Aldrich. The physical properties of HNTs are listed in Table 3.3.

Table 3.3 Properties of HNTs [81].

Physical Property	Unit	Value
Average Diameter	nm	30-70
Length	μm	1-3
Surface Area	m^2/g	64
Color	-	White

3.1.4 Solvents

Chloroform (CHL) and dimethylformamide (DMF), both with 99% purity, were procured from Isolab Chemicals and used as solvents in the electrospinning process.

3.2 Experimental Procedure

3.2.1 Preparation of Polymer Solutions

In this study, different polymer solution preparation methods were applied in order to investigate the effect of solution preparation methods on fiber morphology, thermal and mechanical properties. While preparing neat PLA and PLA/PEG solutions, same method was applied, and for this method only magnetic stirrer was used. On the other hand, during the preparation of PLA/HNT and PLA/PEG/HNT systems, various methods were applied. While preparing PLA/HNT suspensions, the difference between using magnetic stirrer and sonication bath for the HNTs dispersion was examined. Moreover, the insertion order of the solution components to the system was studied in addition to the influence of using sonication bath and magnetic stirrer on the HNTs dispersion while preparing PLA/PEG/HNT solution.

3.2.1.1 Preparation of Neat PLA and PLA/PEG Solutions

In the preparation of neat PLA solution, CHL and DMF with 80:20 by volume ratio (v/v) was selected as the solvent system. In all experiments, 20 ml of solvent system was used to dissolve the PLA granules. The amount of PLA, which was necessary for the preparation of polymer solution with the predetermined polymer concentrations (7, 11, and 13 wt. %), was weighed with high precision balance (Precisa-XB 220A-SCS) and dissolved in the solvent system. The prepared solution was mixed with a magnetic stirrer (Velp Scientifica, Arex heating magnetic) for 5

hours at room temperature until observing a homogeneous solution. The schematic representation of the procedure can be seen in Figure 3.3.

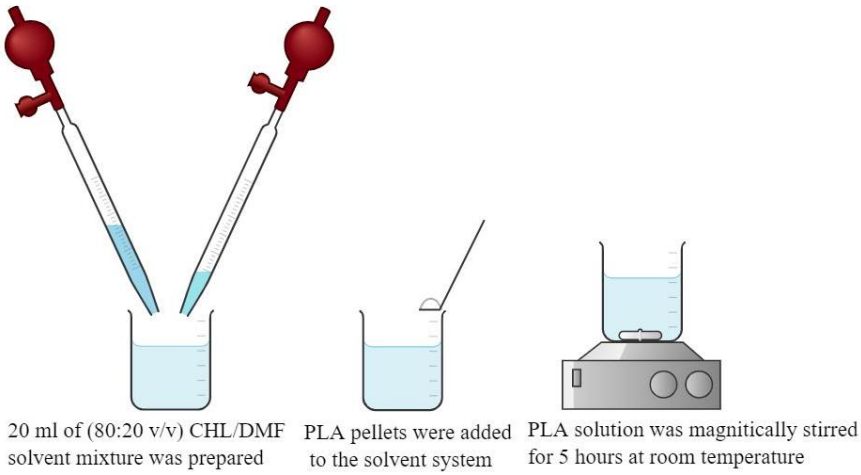

Figure 3.3 Experimental procedure for preparation of neat PLA solution.

In the preparation of PLA/PEG solution (PLA/xPEG), same procedure in neat PLA solution was applied. The amount of PLA and PEG (x: 4, 7, 10, 15 and 25 wt.% of PLA), were weighed and dissolved in the CHL/DMF solvent system. After reaching the predetermined total solution concentrations (13 wt. %), the prepared solution was mixed with a magnetic stirrer for 5 hours at room temperature until observing a homogeneous solution. The schematic representation of the procedure is given in Figure 3.4.

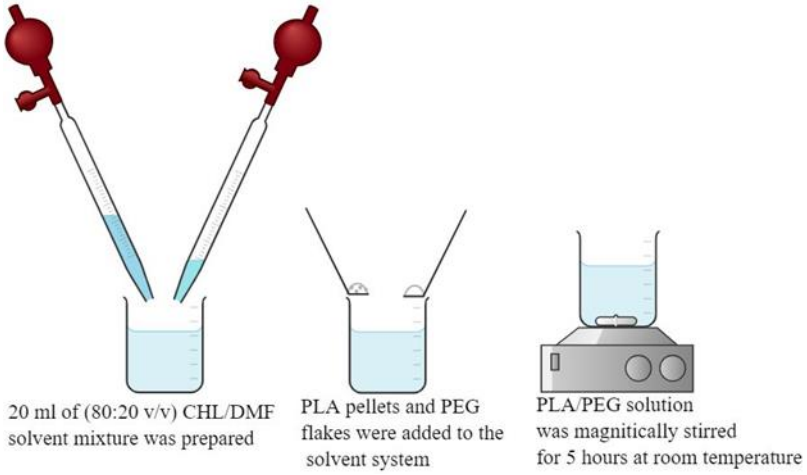

Figure 3.4 Experimental procedure for preparation of PLA/PEG solution.

3.2.1.2 Preparation Methods of PLA/HNT Suspensions

In order to obtain better dispersion of HNT in the polymer solution, different preparation methods of PLA/HNT suspensions were investigated. For the first method (PLA/xHNT-M1), same procedure as neat PLA and PLA/PEG solutions was applied except the stirring duration. The amount of PLA and HNT (x: 0.25, 0.5, 1, 3 and 5 wt.% of PLA), were weighed with high precision balance (Precisa-XB220A) and dissolved in the CHL/DMF solvent system. After reaching the predetermined total solution concentrations of 13 wt. %, the prepared solution was mixed with a magnetic stirrer (Velp Scientifica, Arex heating magnetic) for overnight at room temperature until observing a homogeneous solution. The schematic representation of the procedure is given in Figure 3.5.

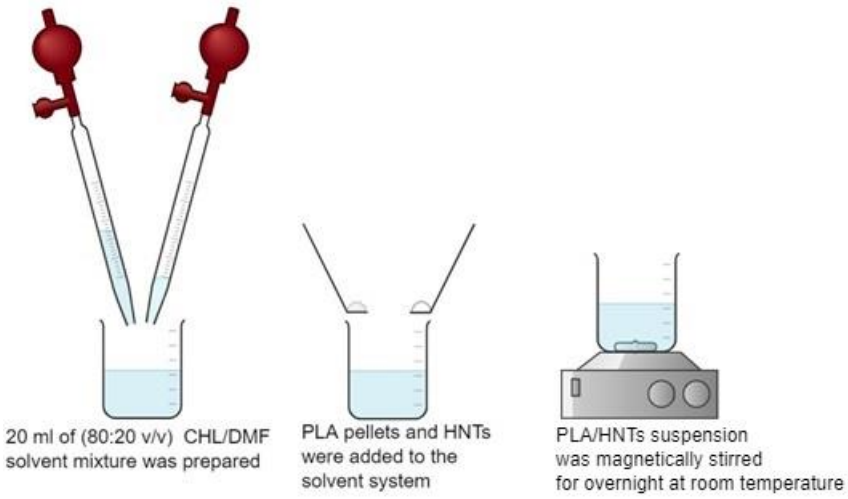

Figure 3.5 Method-1 for preparation of PLA/HNT suspension.

As the second method of PLA/HNT suspension preparation (PLA/xHNT-M2), first HNTs with the predetermined amount (x: 0.5 and 3 wt.% of PLA) was added to the CHL and DMF solvent system. This suspension was sonicated at room temperature for 30 minutes with a Bandelin Sonorex RK 100 sonicator. Then, the PLA pellets were added to reach the predetermined total solution concentration of 13 wt.% and mixed with the magnetic stirrer for 4 hours at room temperature. The schematic representation of the procedure is given in Figure 3.6.

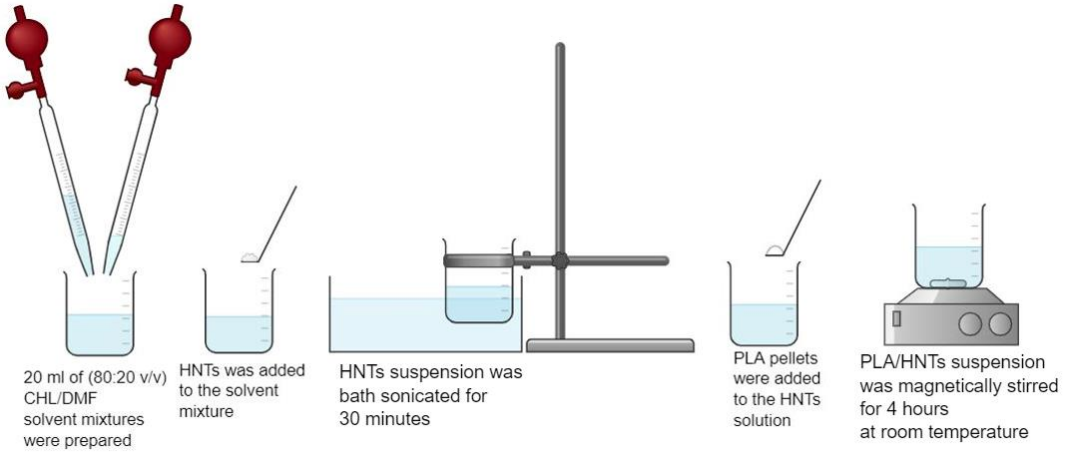

Figure 3.6 Method-2 for the PLA/HNT suspension preparation.

3.2.1.3 Preparation Methods of PLA/PEG/HNT Solutions

In this study, the influence of preparation methods of polymer solutions with three components were investigated. While preparing the polymer solutions, it was aimed to observe the difference caused by the addition order of the components to the solvent system and using a sonication bath or magnetic stirrer. For this purpose, various preparation methods for PLA/PEG/HNT solutions were designed and presented in this section.

In the first preparation method of PLA/PEG/HNT solution (PLA/PEG/HNT-M1), PLA pellets, 0.5 wt. % HNT and 15 wt. % PEG flakes were added to the CHL/DMF solvent system with a total solution concentration of 13 wt.% and magnetically stirred overnight at room temperature. The schematic representation of the procedure is given in Figure 3.7.

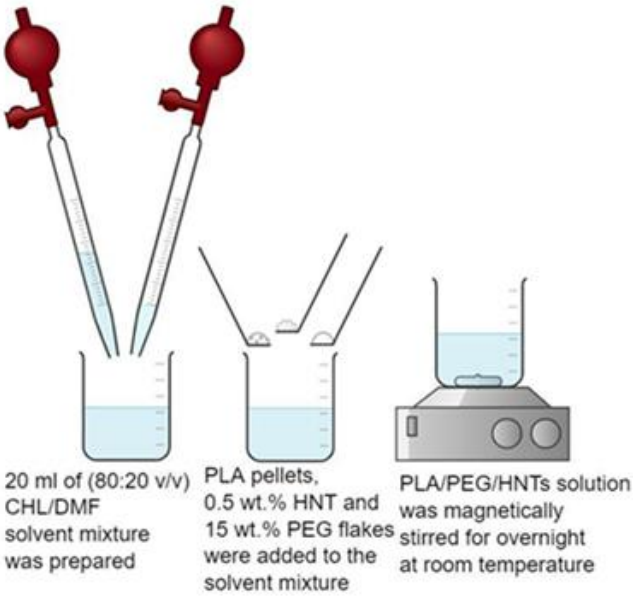

Figure 3.7 Method-1 for PLA/PEG/HNT solution preparation.

As the second method of PLA/PEG/HNT solution preparation (PLA/PEG/xHNT-M2), first HNTs with the predetermined amount (x: 0.5 and 3 wt.% of PLA) was added to the CHL/DMF solvent system. This suspension was sonicated at room temperature for 30 minutes. Then, the PLA pellets and 15 wt. % PEG flakes were added to reach the predetermined total solution concentration of 13 wt.% and mixed with the magnetic stirrer for 4 hours at room temperature.

The schematic representation of the procedure is given in Figure 3.8.

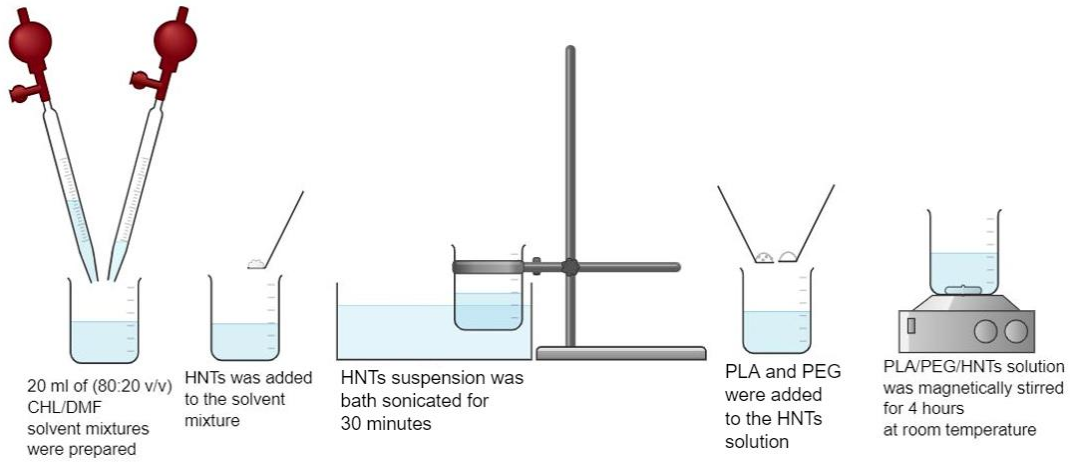

Figure 3.8 Method-2 for PLA/PEG/HNT solution preparation.

For the third method (PLA/PEG/HNT-M3) 0.5 wt.% HNT was added to the solvent mixture and sonicated at room temperature for 30 minutes. Then, PLA pellets were added to the HNTs solution. Finally, 15 wt.% PEG flakes were added gradually, and the solution was magnetically stirred for 4 hours at room temperature. The schematic representation of procedure is given in Figure 3.9.

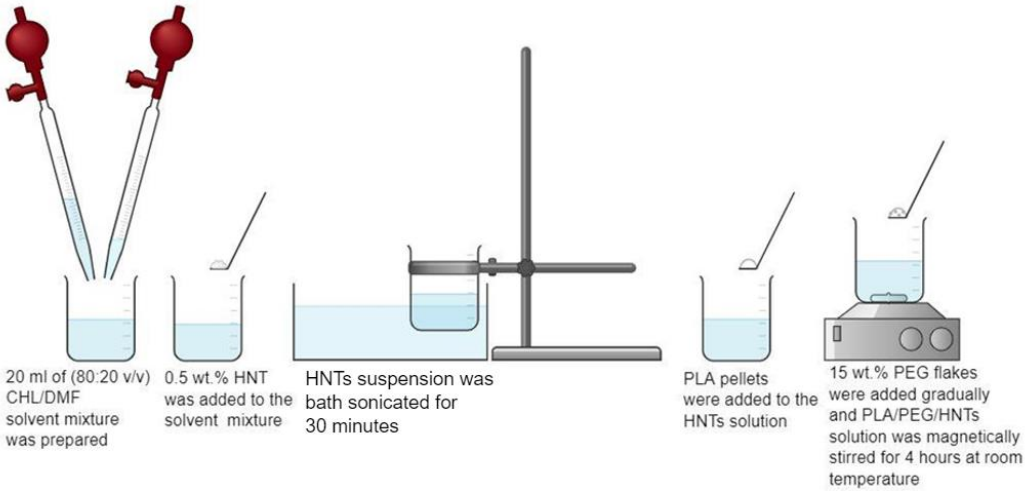

Figure 3.9 Method-3 for PLA/PEG/HNT solution preparation.

In the fourth method (PLA/PEG/HNT-M4), the same procedure was applied with the third method except at first 15 wt.% PEG flakes were added to the HNTs solution after the sonication and then PLA pellets were added gradually and magnetically stirring was carried out for 4 hours at room temperature. The schematic representation of the procedure is given in Figure 3.10.

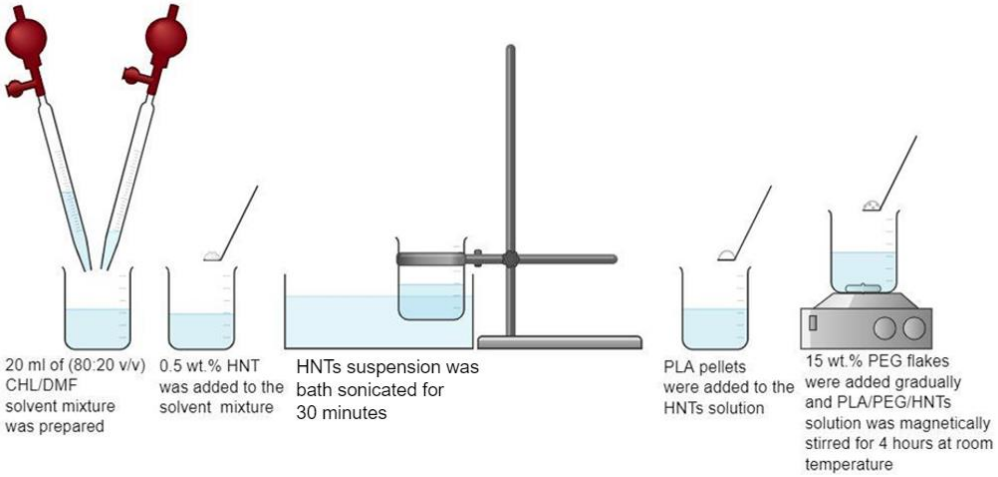

Figure 3.10 Method-4 for PLA/PEG/HNT solution preparation.

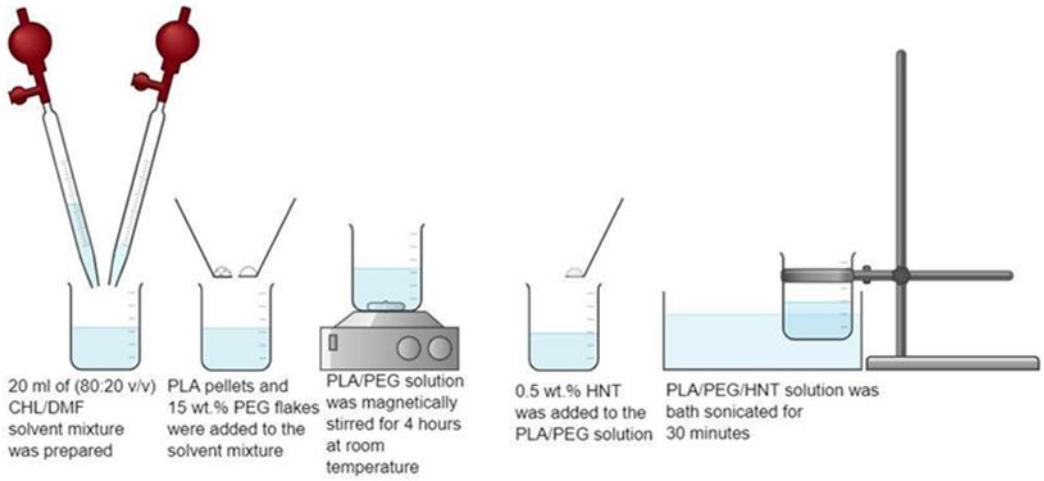

Figure 3.11 Method-5 for PLA/PEG/HNT solution preparation.

The schematic representation of fifth and the last preparation method (PLA/PEG/HNT-M5) is given in Figure 3.11. In this method, first PLA pellets and 15 wt.% PEG flakes were added to the CHL/DMF solvent mixture and magnetically stirred for 4 hours at room temperature. Then, 0.5 wt% HNT was added to the PLA/PEG solution and sonicated at room temperature for 30 minutes.

3.2.2 Electrospinning Process

Uniaxial electrospinning processing were conducted using a bottom-up type Inovenso NE300 electrospinning equipment. The photograph of the used device during the process can be seen in Figure 3.12.

Figure 3.12 Inovenso NE300 Electrospinning Machine.

Technical specifications of the device are given in Table 3.4. Uniaxial electrospinning parameters values that were applied for producing nanofibers can be seen in Table 3.5. All the electrospinning processes were performed in the laboratory conditions at room temperature (23 ± 3ºC) and 35 ± 10% relative humidity. The relative humidity and temperature data were determined by a digital hygro-thermometer in the electrospinning chamber.

Table 3.4 Technical specifications of Inovenso NE300 electrospinning device [82].

Property	Value
Voltage Range (kV)	0-40
Feed Rate Range (mL/h)	0.01-1000
Needle Diameter (mm)	0.8
Distance Range (cm)	5-25
Collector Types	Rotation cylinder or constant plate
Material of Collector	Aluminum
Rotating Cylinder Speed (rpm)	100-500

In this study, the process parameters for optimization included feed rate, tip-to-collector distance, applied voltage, solution concentration. The rotational speed of the cylindrical collector was kept constant at 100 rpm. During the optimization of these parameters, technical specifications of the device and ranges for each parameter were also considered.

Table 3.5 Parameters of the uniaxial electrospinning process.

Optimized Parameter	**Variables**	**Fixed Parameters**
Solution Concentration (wt.%)	7, 11, 13	20 kV, 20 cm, 1 mL/h, CHL/DMF:80/20 v/v
CHL/DMF Solvent Ratio (v/v)	75/25, 80/20, 90/10	13 wt.%, 20 kV, 20 cm, 1 mL/h
Applied Voltage (kV)	17, 20, 23	13 wt. %, 20 cm, 1 mL/h CHL/DMF: 80/20 v/v
Feed Rate (mL/h)	0.8, 1, 1.2	13 wt. %, 20 kV, 20 cm CHL/DMF: 80/20 v/v
Tip-to-collector Distance (cm)	16, 20, 24	13 wt. %, 20 kV,1 mL/h, CHL/DMF: 80/20 v/v
PEG Concentration (wt. %)	4, 7, 10, 15, 25	13 wt. %, 20 kV, 1mL/h, 20 cm, CHL/DMF: 80/20 v/v
HNT Concentration (wt. % based on PLA)	0.25, 0.5, 1, 3, 5	13 wt. %, 20 kV, 1mL/h, 20 cm, CHL/DMF: 80/20 v/v

Furthermore, as the preliminary studies, it was also focused on the influence of electrospinning process duration and drying duration of the samples (xPLA/th/y where x: 11, 13, t: 1, 2, 3 and y: 2d, on) on the morphology, thermal and mechanical properties. In order to investigate the effect of electrospinning duration, the electrospinning process was conducted for 1, 2, and 3 hours at 11 wt.% and 13 wt.% of neat PLA concentrations. The effect of sample drying duration was investigated for the samples obtained from 3 hours of the electrospinning process. These samples

were dried for overnight and 2 days in order to observe the plasticizer effect of the possible residual solvents on the nanofibrous mats. In the following table, the parameters for the investigation of electrospinning and sample drying time can be found. The tabulated values of the inspected parameters can be seen in Table 3.6.

Table 3.6 Parameters for Electrospinning and Sample Drying Durations.

Inspected Parameters	Variables	Fixed Parameters	SC (wt.%)
Electrospinning Duration (h)	1, 2, 3	20 kV, 20 cm, 1 mL/h, CHL/DMF: 80/20 v/v	11, 13
Sample Drying Duration	Overnight, 2 days	ED: 3h, 20 kV, 20 cm, 1 mL/h, CHL/DMF: 80/20 v/v	11, 13

3.3 Characterization Methods

3.3.1 Scanning Electron Microscopy Analysis

The produced nanofiber morphologies were analyzed via a QUANTA 400 F Field Emission High-resolution Scanning Electron Microscope. The nanofibers were collected onto aluminum foil via the electrospinning process. These collected nanofibers were cut into pieces with 1x1 cm^2 dimensions and then adhered to the stubs with the help of the carbon bands. After that, the samples were coated with gold-palladium alloy to provide conductivity on the polymeric nanofiber surface. The analysis on fiber diameter was performed using ImageJ (Fiji) (NIH, USA) software. The average fiber diameter for each sample was determined by measuring the diameters of 100 nanofibers, and then plots depicting average fiber diameter were drawn for each sample.

3.3.2 Thermogravimetric Analysis

Thermogravimetric analyses (TGA) were conducted using a Shimadzu DTG-60 instrument. Neat and composite nanofibrous samples were heated from 25ºC to

800ºC with a heating rate of 10 ºC/min under N_2 flow with 500 ml/min. The decomposition temperature, 10% weight loss temperature (T_{10}), 25% weight loss temperature (T_{25}), and the half weight loss temperature (T_{50}) of nanofibrous samples were determined and thermal stability of the mats were observed by TGA.

3.3.3 Differential Scanning Calorimetry Analysis

A Shimadzu DSC-60A instrument was utilized to perform the differential scanning calorimetry (DSC) analysis. Neat and composite nanofibrous samples were heated from 25ºC to 190ºC with a heating rate of 10 ºC/min under an N_2 atmosphere. Samples with approximately 10 mg of weight was put into the aluminum pans, and a heating program was implemented on each sample. Results were analyzed after the first run. The degree of crystallinity calculations were done by applying Equation (2).

$$X_c = \frac{\Delta H_m - \Delta H_{cc}}{\Delta H_f^\circ} x100 \quad (2)$$

where X_c (%) is the degree of crystallinity (%), ΔH_m (J/g) is the heat of melting, ΔH_{cc} is the heat of cold crystallization (J/g), and ΔH_f° is the heat of fusion for 100% crystalline. The heat of fusion value for fully crystalline PLA was taken as 93.7 J/g [83]. Exo-up DSC graphs were obtained after the analysis of each sample.

3.3.4 Tensile Test

The tensile test was conducted using a Shimadzu Autograph AG-IS 100kN Universal Testing Machine in order to determine the mechanical properties of the nanofibrous samples. The tensile test machine used can be seen in Figure 3.13.

Figure 3.13 Shimadzu Autograph AG-IS 100kN universal testing machine.

Tensile tests conducted on nanofiber films were based on ASTM D882-02 standard. The nanofibrous samples used for the tensile testing had length, gauge length, and width of 50 mm, 30 mm and 10 mm, respectively. The thicknesses of the samples were measured via Micromar Micrometer 40 EWR with a 0.0001 mm precision, and the thickness range of the samples was 60-140 μm.

The cross-sectional area values of the mats were calculated from the average thickness and width values. According to the dimension of the nanofibrous samples, a load cell with a maximum load capacity of 1 kN and a crosshead speed of 15 mm/min was selected for the tensile tests. For each sample used for tensile testing, five measurements were done to obtain both the average and standard deviation values. In order to prepare the sample frames, the sample sizes were drawn on A4 papers. First, the sample-sized papers were cut and then, a double-sided tape was used to stick those papers to the electrospun samples with aluminum foils on the other side. The samples were cut by taking the paper frame as the basis. After this,

samples with a paper frame on one side and aluminum on the other side were obtained. The aluminum foil was carefully peeled off from the samples without harming them. Finally, papers were cut with a scissor to obtain frames on both ends of the samples with 10x10 mm^2 dimensions. In this characterization method, nonwoven fibrous mats were used. Therefore, the obtained tensile strength, elongation at break, and tensile modulus data reflect the properties of the mat with a nanofibrous morphology but not the properties of an individual nanofiber.

3.3.5 Water Contact Angle Measurements

Water contact angle measurements (WCA) of the selected samples were performed at room temperature by applying the sessile drop method according to ASTM D7490-08 standard. The analyses were carried out using Image J (Fiji) (NIH, USA) software with the Drop Analysis-LB-ADSA plug-in. While conducting the analysis, 10 μL of distilled water droplets were dropped on the nanofibrous mats by using micropipette, and the droplet images were taken after ten seconds. In order to calculate average water contact angle and standard deviation values, number of five droplets were dropped on different parts on the surface of the nanofibrous samples, and their average WCA results were taken into account.

CHAPTER 4

RESULTS AND DISCUSSION

4.1 Parameter Optimization on Electrospinning of Neat PLA

As it was mentioned in the previous sections, one of the main purposes of this study was to generate bead-free, smooth, uniform, and fine fibrous structures. In order to achieve this purpose, solution parameters (solution concentration and solvent ratio) and process parameters (applied voltage, solution feed rate, and tip-to-collector distance) were optimized. Before performing the parametric studies, many attempts have been made to get familiar with the electrospinning process of neat PLA and to determine the value range of the parameters to be optimized for producing desired fibrous morphologies.

4.1.1 Scanning Electron Microscopy Analysis

The effect of solution concentration on the fiber morphology was investigated by trying different concentrations of 7, 11, and 13 wt.% of PLA while keeping the applied voltage, solution feed rate, and tip-top-collector distance parameters at constant values of 20 kV, 1 ml/h and 20 cm, respectively. The electrospinning experiments were conducted for 3 hours using a rotating cylinder collector with a rotational speed of 100 rpm.

The SEM micrographs of the resulting nanofibers are shown in Figure 4.1. It can be clearly deduced that solution concentration of 7 wt.% PLA was inadequate to generate nanofibers. Since the molecular entanglements are too low, due to the surface tension and stretching, there is no continuous fiber formation. As a result, a mixture of fibers and beads was obtained at 7 wt.% of solution concentration.

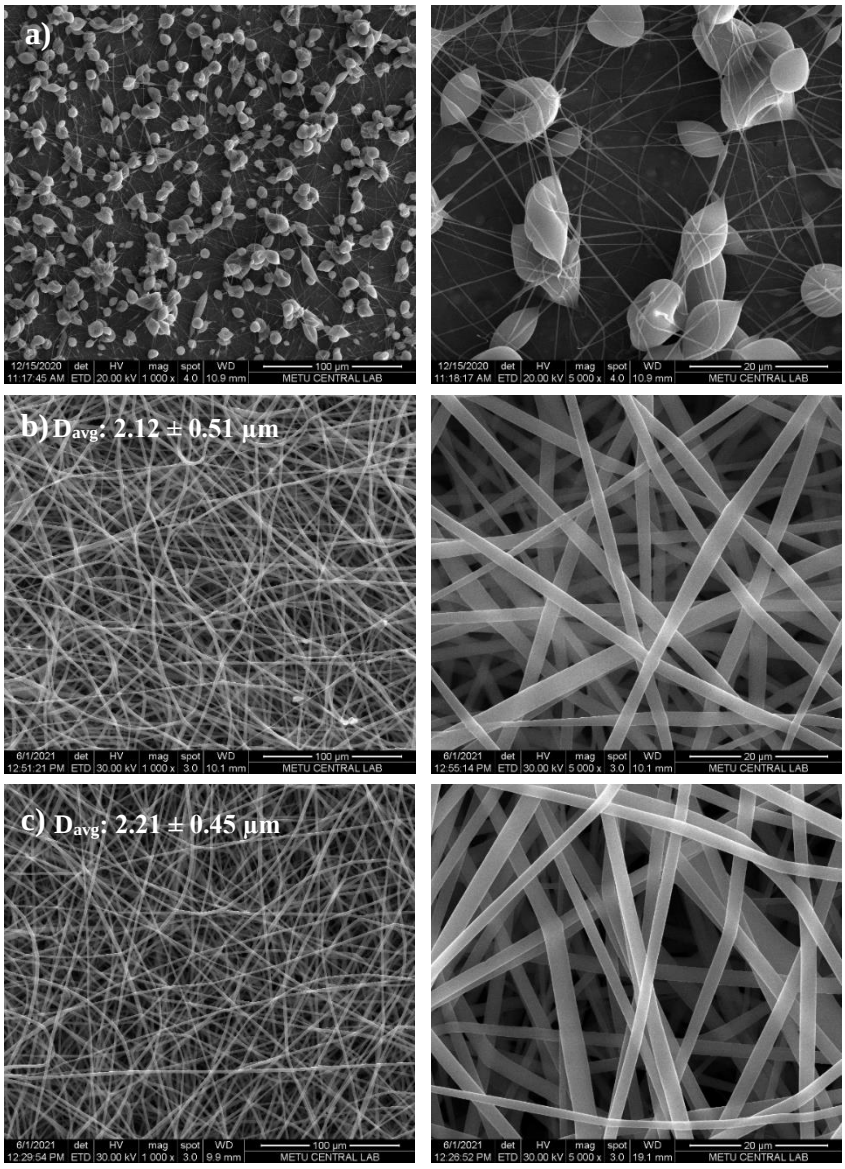

Figure 4.1 SEM micrographs of electrospun neat PLA with concentrations of a) 7, b) 11, c) 13 wt. % (AV: 20 kV, TCD: 20 cm, SFR: 1 ml/h CT: cylinder RS: 100 rpm ED: 3 h, SR: 80/20 v/v).

As the solution concentration was increased to 11 wt.% PLA, the beaded structure changed to fibers. The formation of fibers can be explained by the increase in the solution viscosity and thus in the chain entanglements with the increasing solution concentration. The chain entanglements were able to overcome the surface tension and hence fiber formation was observed at 11 wt.% concentration [3]. From the SEM analysis and the average fiber diameter measurements (presented in Figure 22), it can be concluded that as the PLA concentration was increased from 11 wt.% to 13

wt.%, the average fiber diameter did not show a significant change. However, fibers obtained from polymer solution with 13 wt.% concentration had a slightly smaller standard deviation value than the ones obtained from 11 wt.% concentration. Therefore, increasing the polymer concentration to 13 wt.% resulted in a relatively more uniform distribution of fiber thickness.

Optimization studies on solution feed rate were conducted by using a polymer solution with 13 wt.% concentration. During the electrospinning process, the applied voltage and tip-to-collector distance values were kept constant at 20 kV and 20 cm, respectively. The duration of the electrospinning process was 3 hours and the fibers were collected on a rotating cylinder collector.

In the electrospinning process, it is important to eject an adequate amount of solution to the nozzle tip in order to have sufficient time for solvent evaporation and to form Taylor Cone [84]. Therefore, in order to determine the maximum and minimum values for the solution feed rate optimization studies, electrospinning was done at feeding rates of 0.8, 1 and 1.2 ml/h. A stable Taylor Cone could not be observed at the solution feed rates below 0.8 ml/h due to the lack of adequate material transfer rate. Therefore, fibers could not be produced at feeding rates smaller than 0.8 ml/h. SEM micrographs and bar chart depicting the average fiber diameters of resulting nanofibers are given in Figures 4.2 and 4.6, respectively. SEM micrographs and average fiber measurements pointed out that as the solution feed rate was increased from 0.8 ml/h to 1 ml/h, the average fiber diameter did not show a crucial change. However, fibers obtained with a 0.8 ml/h feed rate had a greater standard deviation value than the ones obtained with a feed rate of 1 ml/h. Therefore, increasing the solution feed rate to 1 ml/h led to obtain a more uniform distribution in fiber thickness. On the other hand, as the solution feed rate was increased to 1.2 ml/h, excess solution accumulation at the nozzle tip occurred. This resulted in rapid tip blocking and hence the shape of the Taylor Cone could not be preserved. Higher standard deviations in the average fiber diameter measurement resulted from this highly unstable Taylor Cone [85]. Moreover, when the standard deviation values

were taken into account, increasing feed rate was not resulted in a significant change in the fiber thickness. Parameter optimization studies continued with the solution feed rate of 1ml/h due to the most uniform distribution of fiber thickness at this feed rate.

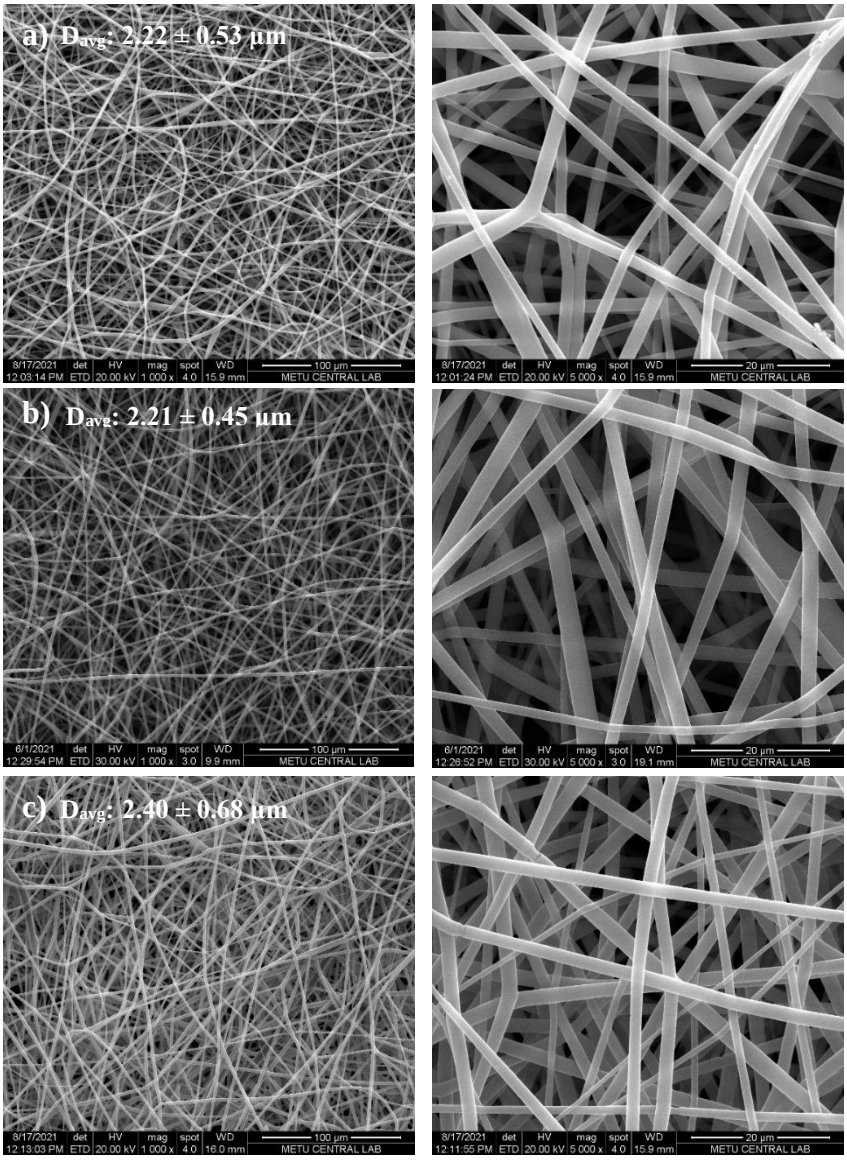

Figure 4.2 SEM micrographs of electrospun neat PLA with SFR of a) 0.8, b) 1, c) 1.2 ml/h (AV: 20 kV, TCD: 20 cm, SC: 13 wt. % CT: cylinder RS: 100 rpm ED: 3 h, SR: 80/20 v/v).

Tip-to-collector distance optimization studies were carried out by using polymer solution with 13 wt.% concentration of PLA. While implementing the electrospinning process, the solution feed rate and applied voltage values were adjusted to 1 ml/h and 20 kV, respectively. During the 3 hours of electrospinning process, the produced fibers were collected on the rotating cylinder.

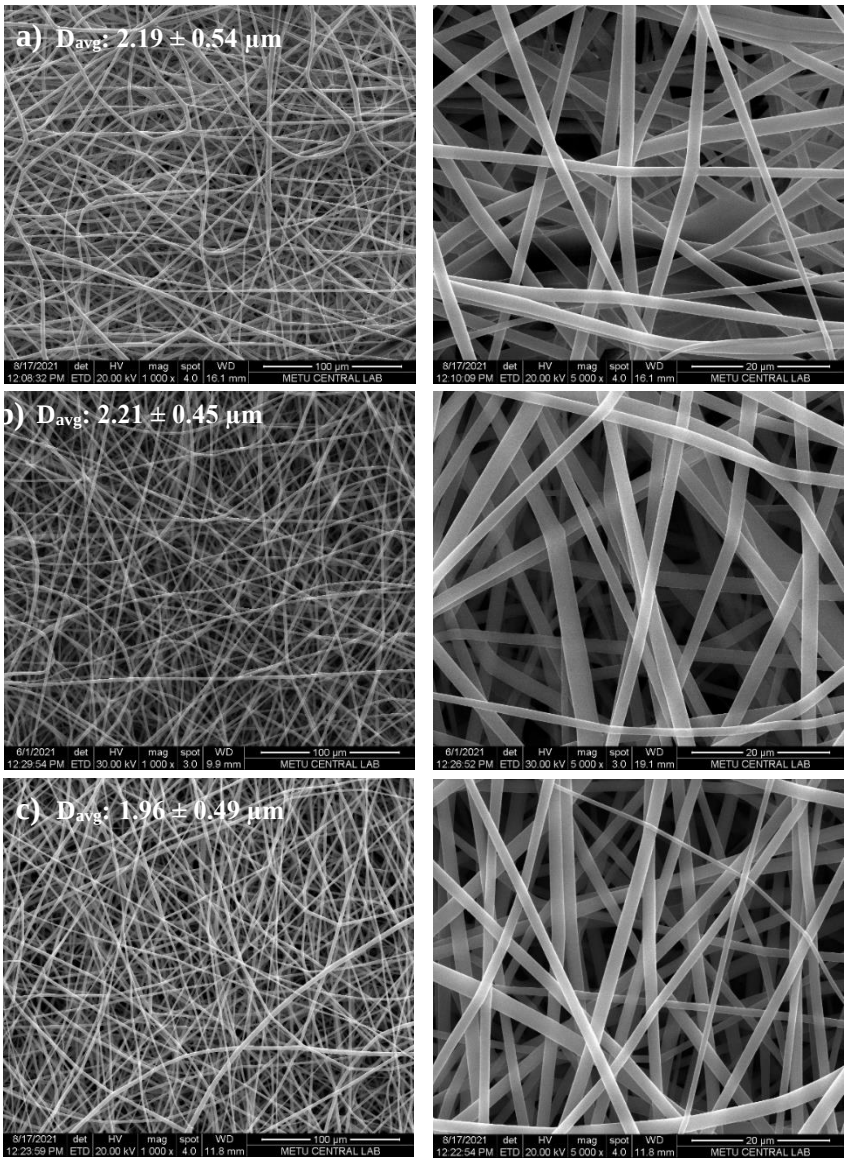

Figure 4.3 SEM micrographs of electrospun neat PLA with TCD of a) 16 b) 20, c) 24 cm (AV: 20 kV, SFR: 1 ml/h, SC: 13 wt. % CT: cylinder RS: 100 rpm ED: 3 h, sr: 80/20 v/v).

Tip-to-collector distance values were selected as 16, 20, and 24 cm for the optimization of this parameter. At distances shorter than 16 cm, the formation of a stable Taylor Cone could not be observed, which is caused by the inadequate tip-to-collector distance. The electric field is inversely proportional to the distance (i.e., E=V⁄d where; E: electric field, V: applied voltage, and d: distance). At the small values of tip-to-collector distance, unstable Taylor Cone results from the excessive stretching of the polymer jets [86, 87]. For this reason, fibers could not be generated at distances shorter than 16 cm. The SEM micrographs and bar chart depicting the average fiber diameter of the resulting nanofibers are given in Figures 4.3 and 4.6, respectively. According to the SEM micrographs and average fiber measurements, as the solution tip-to-collector distance was increased from 16 to 20 cm, the average fiber diameter did not show a significant change. Increasing the distance to 24 cm enabled fibers to have an increase in flight time. Therefore, longer time for solvent evaporation was provided [3]. This resulted in a decrease in the average fiber diameter value. A more uniform distribution of fiber diameter was obtained at the tip-to-collector distance of 20 cm.

After the determination of the optimum solution concentration, solution feed rate and tip-to-collector distance values, applied voltage optimization studies were carried out in order to generate more uniform fibers via uniaxial spinning. For this purpose, electrospinning was conducted at applied voltage values of 17, 20 and 23 kV. Polymer solution concentration, solution feed rate and tip-to-collector distance values were set at 13 wt.% PLA, 1 ml/h and 20 cm, respectively. Electrospinning was conducted for 3 hours, and collector type was chosen as rotational cylinder with 100 rpm of rotational speed. At voltage values smaller than 17 kV, the electrostatic forces applied on the PLA solution in the nozzle tip was insufficient to overcome to solution surface tension. Hence, polymer jet could not be formed at these electrical potential values.

The SEM micrographs and bar chart depicting the average fiber diameters of resulting nanofibers are given in Figures 4.4 and 4.6, respectively. As the applied

voltage was increased to 17 kV, polymer jet could be formed, and fiber generation was observed. SEM micrographs and average fiber measurements pointed out that as the applied voltage was increased from 17 kV to 20kV, the average fiber diameter did not show a significant change.

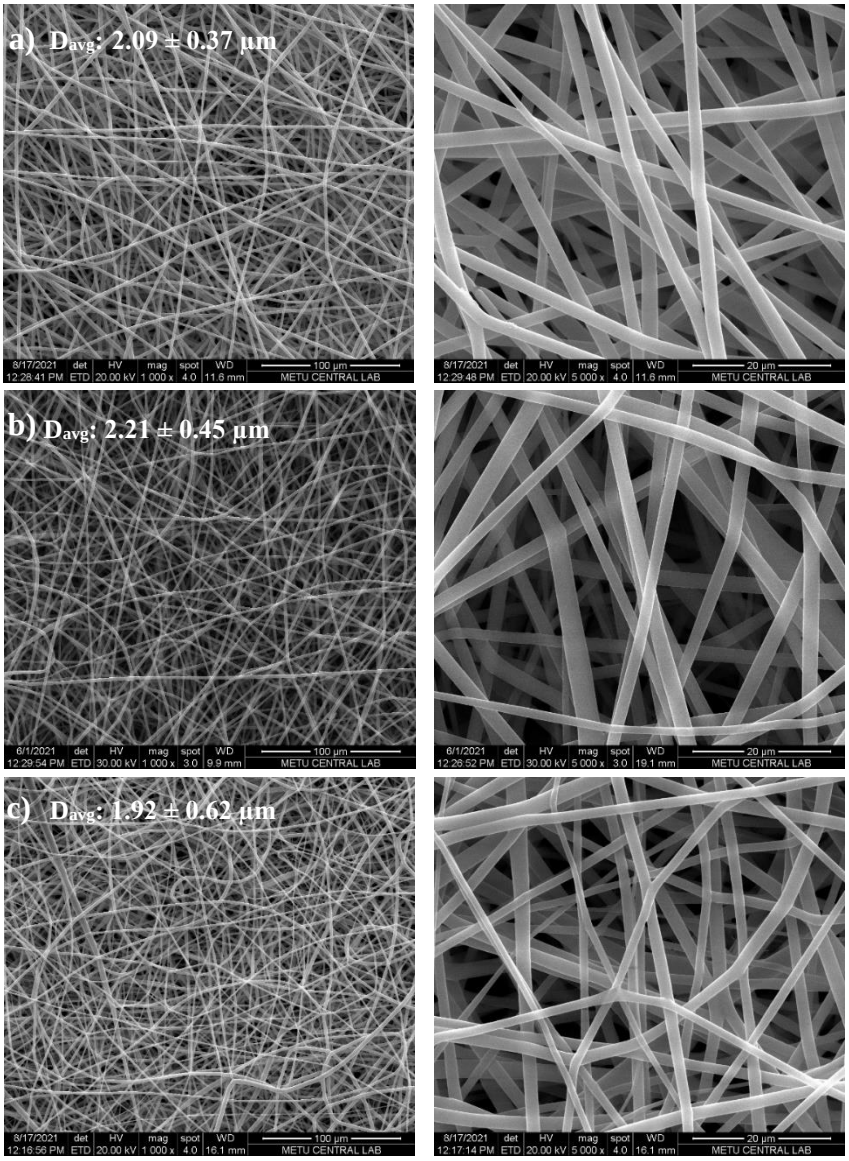

Figure 4.4 SEM micrographs of electrospun neat PLA with AV of a) 17 b) 20, c) 23 kV (TCD: 20 cm, SFR: 1 ml/h, SC: 13 wt. % CT: cylinder RS: 100 rpm ED: 3 h, SR: 80/20 v/v).

Fibers obtained with a 20 kV applied voltage had a greater standard deviation value than the ones obtained with an applied electrical potential of 17 kV. Therefore, increasing the electrical potential to 20 kV caused to obtain a less uniform distribution in fiber diameter. In addition, a decrease in the average fiber diameter was obtained as the applied voltage value was increased to 23 kV. Higher voltage values cause an increase in the polymer solution stretching and acceleration of polymer jet. This results in a diminution in the fiber diameter.

The electrostatic repulsive forces, thus the electrical potential increases on the polymer jet with the increasing applied voltage, which favors reducing the fiber diameter [3]. On the other hand, as it can be seen in Figure 4.4, thick fibers were generated besides the thin ones. Since excess electrostatic forces were exerted on the PLA solution at 23 kV during the electrospinning process, unstable Taylor Cone formation was obtained.

Solvent ratio optimization studies were performed by using polymer solution with 13 wt.% concentration. While implementing the electrospinning process, the solution feed rate, tip-to-collector distance, and applied voltage values were adjusted to 1 ml/h, 20 cm and 20 kV, respectively. Throughout the electrospinning process of 3 hours, the produced fibers were collected on the rotating cylinder collector rotating with a speed of 100 rpm.

The ratios of solvents were selected as 75/25, 80/20, and 90/10 v/v CHL/DMF for the optimization of this parameter. The solvent ratio of 70/30 v/v CHL/DMF was also tried. However, at 13 wt.% of polymer concentration, PLA could not be dissolved at this solvent ratio by applying the determined solution preparation method. Therefore, electrospinning cannot be conducted for the solution with the solvent ratio of 70/30 v/v. The SEM micrographs and bar chart depicting the average fiber diameters of resulting nanofibers are given in Figures 4.5 and 4.6, respectively. SEM images and measurements of average fiber values indicate that as the solvent ratio was changed from 75/25 to 80/20 and 90/10 v/v CHL/DMF, the average diameter of the fibers was increased. In other words, when the DMF concentration

was decreased, the properties of the polymer solution changed. This change affected the average diameter of the fibers. The properties of the solvents used in this study can be found in the following table.

Table 4.1 Properties of Solvents Used for the Electrospinning Process [43, 88].

Solvents	**Boiling Point (°C)**	**Electrical Conductivity (µS/cm)**	**Dielectric Constant**	**Vapor Pressure at 25 °C (kPa)**
Dimethylformamide	153	6.0E-02	36.70	0.501
Chloroform	61	1.0E-04	4.80	26.22

As it can be seen from the tabulated data, dimethylformamide has higher boiling point, electrical conductivity, and dielectric constant than chloroform. Solvents with greater boiling points has a low evaporation rate from the ejected polymer jet. Therefore, a change in the viscoelastic properties of the jet occurs. This change results in polymer jet stretching to lower fiber diameter values [43]. In addition, it was reported that fiber diameter decreases with the increase of the solution charge density or electrical conductivity. This is caused by the polymer jet carrying more charges. Hence, greater stretching occurs due to the higher conductivity, resulting in uniform fibers with fewer defects and smaller fiber diameters [89].

When the DMF concentration was decreased in the polymer solution, the boiling point, electrical conductivity, and the dielectric constant of the solution also decreased. Therefore, as expected, the average fiber diameter increased with decreasing DMF concentration. Since applying different ratios of solvents did not affect crucially the standard deviation values, the uniformity of the fiber thickness distribution was not significantly affected. According to the obtained results, the optimum process parameters were determined for the further studies as 13 wt.% of polymer solution concentration, 1ml/h of solution feed rate, 20 cm of tip-to-collector distance, 20 kV of applied voltage and 80/20 v/v CHL/DMF of solvent ratio.

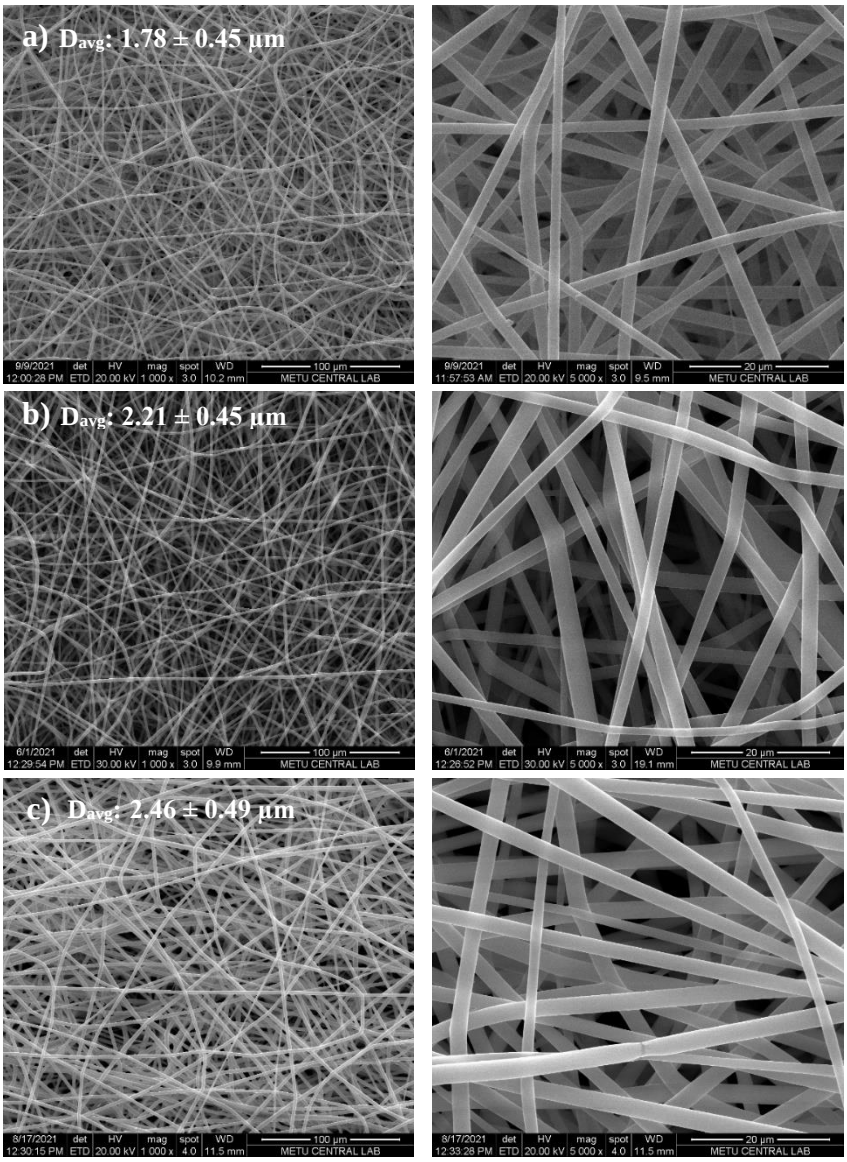

Figure 4.5 SEM micrographs of electrospun neat PLA with SR of a) 75/25 b) 80/20, c) 90/10 v/v CHL/DMF (TCD: 20 cm, AV: 20 kV, SFR: 1 ml/h, SC: 13 wt. % CT: cylinder RS: 100 rpm ED: 3 h).

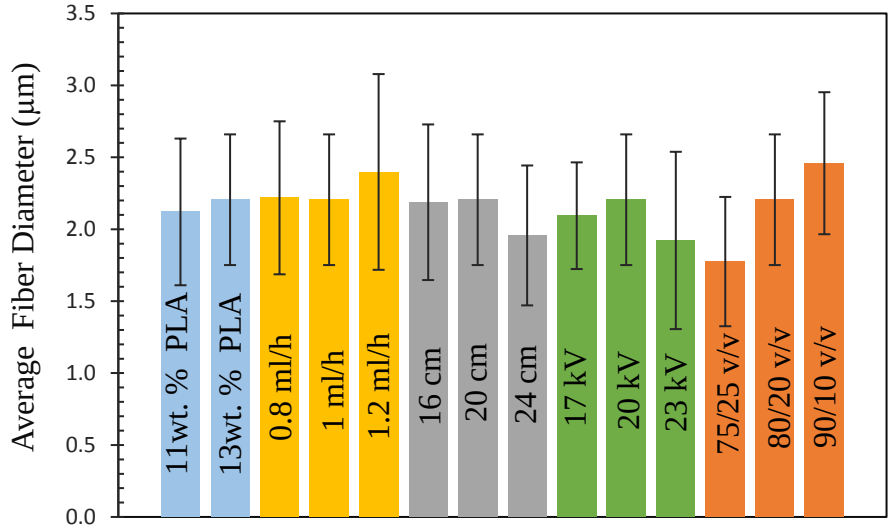

Figure 4.6 Bar chart depicting the average fiber diameters of nanofibers generated by parameter study.

4.1.2 Differential Scanning Calorimetry Analysis

DSC analysis was carried out for the nanofibers generated applying different values of solution parameters (solution concentration and solvent ratio) and process parameters (applied voltage, solution feed rate, and tip-to-collector distance). The obtained DSC curves are presented in Figure 4.7. Moreover, thermal properties (i.e., glass transition temperature (T_g), cold crystallization temperature (T_{cc}), enthalpy of cold crystallization (ΔH_{cc}), melting temperature (T_m), enthalpy of melting (ΔH_m) and degree of crystallization (X_c)) values are given in Table 4.2.

As it can be seen in Figure 4.7, peaks around T_g were observed due to the physical aging. According to the tabulated data in Table 4.2, it can be concluded that as-received PLA pellets (bulk PLA) have a higher degree of crystallization value than the value obtained for the electrospun PLA fibers at the different process and solution parameters. Concerning the influence of the electrospinning process on the crystallinity of the polymers, electrospun fibers have generally been reported to have

lower crystallinity than the degree of crystallinity of the as-received polymers, films cast from polymer solutions, and polymer melts. This can be explained by the rapid solidification of the stretched polymer jets during the electrospinning, which results in insufficient time for the occurrence of the crystallization [49]. Moreover, all of the samples except the bulk PLA showed exothermic peaks, which were associated with the cold crystallization. During heating the polymer above T_g, the polymer chains gain adequate energy to have mobility and arrange themselves into a more ordered structure. This exothermic transition is called cold crystallization. The occurrence and extent of the cold crystallization transition depend on the sample processing history [90].

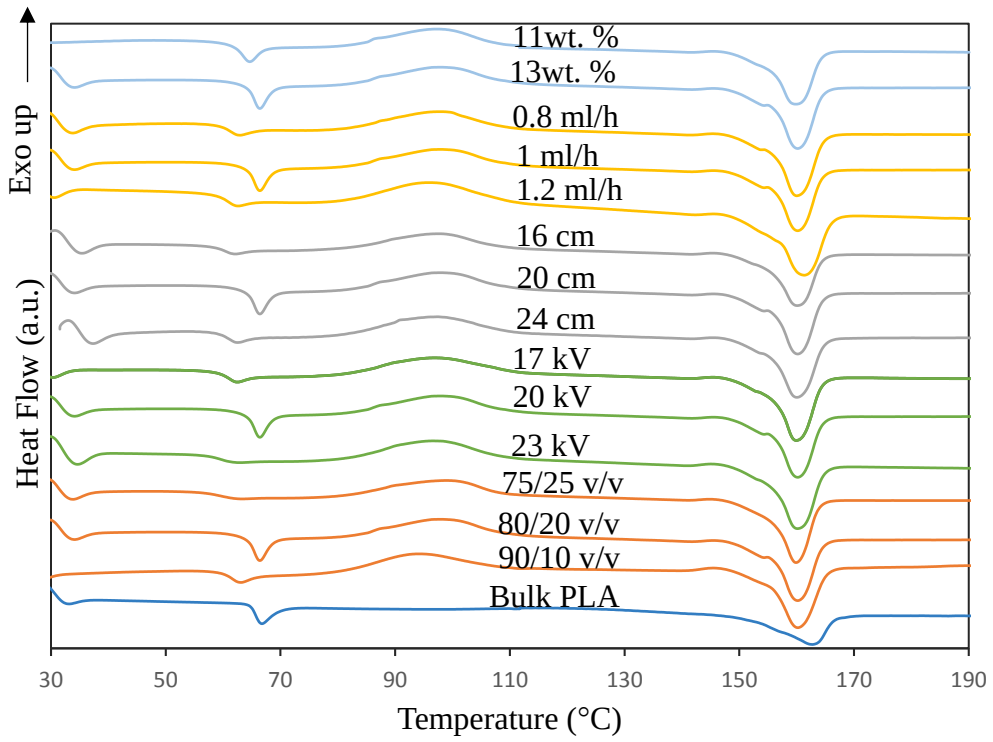

Figure 4.7 DSC curves for Parameter Studies on Electrospinning of Neat PLA.

Table 4.2: DSC data for Parameter Studies on Electrospinning of Neat PLA.

Sample	T_g (°C)	T_{cc} (°C)	ΔH_{cc} (J/g)	T_m (°C)	ΔH_m (J/g)	X_c (%)
Bulk PLA	64.43	-	-	161.90	30.40	32.69
11 wt.%	61.94	97.26	18.17	159.72	33.49	16.47
13 wt.%	64.33	98.37	17.26	160.15	31.38	15.07
0.8 ml/h	60.56	96.86	22.34	161.24	43.81	22.91
1 ml/h	64.33	98.37	17.26	160.15	31.38	15.07
1.2 ml/h	60.67	97.80	17.67	160.21	31.4	14.76
16 cm	60.73	97.23	16.62	160.12	31.41	15.78
20 cm	64.33	98.37	17.26	160.15	31.38	15.07
24 cm	60.11	97.88	12.61	160.11	31.61	20.28
17kV	59.94	97.64	12.89	160.24	33.48	21.97
20 kV	64.33	98.37	17.26	160.15	31.38	15.07
23kV	60.59	97.44	20.5	160.06	34.30	14.73
75/25 v/v	61.09	94.24	14.83	160.14	35.59	22.32
80/20 v/v	64.33	98.37	17.26	160.15	34.22	18.24
90/10 v/v	59.47	99.15	17.01	159.80	31.79	15.77

First, the DSC analysis was discussed for the solution concentration parameter. Since the non-uniform and beaded structure was obtained at the concentration of 7 wt.% PLA, the analysis was not performed for that sample. The DSC analysis results for polymer concentration pointed out that increasing the solution concentration from 11 wt.% to 13wt.% did not necessarily change the thermal properties presented in Table 4.2. A slight decrease in the degree of crystallization value was obtained while increasing the solution concentration. Since the number of chain entanglements is lower at low solution concentrations, the polymer chains have more mobility than those at higher concentrations. Therefore, having more mobile polymer chains gives rise to have a higher molecular orientation during the electrospinning process. As a consequence, samples obtained via electrospinning at low concentrations tend to have a greater degree of crystallization [91].

When the DSC analysis results for solution feed rate were assessed, it can be concluded that T_g, T_{cc}, and T_m of the nanofibrous neat PLA samples did not show a significant change with the increase in the solution feed rate. On the other hand, as the solution feed rate increased from 0.8 ml/h to 1 ml/h, the melting enthalpy and crystallization enthalpy values reduced. Hence, the degree of crystallization was

found to be decreased as the solution feed rate increased. This was resulted from the rapid deposition rate of the fibers from the nozzle to the collector during electrospinning, which provides a minimal time for crystallization to occur [92]. For this reason, a reduction in the degree of crystallization due to the solution feed rate increment was obtained. Furthermore, due to the overstretching of the polymer jet, lower solution flow rates are not suitable for generating continuous nanofiber generation [93]. According to the results in Table 4.2, increasing the solution feed rate to 1.2 ml/h did not cause a crucial change in the enthalpy of melting and enthalpy of crystallization. Thus, the degree of crystallization value did not show a significant change compared to the value evaluated for 1 ml/h solution feed rate.

DSC analysis was also performed for the determination of the tip-to-collector distance influence on the thermal properties and crystallinity. The obtained results indicated that changing tip-to-collector distance did not affect T_g, T_{cc}, T_m and ΔH_m of the nanofibrous neat PLA samples crucially. In addition, increasing the distance from 16 cm to 20 cm also did not cause an essential effect on the degree of crystallization. On the other hand, as the tip-to-collector distance was increased to 24 cm, an increase in the degree of crystallization value was obtained. Theoretically, the flight time of the ejected polymer jet to the collector increases with the increasing tip-to-collector distance. Flight time increment is considered to lead to an increase in the molecular orientation and thus, the degree of crystallization is expected to increase [49].

According to Figure 4.7 and tabulated data in Table 4.2, the degree of crystallinity of the electrospun samples produced with increasing applied voltage from 17 kV to 23 kV decreased. As it was mentioned before, the degree of crystallinity is affected by the flight time of the ejected polymer jet. At higher applied electrical voltage values the polymer jet has more acceleration while reaching the collector which reduces the flight time. Hence, there is not enough time for the polymer to crystallize [48]. Increasing the applied voltage from 20 kV to 23 kV did not result in a significant decrease in the degree of crystallinity. In addition, increasing applied

voltage did not have a vital influence on T_g, T_{cc}, T_m of the nanofibrous neat PLA samples.

As the last step of the DSC analysis, the effect of solvent ratio on thermal properties and the degree of the crystallization was investigated. The obtained results show that the degree of the crystallinity of the electrospun fiber generated at a solvent rate of 75/25 v/v CHL/DMF was higher compared to the ones with the solvent ratios of 80/20 and 90/10 v/v CHL/DMF. In other words, as the DMF concentration on the binary solvent system increased, the degree of crystallization also increased. As it can be seen in Table 4.1, DMF has a greater boiling point and lower vapor pressure value than CHL. Consequently, DMF could have more time to stay with the electrospun polymer fibers due to its slower evaporation rate. Therefore, PLA fibers had more time for developing a relatively high crystalline structure. For this reason, as the amount of DMF increased in the polymer solution, a higher degree of crystallinity was obtained [94]. Furthermore, when the solvent ratio changed from 90/10 v/v/ to 80/20 v/v, the degree of crystallization showed a slight increase due to the same reason given above. In addition, varying solvent ratio did not have a significant effect on T_g, T_{cc}, T_m of the nanofibrous neat PLA samples.

4.1.3 Thermogravimetric Analysis

TGA was conducted for the nanofibers generated applying different values of process parameters (applied voltage, solution feed rate, and tip-to-collector distance) and solution parameters (solution concentration and solvent ratio). Percent weight loss versus temperature graphs of neat PLA fibers at different process parameters and solution parameters can be seen in Figures 4.8 and 4.9, respectively. TGA analysis was performed for investigating the thermal stability of the obtained nanofibrous samples. Furthermore, the decomposition temperature, 10% weight loss temperature (T_{10}), 25% weight loss temperature (T_{25}), and the half weight loss temperature (T_{50}) of nanofibrous samples at different parameters are presented in

Table 4.3. All of the samples that were uniaxially electrospun at different parameter values and as-received PLA pellets showed similar characteristics of decomposition.

According to the tabulated data in Table 4.3, it can be concluded that as-received PLA pellets (bulk PLA) have a higher decomposition temperature than the values obtained for the electrospun PLA fibers at the different process and solution parameters. Concerning the influence of the electrospinning process on the morphology, this result can be attributed to randomly oriented PLA nanofiber structures obtained by the stretching of the polymer solution throughout the electrospinning process which resulted in lower thermal stabilities than pristine PLA pellets [95]. According to the obtained results of thermogravimetric analysis, the decomposition temperature did not show a significant change with the varying process and solution parameters.

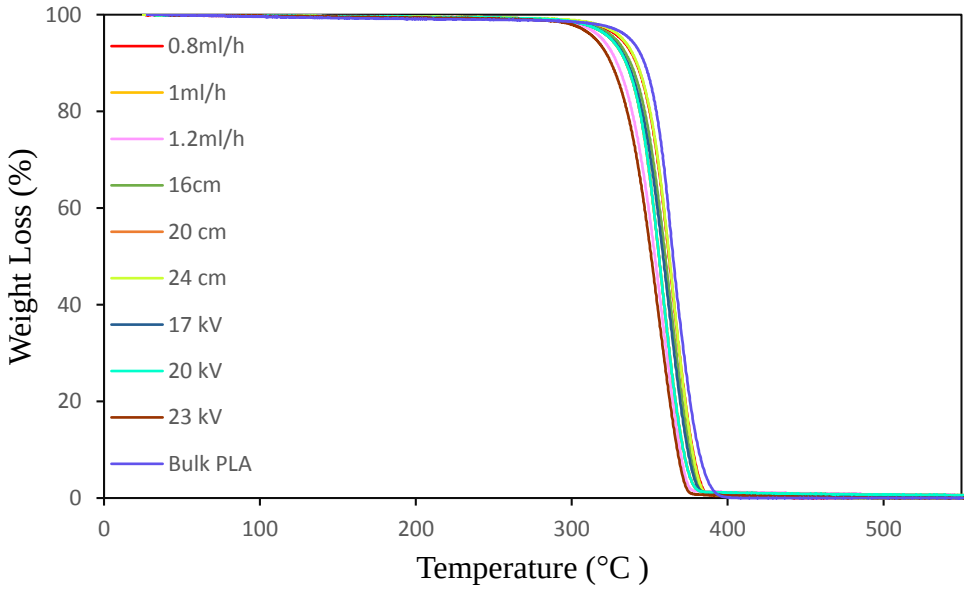

Figure 4.8 TGA curves for Process Parameters Studies on Electrospinning of Neat PLA.

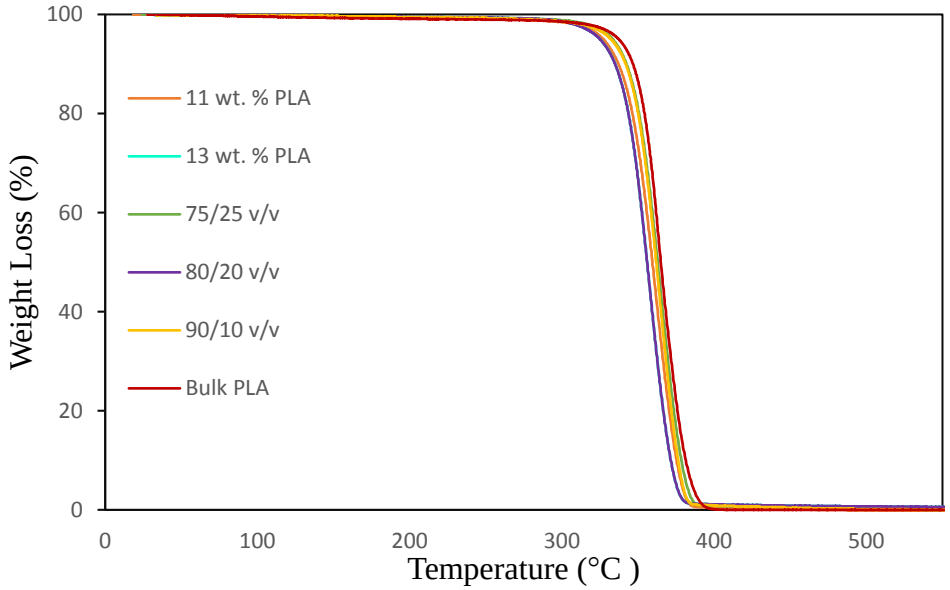

Figure 4.9 TGA curves for Solution Parameters Studies on Electrospinning of Neat PLA.

Table 4.3 TGA data for Parameter Studies on Electrospinning of Neat PLA.

Sample	**Decomposition Temperature (°C)**	**T_{10} (°C)**	**T_{25} (°C)**	**T_{50} (°C)**
Bulk PLA	371.48	346.7	356.62	364.81
11 wt.%	365.56	337.17	349.28	359.46
13 wt.%	362.45	334.99	346.48	356.07
0.8 ml/h	367.65	341.5	352.67	362.19
1 ml/h	362.45	334.99	346.48	356.07
1.2 ml/h	358.92	329.02	341.67	353.26
16 cm	366.18	337.58	349.62	360.18
20 cm	362.45	334.99	346.48	356.07
24 cm	366.80	341.95	352.93	362.49
17kV	364.37	335.95	348.05	358.52
20 kV	362.45	334.99	346.48	356.07
23kV	359.92	325.37	338.9	350.85
75/25 v/v	368.10	342.43	353.26	362.83
80/20 v/v	362.45	334.99	346.48	356.07
90/10 v/v	367.24	341.75	352.82	361.94

4.1.4 Tensile Test Results

Tensile test was performed to the samples produced by different values of process parameters (applied voltage, solution feed rate, and tip-to-collector distance) and solution parameters (solution concentration and solvent ratio). The obtained results are presented in Figures 4.10-4.12. Moreover, the representative stress-strain graphs and tabulated tensile data (i.e., tensile strength, tensile modulus, and elongation at break) including average and standard deviation values are given in Figure A.1 of Appendix A and Table B.1 of Appendix B, respectively.

As mentioned before, at the solution concentration of 7 wt.% PLA, a mixed morphology of fibers and beads mixed was obtained. The existence of beaded structure results in low fiber-to-fiber interaction, causing low mechanical properties [96]. Therefore, tensile test was not carried out for the samples produced at the solution concentration of 7 wt.% PLA. As the concentration increases, smoother fibers with uniform fiber diameter are generated, which reveals an increase in the fiber cohesion points. As a results, fibrous mats with higher tensile strength value can be obtained [96]. By increasing polymer solution concentration from 11 wt.% to 13 wt.% PLA, a slight decrease in the standard deviation of the average fiber diameter was observed. However, this small change did not have a substantial impact on the tensile strength value. In addition, the tensile modulus was also not affected significantly by the increment in the solution concentration. On the other hand, elongation at break increased with the increasing solution concentration. In accordance with the literature [53], low tensile strength and tensile modulus values were obtained compared to aligned nanofibrous mats since the orientation of the produced fibers was random. Moreover, random orientation resulted in high elongation values. By considering all of these results and observations, polymer solution concentration of 13 wt.% PLA was selected as the optimum.

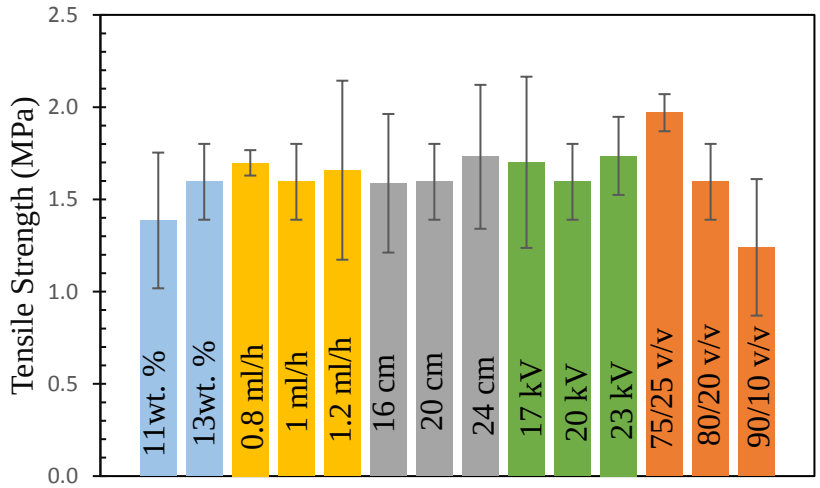

Figure 4.10 Tensile strengths of electrospun Neat PLA for Parameter Optimization Studies.

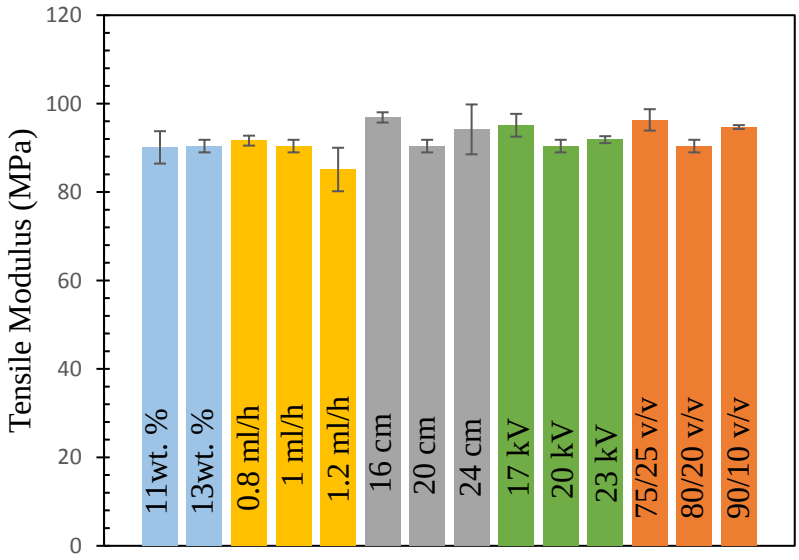

Figure 4.11 Tensile Moduli of electrospun Neat PLA for Parameter Optimization Studies.

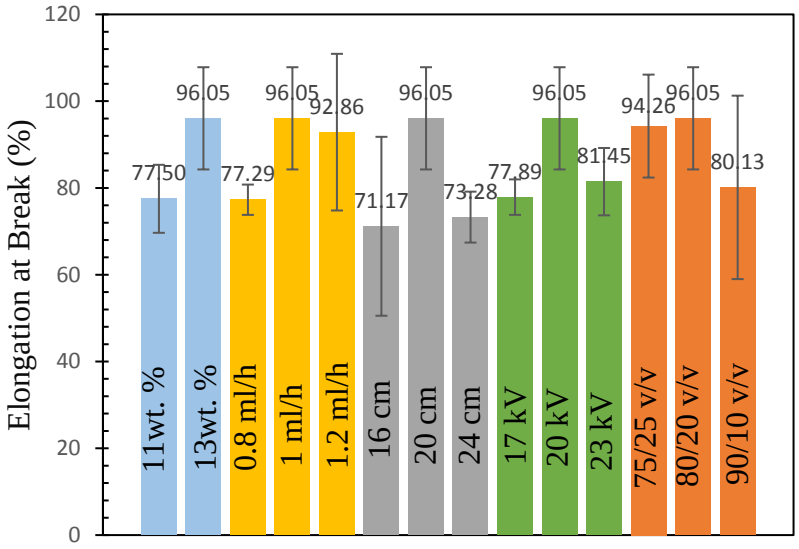

Figure 4.12 Elongation at break of electrospun Neat PLA for Parameter Optimization Studies.

According to the results, the standard deviation increased with the increments in the feed rate. Hence, it can be said that selecting very high feed rates are not convenient for the generation of smooth and continuous fibers. Although the tensile strength at the feed rate of 1.2 ml/h resulted in higher value than the lower feed rates, the solution feed rate of 1 ml/h was efficient in terms of having longer time period of maintaining stable Taylor cone. Moreover, when the tensile modulus is considered with the standard deviation, it can be deduced that the values were close to each other for the samples produced at 0.8 ml/h, 1 ml/h, and 1.2 ml/h. As it can be seen from Figure 4.12 and the tabulated data, the similar elongation at break values were obtained at the feed rates of 1 ml/h and 1.2 ml/h which are higher than the one at the solution feed rate of 0.8 ml/h. Glass transition temperature did not show a crucial change which implied that applying different values of feed rate did not influence the mobility of the nanofibers. Regarding the average fiber diameter, thermal and mechanical properties of the produced samples, and the observations made during the electrospinning process, the solution feed rate of 1 ml/h was determined as the optimum value.

When the tensile strength values for the samples produced at different tip-to-collector distance values are compared, it can be indicated that the highest tensile strength value was obtained at 24 cm. Mechanical properties are influenced by the fiber morphology. Higher mechanical strength and lower ductility can be obtained as the fiber diameter decreases [97]. The lowest fiber diameter was obtained with the tip-to-collector distance of 24 cm. As a result, greatest tensile strength value was observed at this distance. As it was mentioned before, at the tip-to-collector distances of 16 cm and 20 cm, the average fiber diameters were also obtained at close values to each other. Therefore, as expected, the tensile strength value did not show a significant change as the collector distance was increased from 16 cm to 20 cm. In addition, the tensile modulus of the nanofibrous mats generated at the distances of 16 cm and 24 cm had similar values to each other. Although the tensile modulus at the tip-to-collector distance of 16 cm and 24 cm resulted in higher values than the one at 20 cm, the distance of 20 cm was happened to be better in terms of obtaining desired morphologies. Moreover, at the tip-to-collector distance of 20 cm, the shape of the Taylor Cone was maintained longer time than the ones at other collector distances. Highest elongation value was also obtained at the distance of 20 cm. By considering all of these results and observations, tip-to-collector distance of 20 cm was selected as the optimum value.

When the applied voltage was increased to 23 kV, no crucial influence on the tensile strength value was observed compared to the one at 20 kV, as the standard deviation values were considered. In addition, the highest tensile modulus and elongation values were obtained at the applied voltages of 17 kV and 20 kV, respectively. In the previous studies, it was observed that the decrease in the fiber diameter was resulted in lower ductility and higher mechanical strength [97]. When the average fiber diameters of the samples generated at different applied voltage values were compared, the lowest value was obtained at the applied electrical voltage of 23 kV. Therefore, as expected, the highest tensile strength value belongs to the nanofibrous mat generated at 23 kV. Likewise, the average fiber diameter value was obtained as the highest for the samples produced at 20kV. Hence, these samples have the lowest

tensile strength value. By considering the tensile modulus at 20 kV and 23 kV, it can be seen that these values are very close to each other. Taking into account the morphologies, thermal and mechanical properties of the produced samples, and the observations made during the electrospinning process consideration, the optimum applied voltage value was determined as 20 kV.

As it was indicated before, the selection of the solvent system that is to be used in the electrospinning process has a strong impact on morphology, and thus thermal and mechanical properties. Solvent properties such as conductivity, dielectric constant, boiling point, and volatility determine the solution properties at a specified solution concentration and, hence, the fiber morphology. Eventually, solvent system selection has an essential influence on the mechanical properties [96]. Mechanical strength is enhanced by the decreasing fiber diameter [97]. In accordance with the literature, as the CHL concentration was increased in the polymer solution, the boiling point, electrical conductivity, and the dielectric constant of the solution were decreased. Therefore, as expected, the average fiber diameter increased with the increasing CHL concentration. Consequently, tensile strength value decreased as the average fiber diameter increased. In addition, as the degree of crystallinity increases, an improvement in the tensile strength and the tensile modulus can be observed [98]. The highest degree of crystallinity value was obtained for the samples produced with the solvent ratio of 75/25 v/v CHL/DMF. Hence, the highest tensile modulus was reached at 75/25 v/v CHL/DMF solvent ratio. Chloroform is a highly volatile solvent. However, dimethylformamide is less volatile than chloroform. As the volumetric ratio of DMF increased in the solvent system, the volatility of the CHL/DMF system had lower values. Therefore, there still could be a little solvent left as the fiber reached the rotating cylindrical collector. This might be caused some interactions among the fibers. As a result, fibrous samples generated by the higher DMF ratio in the solvent system have a greater elongation [99].

4.2 Effect of Electrospinning Process Duration and Sample Drying Duration on Neat PLA Nanofibers

As it was mentioned in the previous sections, one of the main purposes of this study was to investigate the effect of the electrospinning process duration on the properties and morphology of fibrous structures. Electrospinning process durations of 1, 2 and 3 hours were determined in order to reach this goal. Moreover, the possible plasticization effect of the retained solvents on the samples was studied by the influence of sample drying duration on the morphology, thermal and mechanical properties of the nanofibrous mats. Therefore, samples obtained after 3 hours of electrospinning process were dried in the furnace for overnight and 2 days. For the investigation of electrospinning process duration and sample drying duration, samples were produced at 11 and 13 wt.% PLA of solution concentration.

4.2.1 Scanning Electron Microscopy Analysis

The effect of electrospinning process duration on the fiber morphology was investigated by applying different time values while keeping the applied voltage, solution feed rate, and tip-top-collector distance parameters at constant values. For the electrospinning time investigation studies, 11 and 13 wt.% of PLA solutions were prepared. During the electrospinning process, the applied voltage, solution feed rate, tip-to-collector distance values were set at 20 kV, 1 ml/h and 20 cm, respectively. The electrospinning experiments were conducted for 1, 2 and 3 hours using a rotating cylinder collector with a rotational speed of 100 rpm.

The SEM micrographs and bar chart depicting the average fiber diameters of nanofibrous mats obtained at different electrospinning process durations and polymer concentration of 11wt.% PLA are given in Figures 4.13 and 4.17, respectively. When the standard deviation values are considered, it can be clearly deduced that increasing electrospinning duration did not result in a significant change in the average fiber values at 11wt.% PLA of polymer concentration.

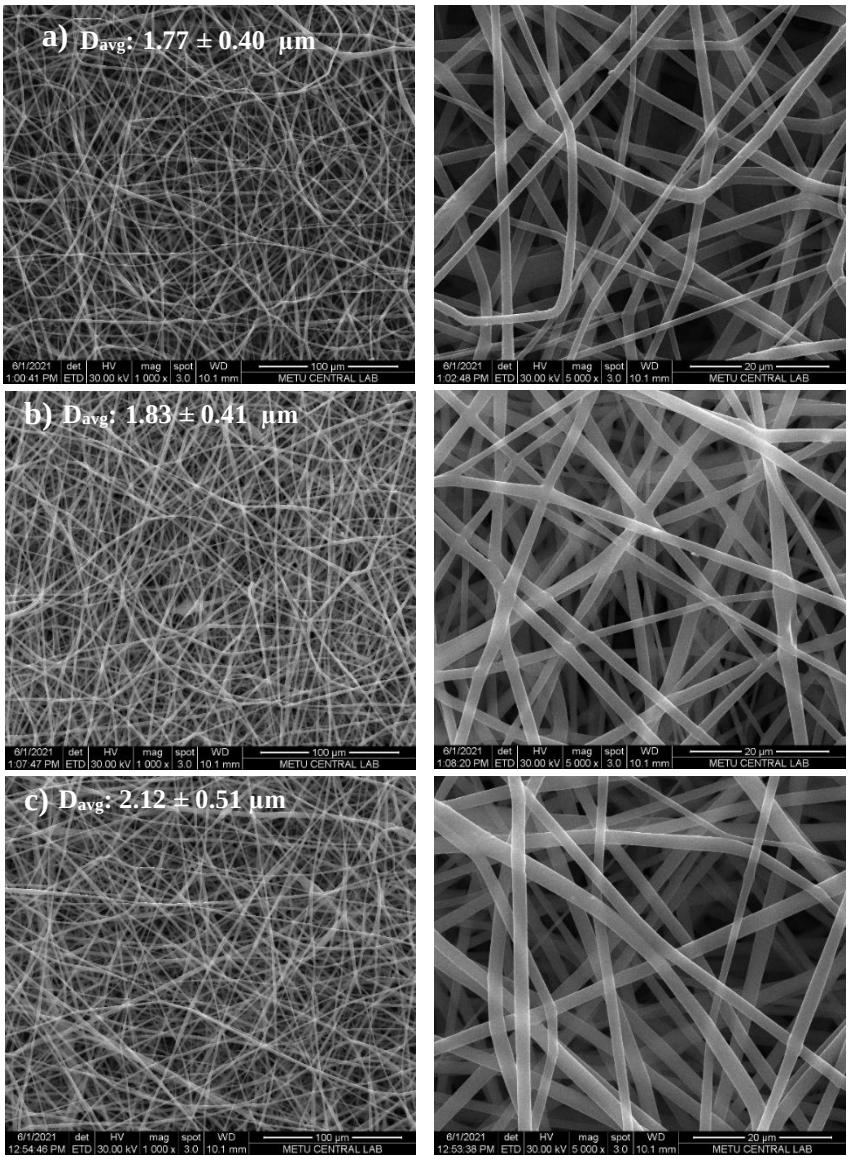

Figure 4.13 SEM micrographs of electrospun neat PLA with ED of a) 1, b) 2, c) 3h (AV: 20 kV, TCD: 20 cm, SC: 11 wt. % CT: cylinder RS: 100 rpm SFR: 1ml/ h, SR: 80/20 v/v SDD: overnight).

Moreover, standard deviation value showed a slight increase with the increasing electrospinning time. The SEM micrographs and bar chart showing the average fiber diameters of nanofibers produced at different electrospinning process durations at the polymer concentration of 13wt.% PLA are shown in Figures 4.14 and 4.17, respectively. As the standard deviation values are taken into account, it can be evidently concluded that increasing electrospinning duration did not cause a crucial

impact on the average fiber values at 13wt.% PLA of polymer concentration. In addition, generated samples had similar standard deviation values.

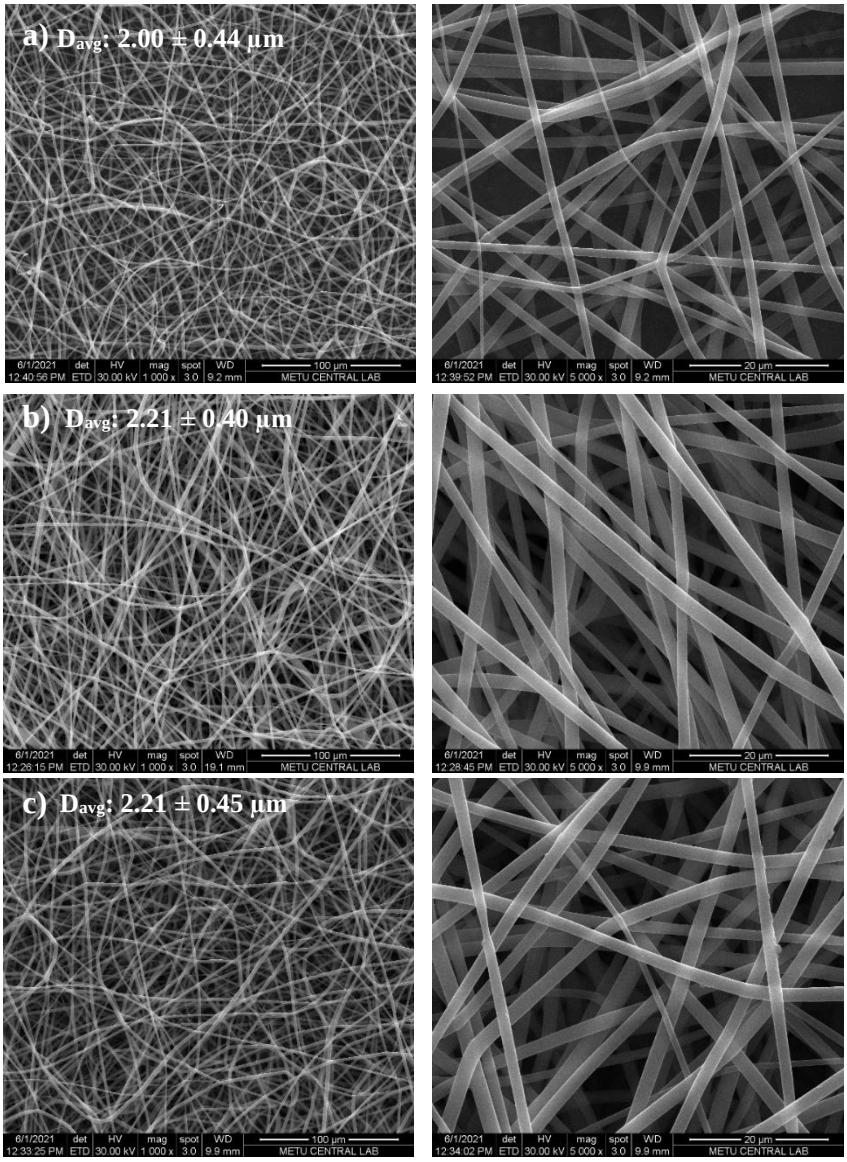

Figure 4.14 SEM micrographs of electrospun neat PLA with ED of a) 1, b) 2, c) 3h (AV: 20 kV, TCD: 20 cm, SC: 13 wt. % CT: cylinder RS: 100 rpm SFR: 1ml/ h, SR: 80/20 v/v SDD: overnight).

The SEM micrographs and bar chart depicting the average fiber diameters of nanofibrous samples obtained at different sample drying durations are presented in Figures 4.15 and 4.17, respectively.

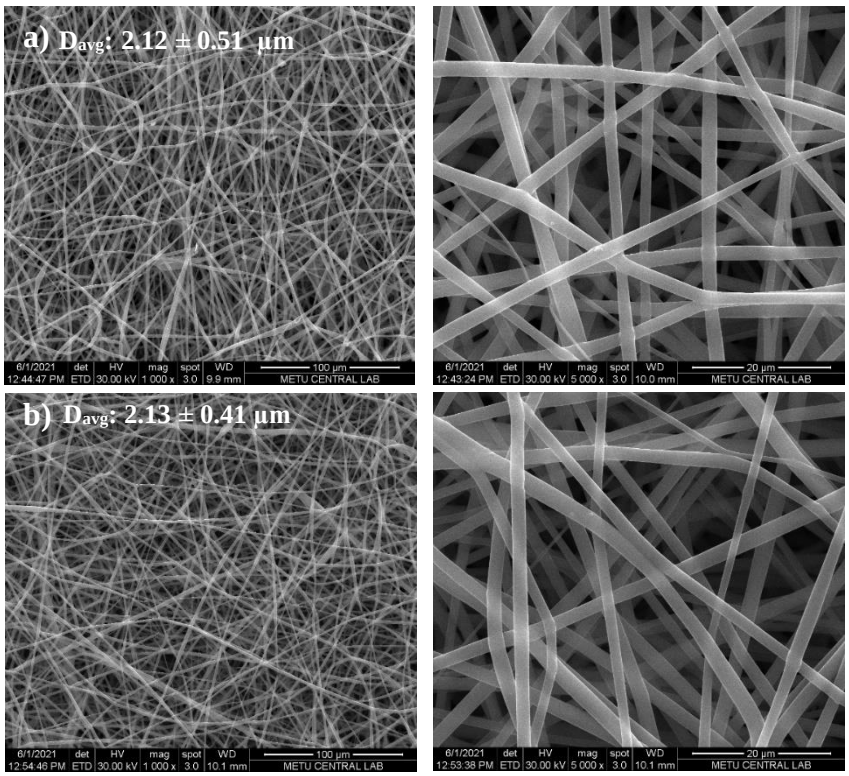

Figure 4.15 SEM micrographs of electrospun neat PLA with SDD of a) overnight, b) 2 days (AV: 20 kV, TCD: 20 cm, SC: 11 wt. % CT: cylinder RS: 100 rpm SFR: 1 ml/ h, SR: 80/20 v/v, ED: 3h).

For Figures 4.15a and b, the samples are generated at the polymer concentration of 11 wt. PLA. As the standard deviation values are considered, it can be determined that the increase in the sample drying duration did not cause a crucial impact on the average fiber values at 11 wt.% PLA of polymer concentration. Furthermore, produced samples had shown a slight decrease in the standard deviation values with increasing sample drying time. Polymer concentration of 13 wt.% PLA was used while producing the samples given in Figures 4.16a and b. As the sample drying duration increases, no important change was observed in the average fiber diameter of the samples when the standard deviation values are regarded. Moreover, generated samples had similar standard deviation values. Therefore, it can be concluded that

electrospinning process duration and sample drying duration did not have a significant influence on the morphology of the obtained nanofibrous samples.

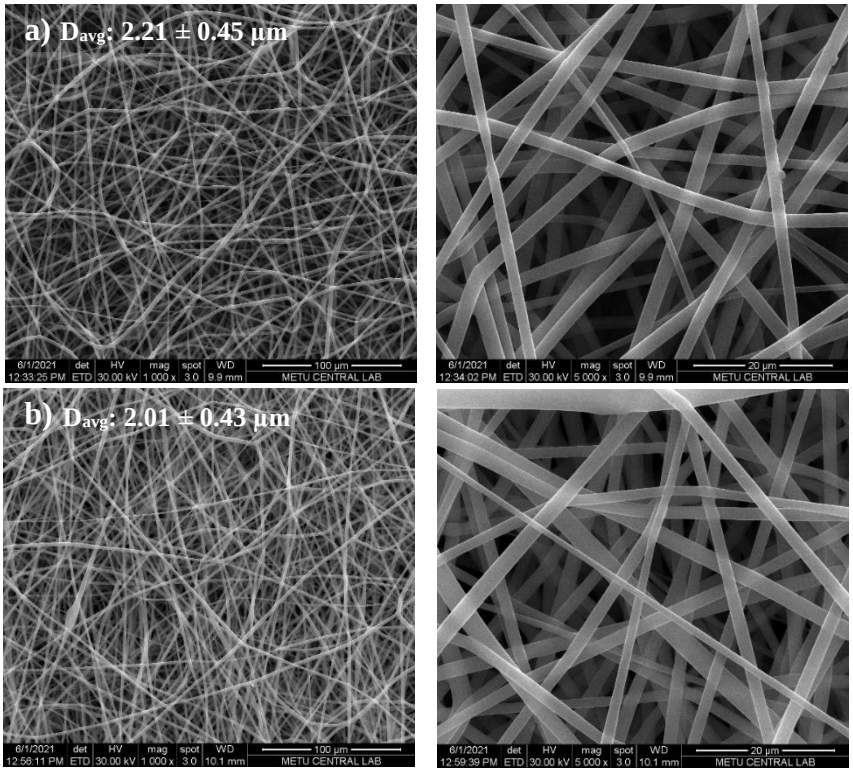

Figure 4.16 SEM micrographs of electrospun neat PLA with SDD of a) overnight d) 2 days (AV: 20 kV, TCD: 20 cm, SC: 13 wt. % CT: cylinder RS: 100 rpm SFR: 1ml/ h, SR: 80/20 v/v ED: 3h).

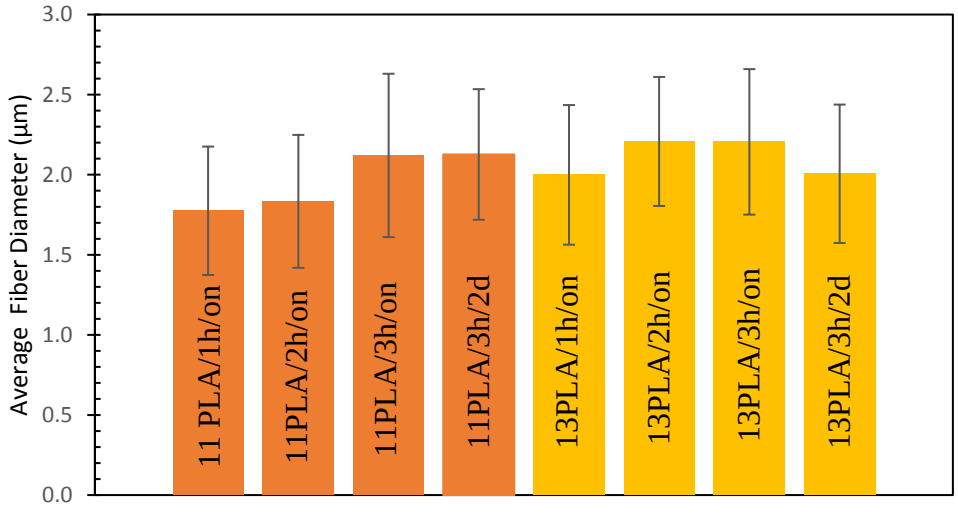

Figure 4.17 Bar chart depicting the average fiber diameters of Neat PLA nanofibers generated by ED and SDD studies.

4.2.2 Differential Scanning Calorimetry Analysis

DSC analysis was carried out for the nanofibers generated at different electrospinning process durations and sample drying durations. The obtained DSC curves are given in Figure 4.18. Furthermore, thermal properties (i.e., glass transition temperature (T_g), cold crystallization temperature (T_{cc}), enthalpy of cold crystallization (ΔH_{cc}), melting temperature (T_m), enthalpy of melting (ΔH_m) and degree of crystallization (X_c)) values are presented in Table 4.4. According to Figure 4.18 and tabulated data in Table 4.4, it can be concluded that increasing electrospinning process and sample drying durations did not lead to a change in the thermal properties determined by DSC analysis.

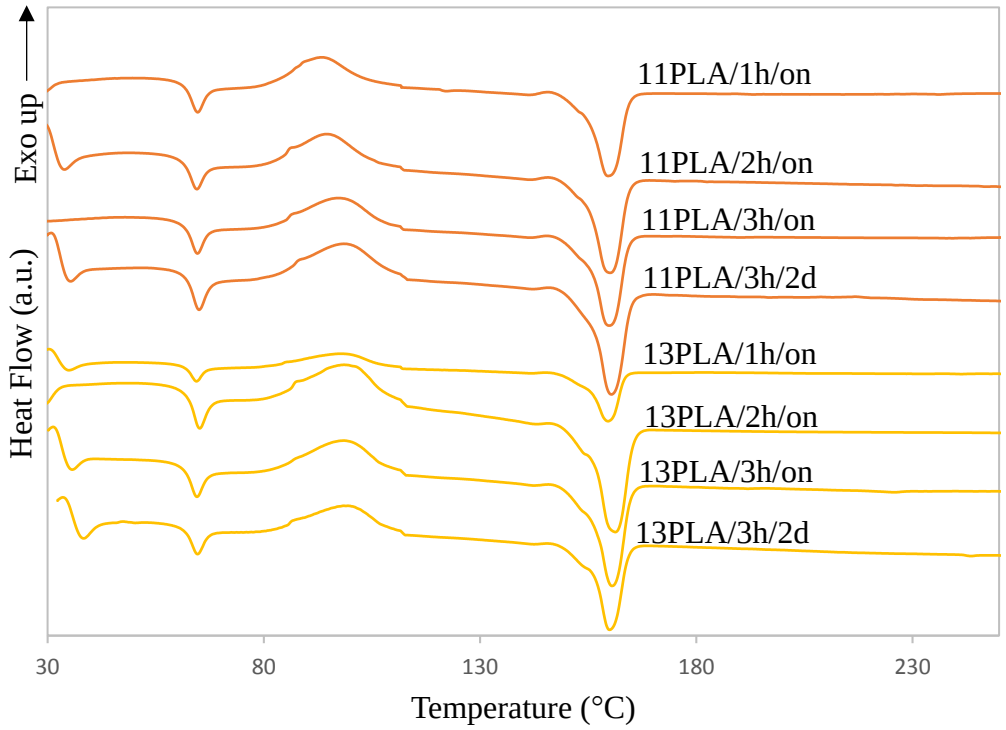

Figure 4.18 DSC curves for ED and SDD studies on Neat PLA nanofibers.

Table 4.4: DSC data for ED and SDD studies on Neat PLA nanofibers.

Sample	T_g (°C)	T_{cc} (°C)	ΔH_{cc} (J/g)	T_m (°C)	ΔH_m (J/g)	X_c (%)
11PLA/1h/on	61.79	93.17	9.76	159.78	36.88	29.16
11PLA/2h/on	61.80	94.59	9.89	159.75	36.28	28.38
11PLA/3h/on	61.94	97.26	8.17	159.72	33.49	27.23
11PLA/3h/2d	62.35	98.35	8.31	160.18	33.14	26.70
13PLA/1h/on	61.48	98.22	10.94	159.21	37.69	28.76
13PLA/2h/on	62.60	98.56	10.19	161.18	35.79	27.53
13PLA/3h/on	61.79	98.25	11.21	160.51	35.15	25.74
13PLA/3h/2d	61.89	98.79	8.99	159.88	32.69	25.48

4.2.3 Thermogravimetric Analysis

TGA was performed for the nanofibrous mats obtained at different electrospinning process durations and sample drying durations. Percent weight loss versus

temperature graphs of neat PLA fibers at polymer concentrations of 11 and 13 wt.% PLA can be seen in Figures 4.19 and 4.20, respectively. TGA analysis was carried out for investigating the thermal stability of the obtained nanofibrous samples. All of the samples that were uniaxially electrospinned at different electrospinning time and dried at different durations showed similar characteristics of decomposition. According to the obtained results of thermogravimetric analysis, the decomposition temperature did not show a significant change with the varying process time and sample drying duration at both polymer concentrations of 11 and 13 wt.% PLA. Therefore, it is possible to conclude that with the increasing process time and drying duration, the effect of solvent retainment on the nanofibrous mats was not observed and hence similar decomposition behaviors were obtained for each sample.

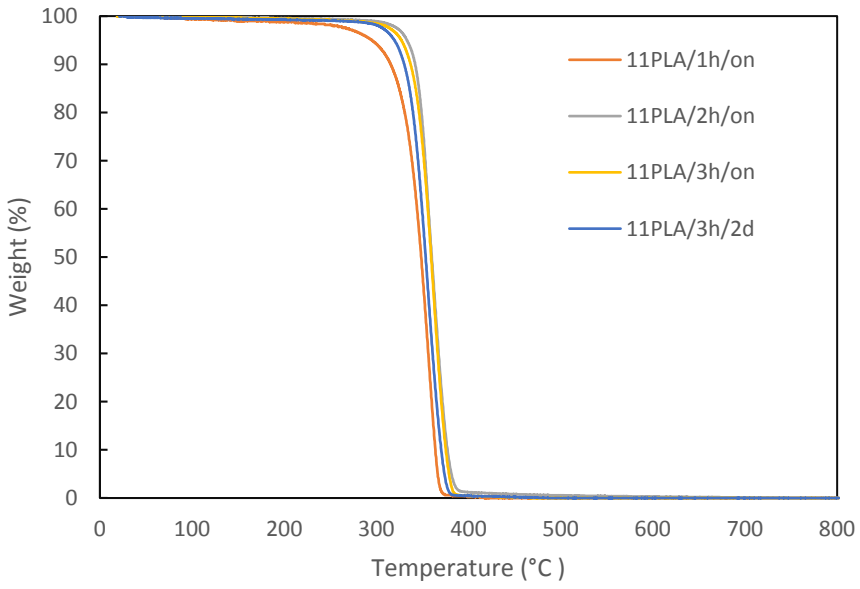

Figure 4.19 TGA curves for Solution Parameters Studies on ED and SDD (SC: 11 wt.%).

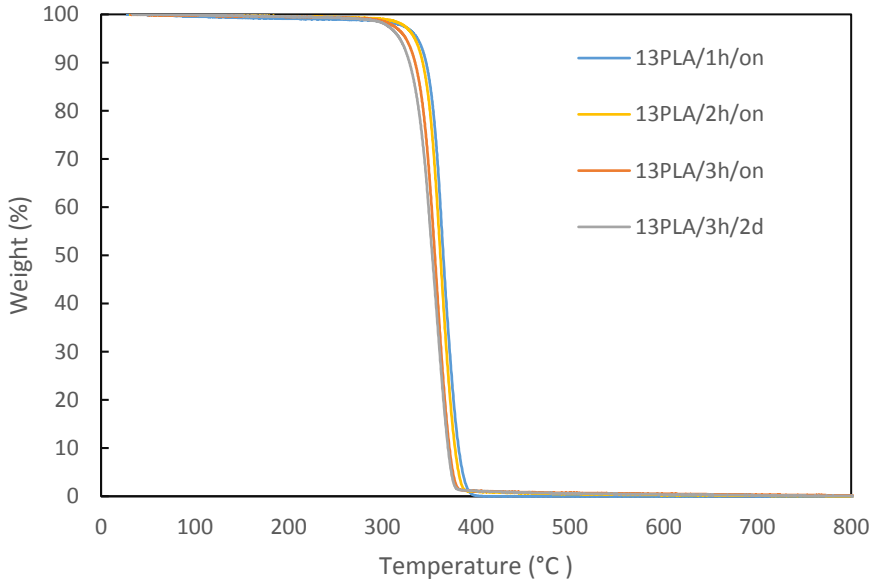

Figure 4.20 TGA curves for Solution Parameters Studies on ED and SDD (SC: 13 wt.%).

4.2.4 Tensile Test Results

Tensile test was conducted for the neat PLA nanofibrous samples produced at different electrospinning process durations. Furthermore, the effect of sample drying duration on mechanical properties was also investigated for electrospun neat PLA samples produced throughout 3 hours of process duration. The obtained results of neat PLA fibers at polymer concentrations of 11 and 13 wt.% PLA are given in Figures 4.21-4.23. Moreover, the representative stress-strain graph and tabulated tensile data (i.e., tensile strength, tensile modulus, and elongation at break) is presented in Figure A.2 of Appendix A and Table B.2 of Appendix B sections, respectively. At 1 hour of electrospinning process duration, the minimum thickness value required for performing tensile test could not be obtained. Therefore, the analysis for determining mechanical properties could not be conducted for the related sample.

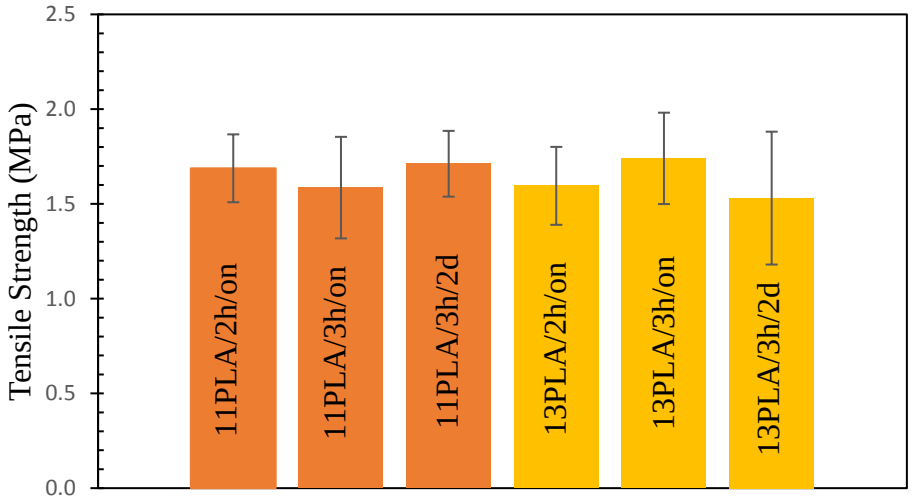

Figure 4.21 Tensile strengths of electrospun Neat PLA nanofibers generated by ED and SDD studies.

According to the obtained results, as the standard deviation values were taken into account, increasing electrospinning process and sample drying durations did not lead to a change in the mechanical properties of the nanofibrous samples electrospun and dried at different durations. Hence, it can be concluded that with the increasing process time and drying duration, the plasticizing effect of solvent retainment on the nanofibrous mats was not observed. Therefore, similar mechanical performances were obtained for each sample. Electrospinning time of 3 hours and overnight sample drying duration were chosen for the further experimental studies.

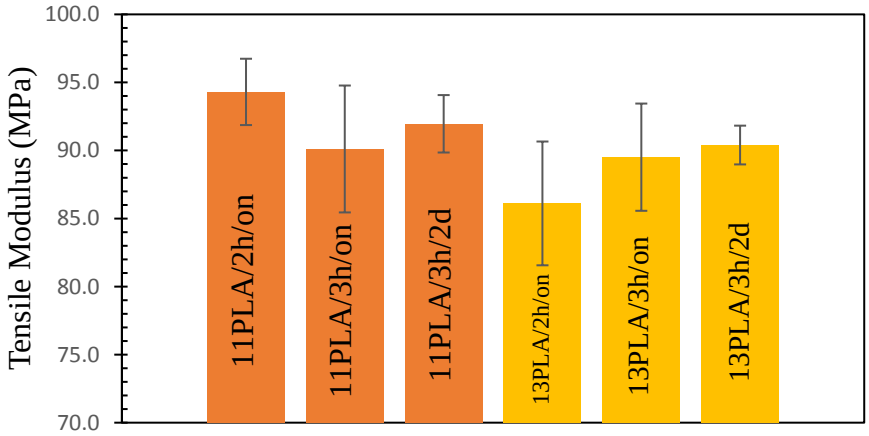

Figure 4.22 Tensile Moduli of electrospun Neat PLA nanofibers generated by ED and SDD studies.

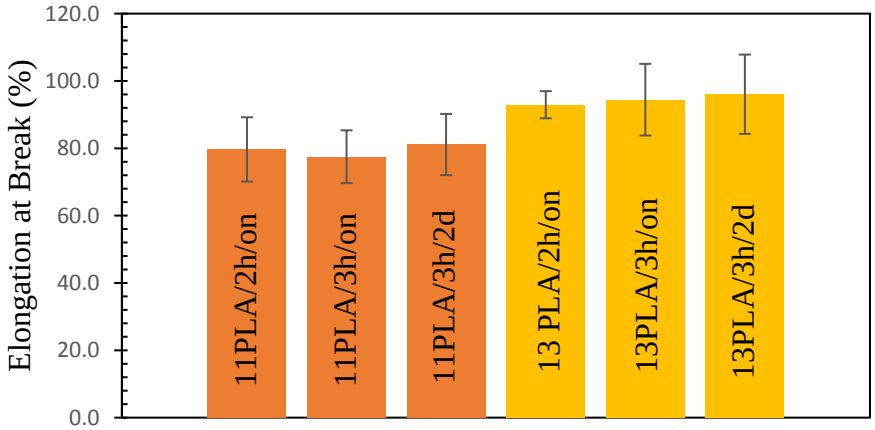

Figure 4.23 Elongation at break of electrospun Neat PLA nanofibers generated by ED and SDD studies.

4.3 Development of PLA/PEG and PLA/HNT Nanofibers

The studies for obtaining the optimum PEG and HNT concentration were carried out after obtaining the suitable parameter values for the electrospinning process by the parameter studies on the electrospinning of the neat PLA. For this purpose, 4, 7, 10, 15, and 25 wt.% PEG were added and mixed with PLA to obtain a homogeneous PLA/PEG polymer solution. Moreover, 0.25, 0.5, 1, 3, 5 wt.% HNT were also added and mixed with PLA to obtain PLA/HNT suspension. While generating nanofibrous

PLA/PEG and PLA/HNT mats, the process parameters were applied as 1 ml/h of solution feed rate, 20 cm of tip-to-collector distance, and 20 kV of applied voltage. Moreover, solution concentration and solvent ratio were kept constant at 13 wt.% and 80/20 v/v CHL/DMF, respectively. In this section, the obtained results are presented in terms of morphology, thermal and mechanical properties.

4.3.1 Scanning Electron Microscopy Analysis

The SEM micrographs of the resulting PLA/PEG nanofibers are given in Figure 4.24. In addition, the average fiber diameter measurements are presented in Figure 4.26. It can be clearly seen that randomly oriented fibers were generated as in the electrospinning of neat PLA. When the standard deviation values are taken into consideration for the PEG concentrations between 4-10 wt.%, it can be concluded that increasing PEG concentration did not have a significant influence on average fiber diameter.

The average fiber diameter has shown a decreasing trend with the increasing PEG concentration at 15 and 25 wt.%. As mentioned before, solution parameters have a substantial impact on fiber morphology. As expected, solution viscosity, which is one of the solution parameters, indicated a crucial effect on the fiber morphology and diameter. The viscosity of the polymer solution decreased as the PEG concentration increased. The reduction in the solution viscosity can be explained by the influence of the flexible PEG chains, which eases the flow of PLA molecules [53]. Therefore, polymer solutions with lower viscosity values resulted in thinner fibers.

Standard deviation values of electrospun PLA/PEG samples decreased at high PEG concentrations. Hence, increasing the PEG concentration to 15 wt.% and 25 wt.% resulted in a relatively more uniform distribution of fiber thickness.

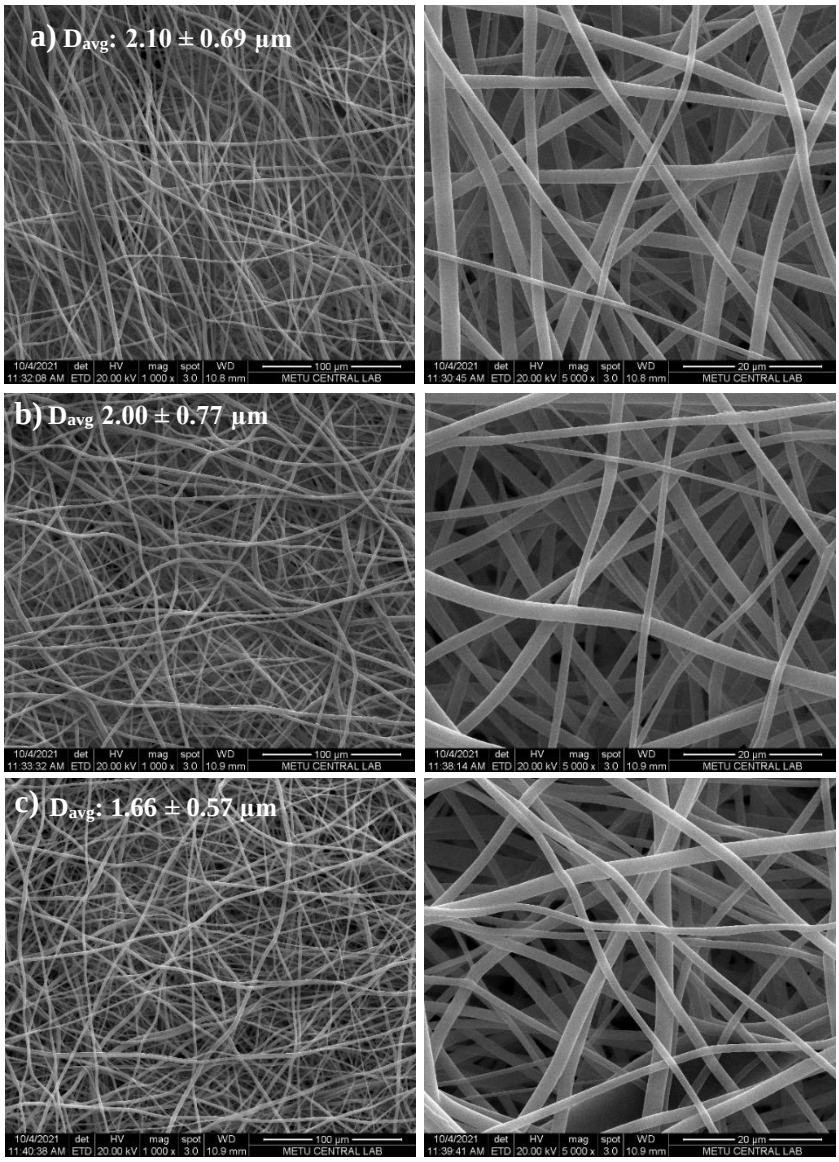

Figure 4.24 SEM micrographs of electrospun PLA/PEG nanofibers with PEG concentrations a) 4, b) 7, c) 10, d) 15, e) 25 wt.% (AV: 20 kV, TCD: 20 cm, SFR: 1 ml/h CT: cylinder RS: 100 rpm ED: 3 h, SR: 80/20 v/v).

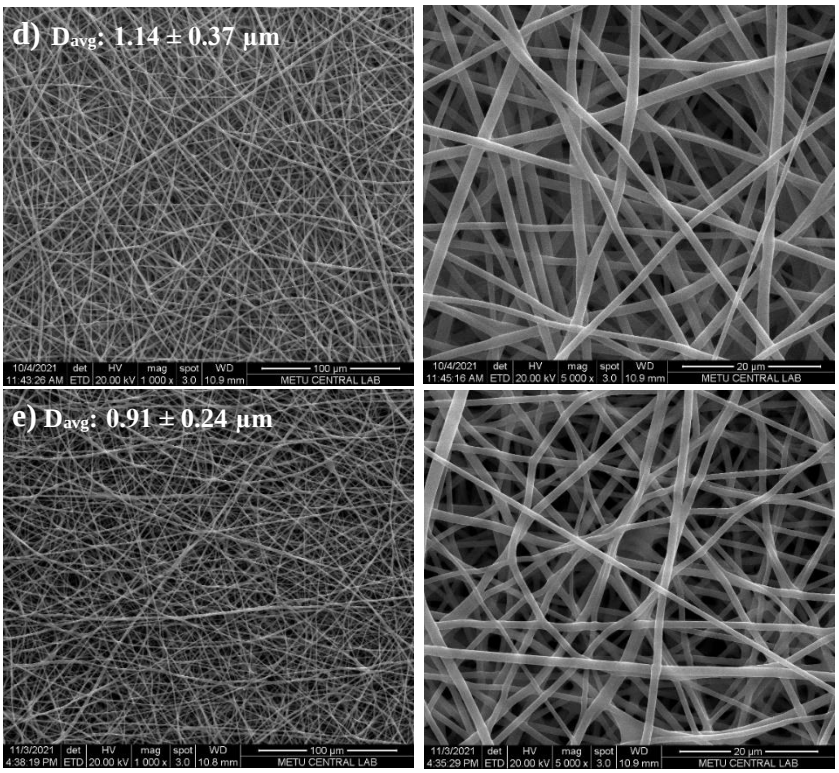

Figure 4.24 (continued) SEM micrographs of electrospun PLA/PEG with concentrations a) 4, b) 7, c) 10, d) 15, e) 25 wt.% PEG (AV: 20 kV, TCD: 20 cm, SFR: 1 ml/h CT: cylinder RS: 100 rpm ED: 3 h, SR: 80/20 v/v).

The SEM micrographs of the produced PLA/HNT nanofibers are presented in Figure 4.25. Moreover, the average fiber diameter data are given in Figure 4.26. It can be clearly deduced that composite mats with randomly oriented fibers were produced as in the electrospinning of neat PLA and PLA/PEG samples. In addition, the average fiber diameter showed an ascending trend with the increment in the HNTs concentration for the polymer solutions prepared by the first method, in which predetermined amounts of PLA and HNTs were added in the CHL/DMF solvent system and mixed with a magnetic stirrer for overnight at room temperature until observing a homogeneous polymer solution with a total solution concentration of 13 wt. %. This finding can be explained by the enhanced solution viscosity due to the inclusion of HNTs to the polymer solution. As a result, the stretching of the jet was restricted during the electrospinning process, and fiber diameter gradually increases with the increasing HNTs concentration [70].

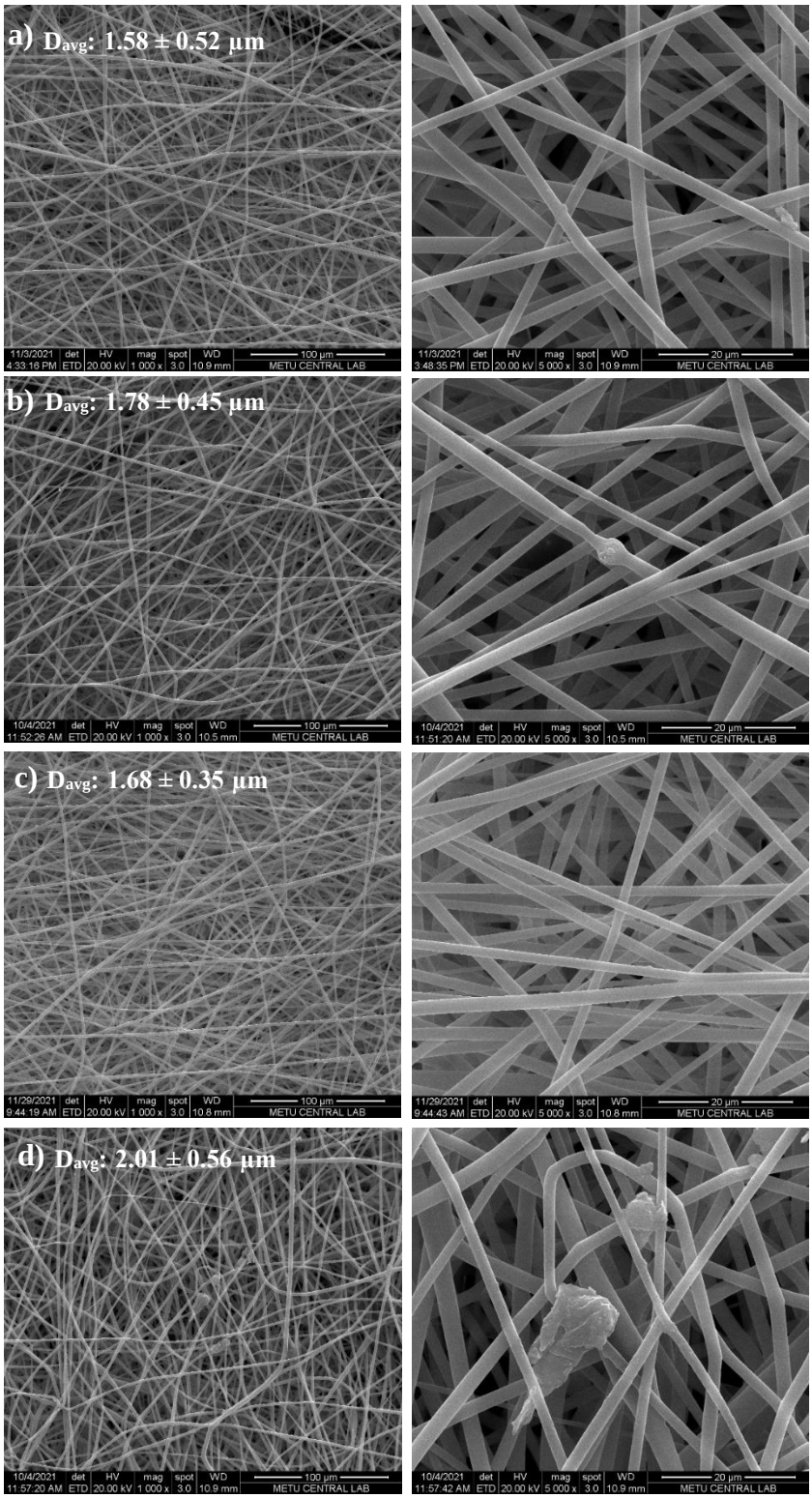

Figure 4.25 SEM micrographs of electrospun PLA/HNT nanofibers with HNT concentrations of a) 0.25 wt.%, b) 0.5 wt.%-M1, c) 0.5 wt.%-M2, d) 1 wt.%, e) 3 wt.%-M1, f) 3 wt.%-M2 g) 5 wt.% (AV: 20 kV, TCD: 20 cm, SFR: 1 ml/h).

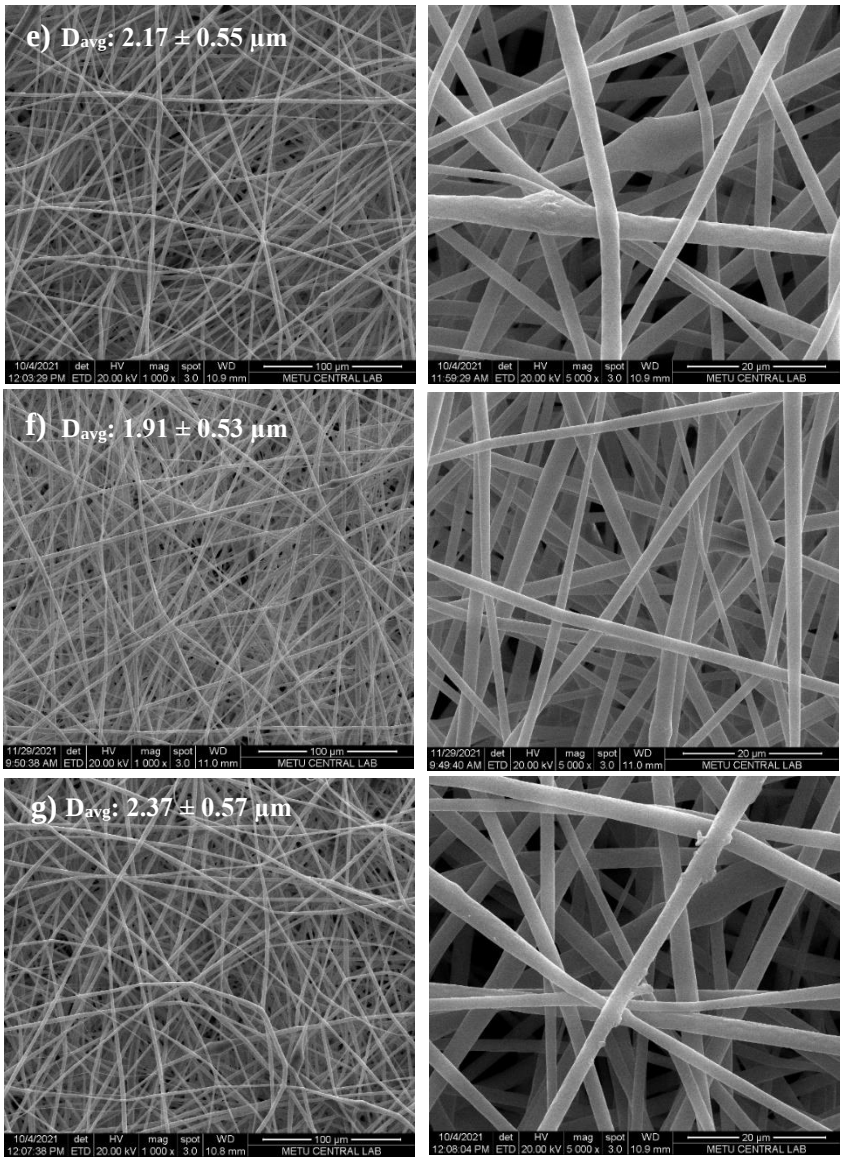

Figure 4.25 (continued) SEM micrographs of electrospun PLA/HNT nanofibers with HNT concentrations of a) 0.25 wt.%, b) 0.5 wt.%-M1, c) 0.5 wt.%-M2, d) 1 wt.%, e) 3 wt.%-M1, f) 3 wt.%-M2 g) 5 wt.% (AV: 20 kV, TCD: 20 cm, SFR: 1 ml/h).

Moreover, when the average fiber diameter results at the HNTs concentrations lower than 5 wt.% are compared with the average fiber diameter value of neat PLA fibers, it can be observed that PLA/HNT system resulted in thinner fibers. As it was discussed before, the electrical conductivity of the polymer solution is another parameter that has an important influence on fiber morphology. Increasing the HNT concentration in the electrospinning solution caused a rise in the electrical

conductivity due to the addition of negatively charged HNTs. As a result, composite fibers with smaller diameters were obtained [100].

The effect of applying different solution preparation methods at the HNT concentrations of 0.5 and 3 wt.% on the morphology and average fiber diameter values was also investigated (Figures 4.25b, c and 4e, f). As the second method of PLA/HNT suspension preparation, first HNTs with the predetermined amounts were added to the CHL and DMF solvent system. The obtained suspension was sonicated at room temperature for 30 minutes with the sonicator. Then, the PLA pellets were added in order to reach the predetermined total solution concentration of 13 wt.% and mixed with a magnetic stirrer for 4 hours at room temperature until observing a homogeneous solution. When the standard deviation values were considered for the electrospinning of PLA/HNT, it can be seen that carrying out the second solution preparation method at the HNTs concentration of 0.5 wt.% resulted in close average fiber diameter values with the ones generated with the electrospinning solution prepared by the first method. Similarly, applying different solution preparation methods did not show an important effect on the fiber morphology and the average fiber diameter values of the PLA/HNT nanofibrous samples at the HNTs concentration of 3 wt.% as the standard deviation values were taken into account. On the other hand, the sample containing PLA and 0.5 wt.% HNT, was prepared by Method-2, (PLA/0.5HNT-M2) has the smallest standard deviation value. Therefore, electrospinning solution prepared by second method with 0.5 wt.% HNTs had more uniform distribution of fiber thickness. Furthermore, samples with HNTs concentrations of 0.25, 1, 3 and 5 wt.% had standard deviation values close to each other. Hence, the generated nanofibrous mats at these HNTs concentrations had similar fiber thickness distribution.

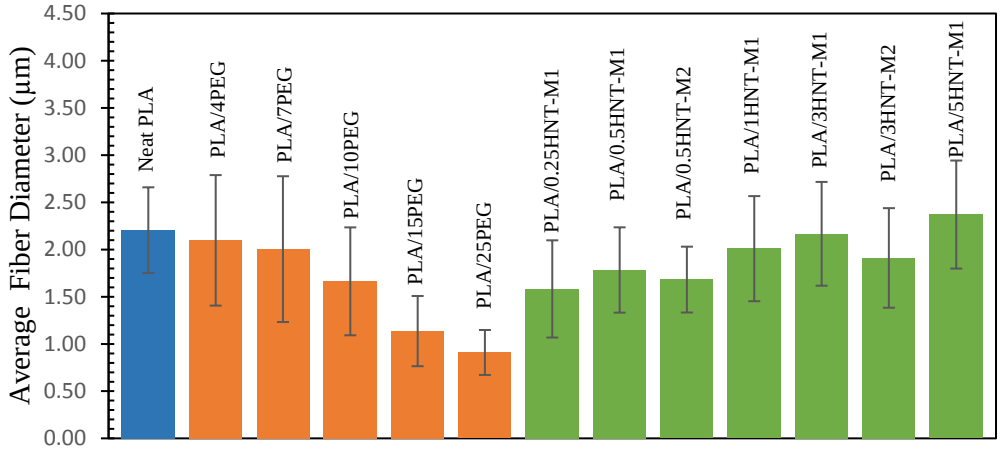

Figure 4.26 Bar chart depicting the average fiber diameters of nanofibers with two components.

4.3.2 Differential Scanning Calorimetry Analysis

DSC analysis was performed for PLA/PEG and PLA/HNT nanofibrous samples generated at different PEG and HNT concentrations, respectively. Moreover, the effect of solution preparation method on thermal properties was also investigated for PLA/HNT samples at the same concentrations. The obtained DSC curves are presented in Figure 4.27. Moreover, thermal properties (i.e., glass transition temperature (T_g), cold crystallization temperature (T_{cc}), enthalpy of cold crystallization (ΔH_{cc}), melting temperature (T_m), enthalpy of melting (ΔH_m) and degree of crystallization (X_c)) values are given in Table 4.5.

According to the results, for PLA/PEG systems, T_g cannot be observed at the temperature range DSC analysis was conducted. Moreover, T_{cc} peak could be observed only at PEG concentration of 25 wt.% at the temperature range of the analysis. This can be attributed to the maximum crystallization of the samples was obtained with the PEG addition to the system so that the cold crystallization did not occur concentrations less than 25 wt.% PEG. Moreover, at the concentration of 25

wt.% PEG T_{cc} peak shifted to a lower temperature. However, T_m values did not change by the presence of PEG in the samples. T_m peak of PEG was observed at the temperatures of 58.84 and 58.06°C for the samples of PLA/15PEG and PLA/25PEG, respectively. Furthermore, PLA/PEG mats have higher degree of crystallization values than the electrospun neat PLA sample. The motion of PLA chains is facilitated with the addition of PEG. Glass transition and cold crystallization temperatures decreased with the chain mobility enhancement. In addition, polymer chains are enabled to have easier rearrangements with the inclusion of PEG to reach higher degree of crystallization values [101].

According to the tabulated data, a slight decrease in T_g occurred with the addition of HNTs compared to the glass transition temperature value of neat PLA nanofibrous mats generated at the optimum electrospinning parameters. Introducing isotropic nanoparticles such as nano diamonds [102] and nano-TiO_2 [103] to PLA matrix usually leads to an increase in T_g. As the nanofillers are added, polymer chains may have interactions with the nanofiller materials via intermolecular attractions (i.e., hydrogen bonding and van der Waals forces) [104]. Therefore, polymer chain mobility can be hindered by the nanofiller materials [105]. On the other hand, the addition of anisotropic nanofillers may have a different influence on the glass transition temperature of the polymer matrix due to the nanofillers having a greater size in at least one dimension [106, 107]. Although the diameter of the HNTs is in nanoscale, their length is in microscale. As a consequence, polymer chain packing is reduced and an increment in free volume is obtained [108]. Hence, the increase in the free volume enables to obtain an increase in polymer chain mobility which tends to result in a decrease in T_g [100].

For the cold crystallization temperature (T_{cc}), no crucial change was observed except in samples PLA/3HNT-M1 and PLA/5HNT-M1, in which the first solution preparation method was applied by adding the predetermined amounts of PLA and HNTs in the CHL/DMF solvent system and mixing with a magnetic stirrer for overnight at room temperature until observing a homogeneous polymer solution with a total solution concentration of 13 wt. %.

According to the tabulated data, for the first PLA/HNT suspension preparation method, a reduction in T_{cc} value was observed at higher HNTs concentrations compared to electrospun neat PLA samples. This reduction in the T_{cc} can be explained by the nucleation effect of HNTs to expedite the cold crystallization process [70]. Due to the nucleation effect of HNTs, a slight increase in the X_c of PLA/HNT nanocomposite fibers was observed compared to neat PLA nanofibrous samples [100]. T_m values of PLA/HNT nanocomposite fibers did not show a significant change since halloysites are mineral fillers [109].

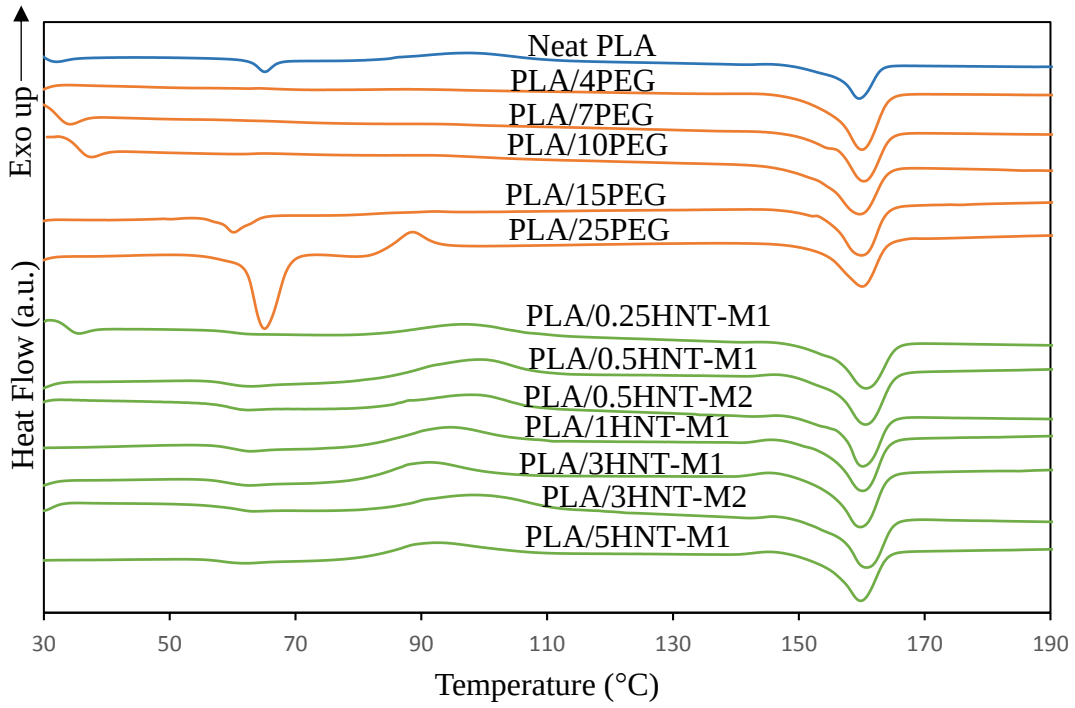

Figure 4.27 DSC curves for electrospun PLA/PEG and PLA/HNT.

Table 4.5: DSC data for electrospun PLA/PEG and PLA/HNT.

Sample	T_g (°C)	T_{cc} (°C)	ΔH_{cc} (J/g)	T_m (°C)	ΔH_m (J/g)	X_c (%)
Neat PLA Fibers	64.33	98.37	17.26	160.15	31.38	15.07
PLA/4PEG	-	-	-	159.98	38.65	43.29
PLA/7PEG	-	-	-	160.38	34.32	39.68
PLA/10PEG	-	-	-	159.75	36.80	43.97
PLA/15PEG	-	-	-	159.99	31.50	39.85
PLA/25PEG	-	88.67	10.59	160.08	29.59	27.24
PLA/0.25HNT-M1	59.80	96.86	13.63	160.75	32.63	20.48
PLA/0.5HNT-M1	59.58	99.31	13.92	160.60	35.6	23.43
PLA/0.5HNT-M2	59.41	98.01	19.57	160.20	39.44	21.47
PLA/1HNT-M1	59.52	94.60	15.97	160.14	37.03	22.87
PLA/3HNT-M1	59.07	91.38	15.75	159.77	35.23	21.59
PLA/3HNT-M2	60.47	98.24	18.79	160.76	35.57	18.60
PLA/5HNT-M1	58.04	92.56	10.46	159.90	32.82	25.31

4.3.3 Thermogravimetric Analysis

TGA was conducted for the PLA/PEG and PLA/HNT nanofibrous samples generated at different PEG and HNT concentrations, respectively. Moreover, the effect of solution preparation method on thermal properties was also investigated for PLA/HNT samples at the HNTs concentrations of 0.5 and 3 wt.%. Percent weight loss versus temperature graphs of PLA/PEG and PLA/HNT fibers can be seen in Figures 4.28 and 4.29, respectively. In addition to obtaining thermal stability information of the nanofibrous samples, the decomposition temperature, 10% weight loss temperature (T_{10}), 25% weight loss temperature (T_{25}), and the half weight loss temperature (T_{50}) of nanofibrous samples at different parameters were determined and presented in Table 4.6. The decomposition temperature of the produced nanofibrous samples was determined from the first derivative of percent weight loss data with respect to increasing temperature. The peak value of this curve gives the decomposition temperature of the samples.

TGA results of PLA/PEG samples demonstrate that all of the electrospun mats had a single-step decomposition. Furthermore, increasing PEG content did not have a

crucial influence on the decomposition temperature. Therefore, it can be concluded that the amount of PEG added in the polymer solution did not have a significant impact on the thermal stability of the nanofibrous mats. According to the results, PLA/HNT composite nanofibrous mats decomposed at higher temperature values than of neat PLA nanofibers. In addition, there was no residue left after the decomposition of nanofibrous neat PLA samples. On the other hand, PLA/HNT samples could not completely decompose. As the temperatures of T_{10}, T_{25}, and T_{50} of neat PLA and PLA/HNT samples are compared, it can be seen that PLA/HNT nanocomposite fibrous samples had higher values than the electrospun neat PLA sample. Hence, PLA/HNT nanocomposite mats came up with a better thermal stability than neat PLA nanofibers. This result can be attributed to the relatively dispersed HNTs in the polymer matrix acting as a mass transfer barrier to the volatile pyrolyzed PLA products. As a result, the thermal decomposition of PLA/HNT nanocomposite fibers was retarded [110].

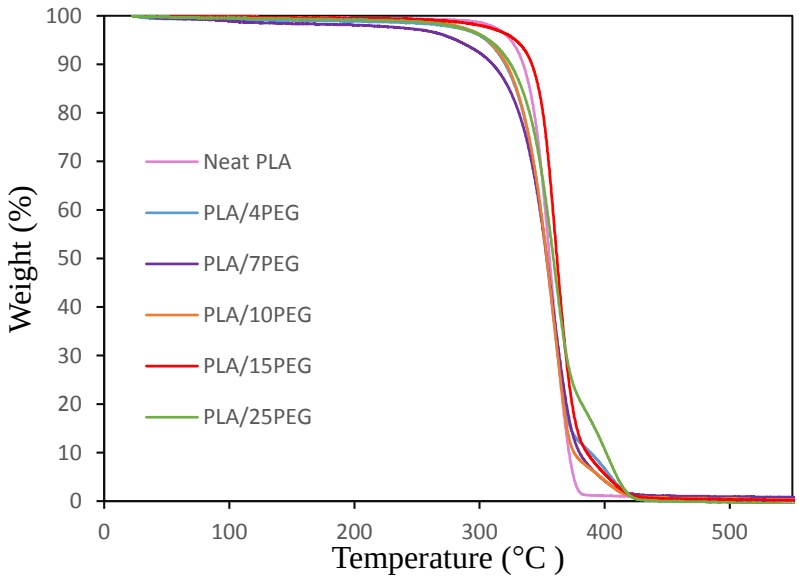

Figure 4.28 TGA curves for electrospun PLA/PEG samples.

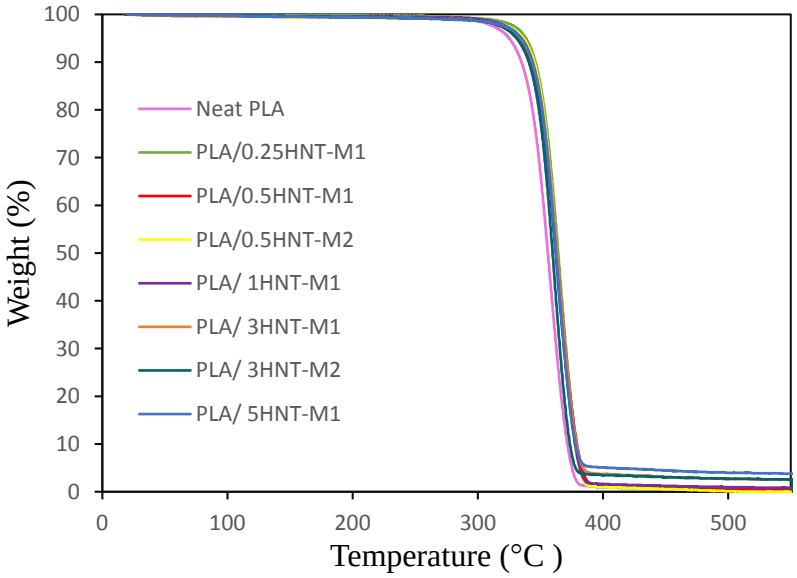

Figure 4.29 TGA curves for electrospun PLA/HNT samples.

Table 4.6 TGA data for electrospun PLA/PEG and PLA/HNT samples.

Sample	Decomposition Temperature (°C)	T_{10} (°C)	T_{25} (°C)	T_{50} (°C)
Neat PLA Fibers	362.45	334.99	346.48	355.87
PLA/4PEG	362.47	332.88	344.87	353.35
PLA/7PEG	363.81	343.06	352.90	360.74
PLA/10PEG	360.50	321.44	339.87	353.90
PLA/15PEG	364.68	331.35	347.43	359.41
PLA/25PEG	362.35	324.93	344.59	358.90
PLA/0.25HNT-M1	368.24	345.98	355.49	364.31
PLA/0.5HNT-M1	367.86	342.12	353.16	362.86
PLA/0.5HNT-M2	367.74	345.18	354.74	362.97
PLA/1HNT-M1	366.27	342.29	352.65	362.09
PLA/3HNT-M1	367.77	343.65	354.44	363.32
PLA/3HNT-M2	364.50	339.63	351.39	359.67
PLA/5HNT-M1	367.74	343.88	353.90	363.57

4.3.4 Tensile Test Results

Tensile test was carried out for PLA/PEG and PLA/HNT nanofibrous samples generated at different PEG and HNT concentrations, respectively. Moreover, the effect of solution preparation method on mechanical properties was also investigated for PLA/HNT samples at the same concentrations. The obtained results are presented in Figures 4.30-4.32. Moreover, the representative stress-strain graph and tabulated tensile data (i.e., tensile strength, tensile modulus, and elongation at break) are given in Figures A.3 and A.4 of Appendix A and Table B.3 of Appendix B, respectively.

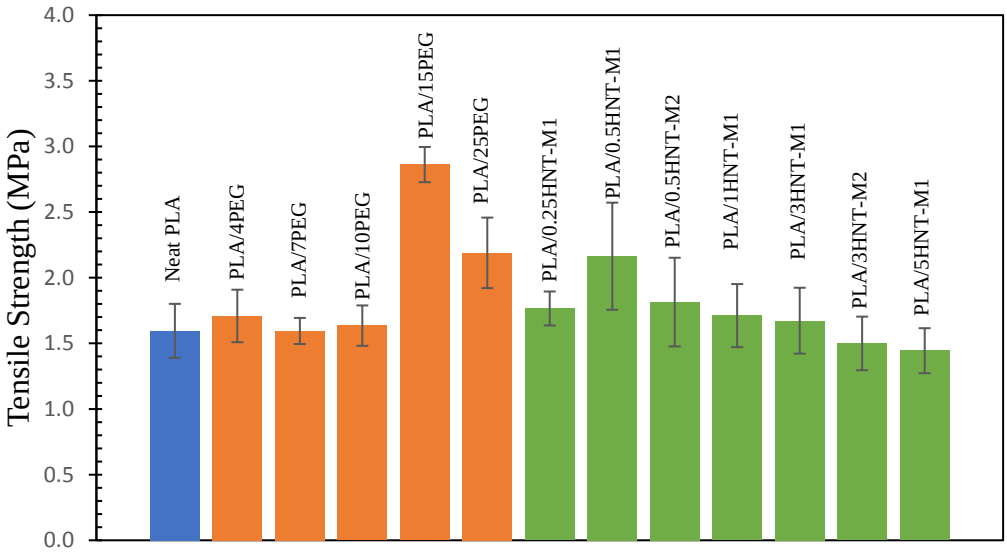

Figure 4.30 Tensile strengths of electrospun PLA/PEG and PLA/HNT.

According to the results, up to PEG concentration of 15 wt.%, tensile strength did not indicate a significant change as the standard deviation values are considered. When PEG concentration increased to 15 wt.%, tensile strength increased and then declined at 25 wt.% of PEG concentration when compared to neat PLA samples. On the other hand, increasing PEG concentration up to 15 wt.% caused a decreasing trend in the tensile modulus. At higher concentrations than 10 wt.% PEG, tensile modulus reached higher values. Elongation at break reached a maximum value at 15 wt.% of PEG concentration and as the concentration was increased to 25 wt.% PEG,

elongation showed a decline. These results can be attributed to the fact that PEG may behave as a plasticizer at a certain level of PEG concentration and then this behavior was broken with the increasing PEG concentration due to the excessive addition of PEG to the system [111]. This behavior could be attributed to the PEG and PLA having limited miscibility due to the surface energy difference, which leads to a phase separation at the surface of the generated fibers [116].

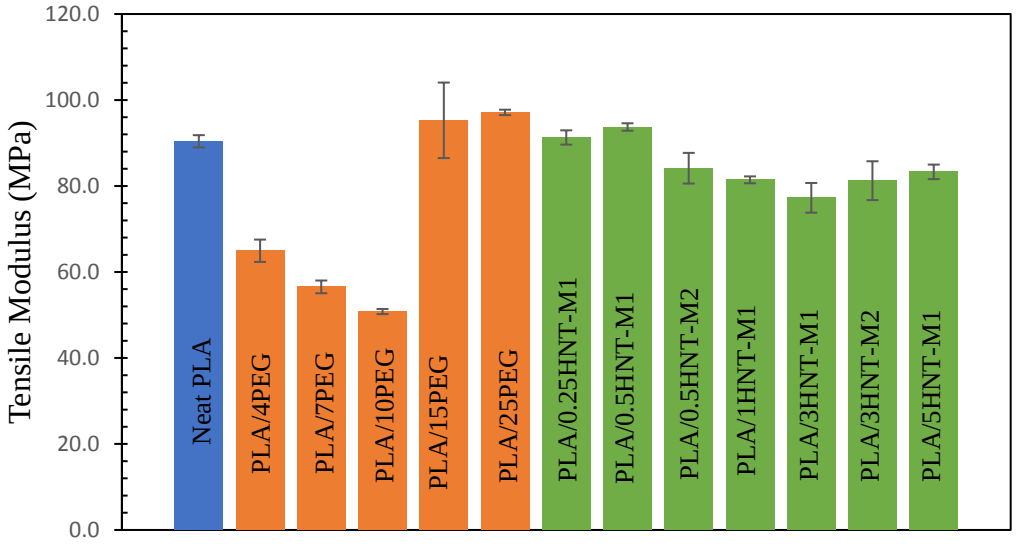

Figure 4.31 Tensile Moduli of electrospun PLA/PEG and PLA/HNT.

From the results, it can be deduced that improvement of the tensile strength and tensile modulus achieved on the nanocomposite samples of PLA/0.25HNT-M1 and PLA/0.5HNT-M1. This result indicates that these composite nanofibrous mats became stronger and stiffer, when compared to neat PLA nanofibers. The enhancement in mechanical performance of nanofillers on composite materials depends on the effective load transfer from the polymer matrix to the nanofillers [112], which can be obtained after the uniform dispersion of reinforcement material and achieving improved interactions of nanofiller and matrix [113]. The mechanism of enhanced nanofiller-matrix interactions can be attained by chemical bond formation and micromechanical interlocking.

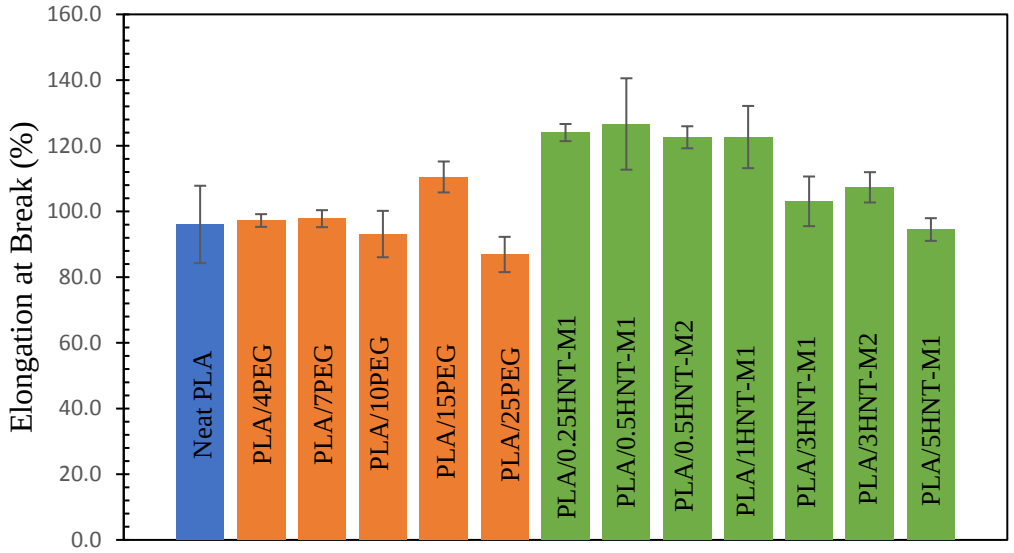

Figure 4.32 Elongation at break of electrospun PLA/PEG and PLA/HNT.

The effective interactions between HNT walls and PLA chains are provided by the hydrogen bonding between the carbonyl groups (C=O) of PLA and the hydroxyl groups of HNT [100]. On the other hand, increasing HNT concentration to values greater than 0.5 wt.% did not further improve the mechanical properties. As the HNT content increases, both tensile strength and tensile modulus showed a decline. This can be caused by the poor dispersion of HNTs in the polymer matrix which resulted in agglomerated nanotubes. The desired nanofiller-matrix interfacial interactions cannot be formed in the samples with agglomerations which weaken the effective load transfer occurring from the matrix to the reinforcement material. Therefore, a reduction in the mechanical performance can be obtained due to the nanotube aggregates behaving as defects [105]. For the concentrations of 0.5 wt.% HNT and 3 wt.% HNT, applying different solution preparation methods did not cause a significant change when the standard deviation values were taken into account. Elongation at break values of generated nanofibrous samples containing HNTs reached higher values than PLA sample with the increasing nanotubes concentration up to 3 wt.%. As it was mentioned before, free volume might increase due the increase in HNT concentration [108]. Therefore, the increase in the free volume

enables to obtain an increase in polymer chain mobility which tends to result in an increase of elongation.

4.4 Effect of Solution Preparation Methods on PLA/PEG/HNT Nanofibers

The studies for determining the optimum solution preparation method were performed after obtaining the optimum PEG and HNTs concentrations (15 and 0.5 wt.%, respectively) by carrying out electrospinning process for the two components systems and using suitable parameter values for the electrospinning process by the parametric studies on the electrospinning of neat PLA. For this purpose, different solution preparation methods were applied. While generating nanofibrous PLA/PEG/HNT mats, the process parameters were applied as 1 ml/h of solution feed rate, 20 cm of tip-to-collector distance, and 20 kV of applied voltage. Moreover, solution concentration and solvent ratio were kept constant at 13 wt.% and 80/20 v/v CHL/DMF, respectively. In this section, the obtained results are presented in terms of morphology, thermal and mechanical properties of the related samples.

4.4.1 Scanning Electron Microscopy Analysis

The SEM micrographs of electrospun PLA/PEG/HNT nanofibers are presented in Figure 4.33. In addition, the average fiber diameter data are given in Figure 4.34. From the SEM micrographs, it can be deduced that randomly oriented fibers were generated as in the electrospinning of neat PLA. Moreover, with the inclusion of PEG and HNTs, the average fiber diameter showed lower values than the value for the neat PLA sample generated at the optimum electrospinning parameters. This result can be attributed to the decrease in the solution viscosity with PEG addition. As the solution viscosity decreases, the polymer chain movement enhances. As a result, thinner fibers are formed.

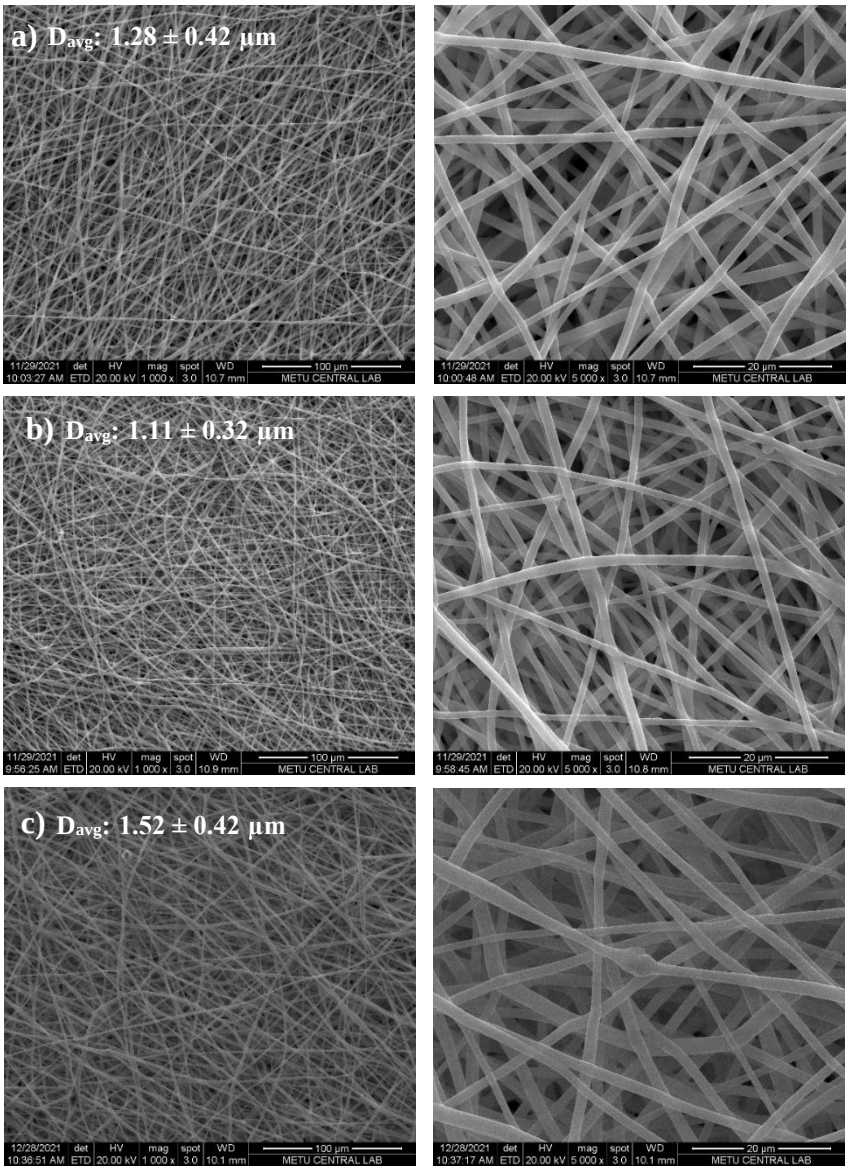

Figure 4.33 SEM micrographs of electrospun PLA/PEG/HNT with solution preparation methods of a) M1, b) 0.5 wt.% HNT-M2 and c) 3 wt.% HNT-M2, d) M3, e) M4 and f) M5 (AV: 20 kV, TCD: 20 cm, SFR: 1 ml/h, CT: cylinder, RS: 100 rpm, ED: 3 h, SR: 80/20 v/v).

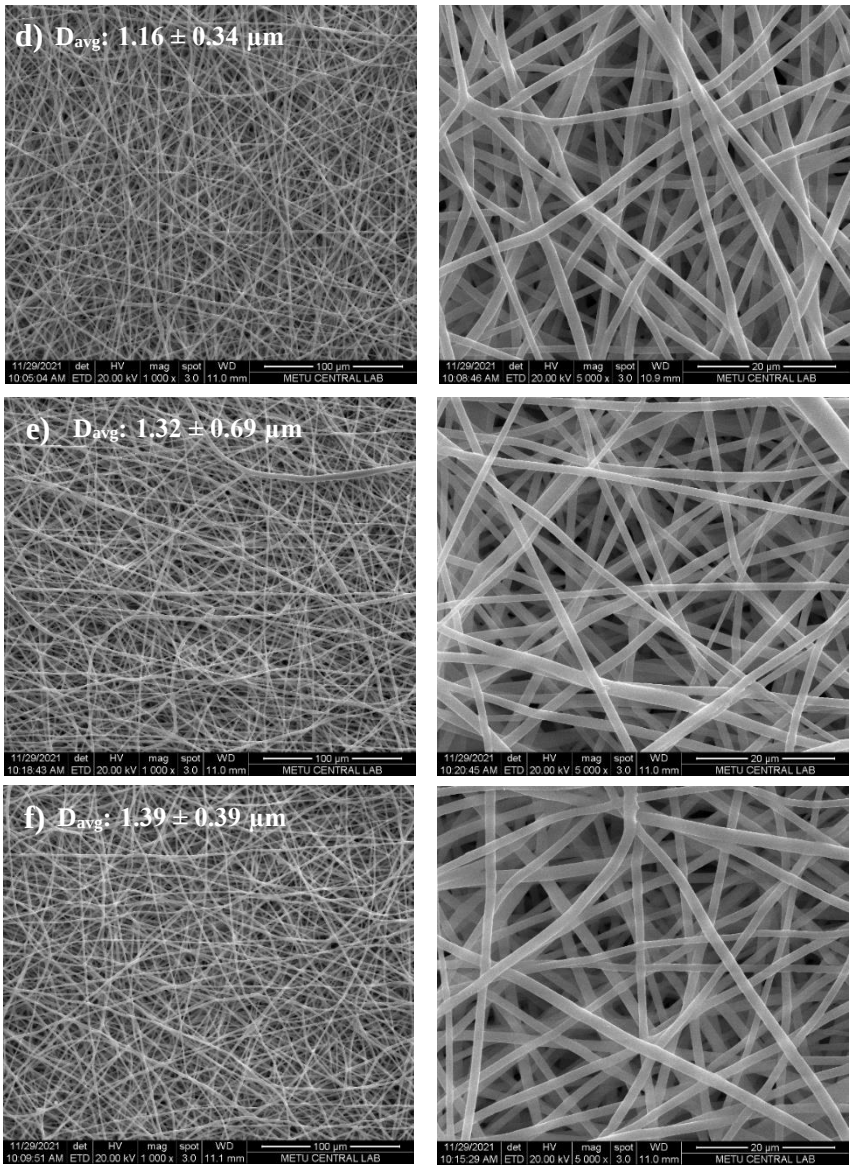

Figure 4.33 (continued) SEM micrographs of electrospun PLA/PEG/HNT with solution preparation methods of a) M1, b) 0.5 wt.% HNT-M2 and c) 3 wt.% HNT-M2, d) M3, e) M4 and f) M5 (AV: 20 kV, TCD: 20 cm, SFR: 1 ml/h, CT: cylinder, RS: 100 rpm, ED: 3 h, SR: 80/20 v/v).

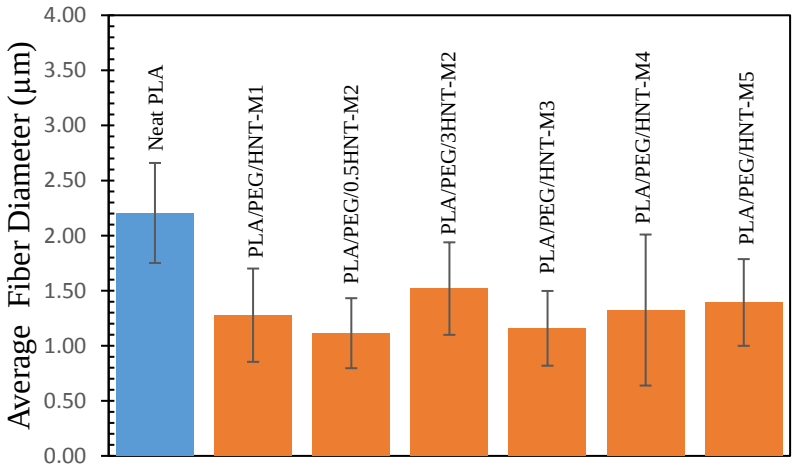

Figure 4.34 Bar graph depicting average fiber diameters of PLAPEG/HNT samples prepared by different solution preparation methods.

In addition, when the standard deviation values are considered for the solution preparation methods of PLA/PEG/HNT-M1 and PLA/PEG/0.5HNT-M2, it can be seen that application of second method did not have a crucial effect on average fiber diameter value compared to first method. On the other hand, increasing the HNTs concentration in the second solution preparation method for PLA/PEG/HNT samples increased the average fiber diameter value. This result can be explained by the enhanced solution viscosity due to the addition of HNTs to the polymer solution. As a result, the stretching of the jet was restricted during the electrospinning process, and fiber diameter increased with the increasing HNTs concentration [70]. The highest standard deviation value belongs to the sample of PLA/PEG/HNT-M4. The lowest standard deviation value was obtained for the sample PLA/PEG/0.5HNT-M2.

4.4.2 Differential Scanning Calorimetry Analysis

DSC analysis was performed for the PLA/PEG/HNT nanofibrous samples generated from the solutions prepared with different methods. The plotted DSC curves are presented in Figure 4.35. Moreover, thermal properties (i.e., glass transition temperature (T_g), cold crystallization temperature (T_{cc}), enthalpy of cold

crystallization (ΔH_{cc}), melting temperature (T_m), enthalpy of melting (ΔH_m) and degree of crystallization (X_c)) values are given in Table 4.7.

According to the results, PLA/PEG/HNT samples had lower T_g values than the T_g of neat PLA fibers. As it was discussed in the previous section, with the inclusion of PEG to the system, polymer chain mobility is enhanced which results in a decrease in glass transition and cold crystallization temperatures [101]. Moreover, with the addition of HNTs, free volume is increased and thus the polymer chain mobility. As a result, a drop in T_g is observed [100]. On the other hand, as the HNTs concentration was increased for the sample PLA/PEG/3HNT-M2, T_{cc} showed an increase. This increase can be caused by the poor dispersion of HNTs in polymer matrix which resulted in agglomerated nanotubes. The melting temperature of PEG was determined as 62.20°C for the sample of PLA/PEG/0.5 HNT-M2. Furthermore, inclusion of PEG and HNTs resulted in PLA/PEG/HNT samples having higher degree of crystallization values than neat PLA fibers. This result can be attributed to the nucleation effect of HNTs [100]. In addition, PEG addition allowed to have such rearrangements so that samples can easily reach higher X_c values [101]. T_m values of PLA/PEG/HNT nanocomposite fibers did not show a significant change.

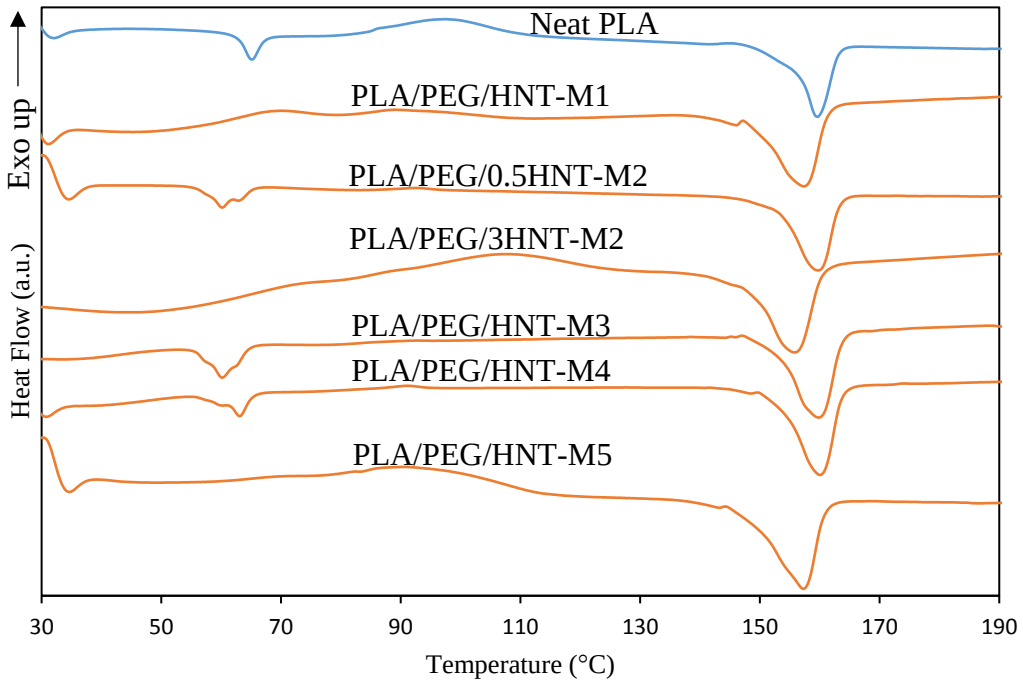

Figure 4.35 DSC curves for electrospun PLA/PEG/HNT.

Table 4.7 DSC data for electrospun PLA/PEG/HNT.

Sample	T_g (°C)	T_{cc} (°C)	ΔH_{cc} (J/g)	T_m (°C)	ΔH_m (J/g)	X_c (%)
Neat PLA Fibers	64.33	98.37	17.26	160.15	31.38	15.07
PLA/PEG/HNT-M1	-	88.97	1.66	157.36	32.20	38.86
PLA/PEG/0.5HNT-M2	58.72	92.56	0.35	159.65	30.76	38.70
PLA/PEG/3HNT-M2	-	107.60	6.79	155.85	30.71	31.37
PLA/PEG/HNT-M3	59.61	-	-	159.87	32.02	40.75
PLA/PEG/HNT-M4	58.71	91.04	0.25	160.08	30.12	38.01
PLA/PEG/HNT-M5	-	91.91	4.59	157.17	30.16	32.54

4.4.3 Thermogravimetric Analysis

Thermogravimetric analysis (TGA) was conducted for PLA/PEG/HNT nanofibrous samples generated from the solutions prepared with different methods. Percent

weight loss versus temperature graphs of PLA/PEG/HNT fibers can be seen in Figure 4.36. In addition to attaining thermal stability information of the electrospun mats, the decomposition temperature, 10% weight loss temperature (T_{10}), 25% weight loss temperature (T_{25}), and the half weight loss temperature (T_{50}) of nanofibrous samples at different parameters were determined and are presented in Table 4.8. As it can be seen from the results, single step degradation was observed for all samples. Except for the sample PLA/PEG/3HNT-M2, the thermal stability was not crucially affected by the solution preparation method. On the other hand, a decrease in the thermal stability of the sample PLA/PEG/3HNT-M2 was obtained. As it was mentioned before, agglomerated structure was observed for the sample PLA/PEG/3HNT-M2. The increase of HNTs concentration might overcome the synergistic effect of HNT and PEG on the PLA.

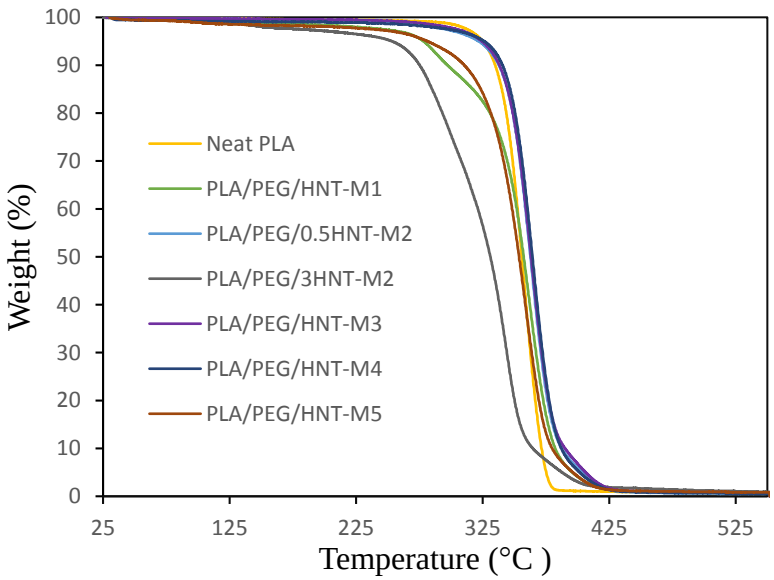

Figure 4.36 TGA curves for electrospun PLA/PEG/HNT.

Table 4.8 TGA data for electrospun PLA/PEG/HNT.

Sample	Decomposition Temperature (°C)	T_{10} (°C)	T_{25} (°C)	T_{50} (°C)
Neat PLA Fibers	362.45	334.99	346.48	355.87
PLA/PEG/HNT-M1	364.80	297.20	338.81	357.40
PLA/PEG/0.5HNT-M2	365.97	337.86	352.08	362.43
PLA/PEG/3HNT-M2	345.15	275.25	300.64	331.18
PLA/PEG/HNT-M3	366.45	338.87	352.31	363.25
PLA/PEG/HNT-M4	368.11	340.63	353.74	364.26
PLA/PEG/HNT-M5	362.22	312.18	337.56	353.84

4.4.4 Tensile Test Results

Tensile Test was carried out for PLA/PEG/HNT nanofibrous samples produced from the solutions prepared with different methods. The obtained results are presented in Figures 4.37-4.39. Moreover, the representative stress-straing graph and tabulated tensile data (i.e., tensile strength, tensile modulus, and elongation at break) are given in Figure A.5 of Appendix A and Table B.4 of Appendix B sections, respectively.

According to the results, when it is compared with neat PLA fibers, an enhancement was observed in tensile strength, tensile modulus and elonftaion at break for the samples PLA/PEG/HNT-M1, PLA/PEG/0.5HNT-M2 and PLA/PEG/HNT-M3. This enhancement can be attributed to the good dispersion of HNTs [113]. In the second method, the sonication of HNTs resulted in greater tensile strength and tensile modulus values than the ones in first method. Sonication of HNTs offered a better dispersion of reinforcement material than the magnetic stirrer, which resulted in an improvement in mechanical properties. Moreover, diminution in the mechanical properties was seen for the samples PLA/PEG/HNT-M4 and PLA/PEG/HNT-M5. For the sample PLA/PEG/HNT-M4, the gradually addition of PEG might cause a poor compatibilizer effect between PLA and HNTs which resulted in a decrease of mechanical properties. In addition, for PLA/PEG/HNT-M5, this decrease might be caused by the poor dispersion of HNTs in the PLA/PEG solution since the

distribution had to occur in a more viscous system than the binary solvent system. On the other hand, when the standard deviation values are taken into account, applying different solution preparation methods did not have a significant impact on the mechanical properties of the samples PLA/PEG/HNT-M4 and PLA/PEG/HNT-M5 since both methods showed similar mechanical property values.

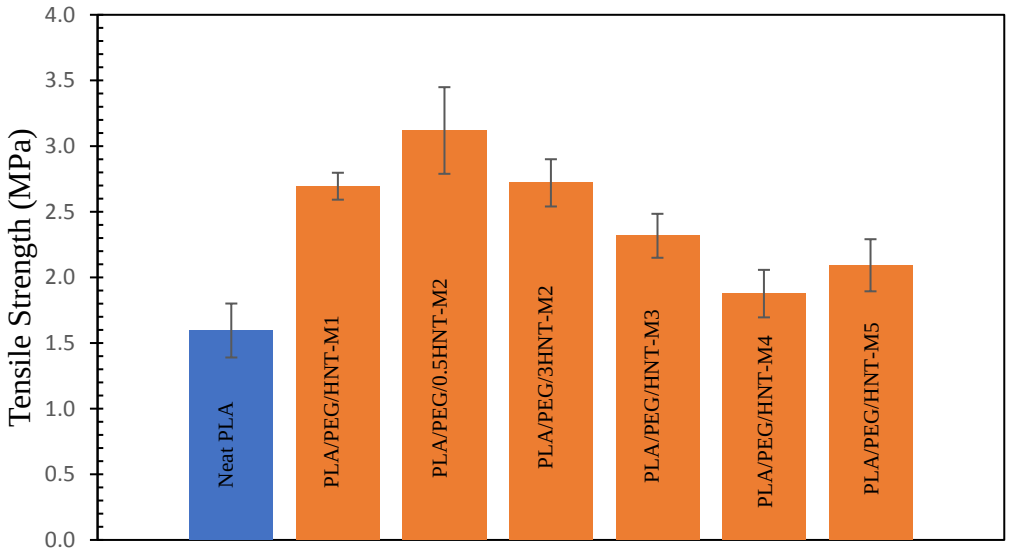

Figure 4.37 Tensile strengths of electrospun PLA/PEG/HNT.

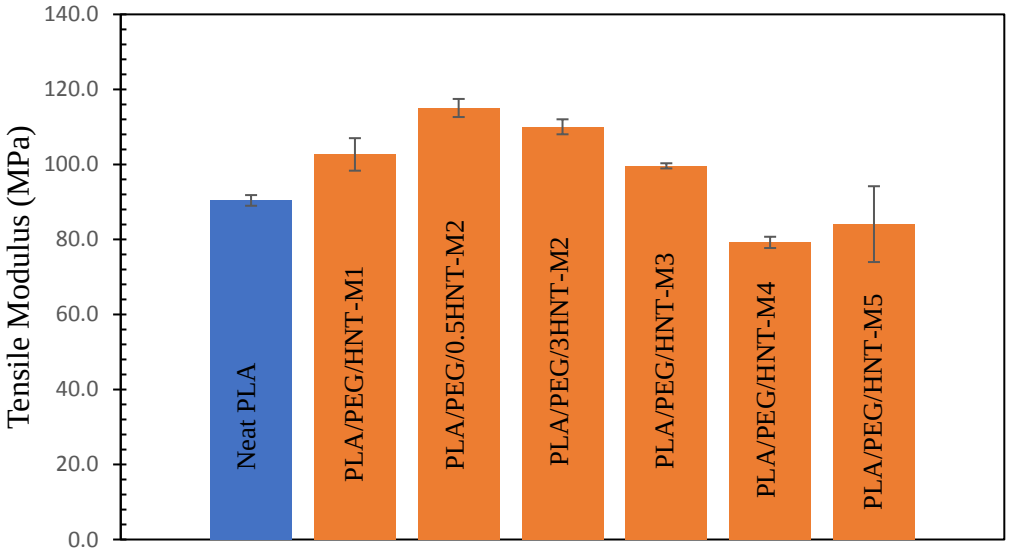

Figure 4.38 Tensile Moduli of electrospun PLA/PEG/HNT.

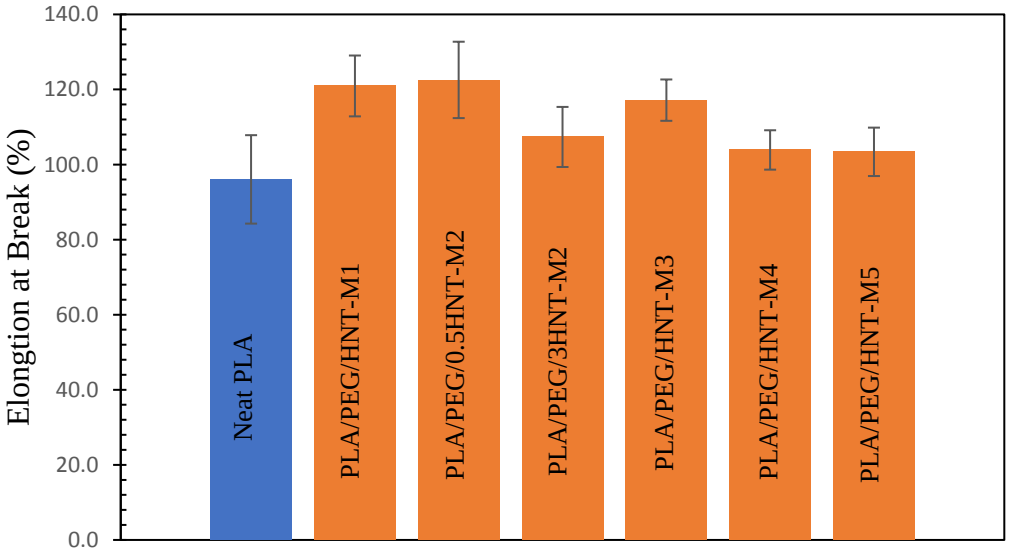

Figure 4.39 Elongation at break of electrospun PLA/PEG/HNT.

4.5 Water Contact Angle Measurements

Water contact angle measurements were performed for the generated samples by electrospinning process. Moreover, neat PLA film was prepared by solvent casting

method in which polymer solution with a concentration of 13 wt.% PLA were prepared and cast on a glass petri dish. Water contact angle measurement was done for the cast PLA film in order to compare the resulting angles with nanofibrous neat PLA mat generated at polymer concentration of 13 wt.%. The resulting contact angles are shown in Figures 4.40-4.43 and the tabulated contact angle data are given in Appendix C.

As it was mentioned before, electrospinning parameters may have an indirect influence on the contact angle values since those parameters affect the sample morphology [65]. According to Figure 4.40, when the standard deviation values are considered, it can be seen that increasing polymer solution concentration, solution feed rate, tip-top-collector distance and binary solvent ratio did not affect the contact angle significantly. As the average fiber diameter values are compared, the increase in the polymer solution concentration, solution feed rate, collection distance and solvent composition did not cause a significant change. Therefore, contact angle values close to each other were obtained for those parameters. Similarly, as the standard deviation values are taken into account, increase in the applied voltage from 17 kV to 20 kV did not result in a change in the water contact angle. On the other hand, the highest standard deviation value was obtained with the applied voltage of 23 kV. This result is caused by the sample morphology. Since excess electrostatic forces were exerted on the PLA solution at 23 kV during the electrospinning process, unstable Taylor Cone formation was obtained. This resulted in the generation of thick fibers besides the thin ones and increased the standard deviation value of the fiber diameter which affecting the surface morphology and thus water contact angle. Furthermore, cast neat PLA film had a smaller water contact angle ($140 \pm 2.0°$) than the value of electrospun neat PLA mats. This result could be attributed to the surface roughness of the samples. As it was claimed before, hydrophobicity is dependent on surface morphology and therefore rougher surfaces resulted in high water contact angle. The PLA film prepared by solvent casting method had a smooth surface which resulted in lower contact angle [67].

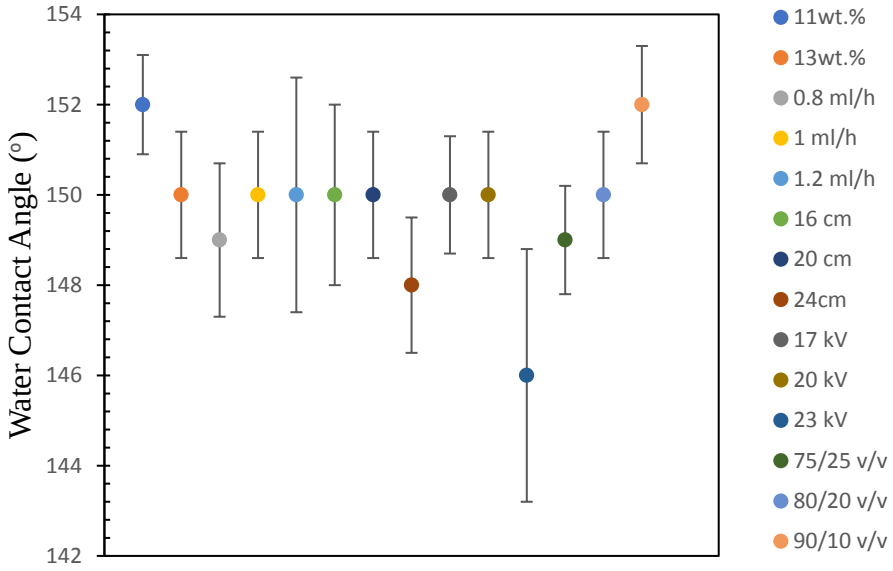

Figure 4.40 Contact angle measurements of nanofibers generated by parameter study.

In order to investigate the influence of PEG concentration on the wetting ability of electrospun PLA/PEG samples, water contact angle measurements were conducted with samples generated at different PEG concentrations. It can be clearly seen in Figure 4.41 that among all samples, the highest water contact angle value at 150° was reached at the neat PLA nanofibrous mat. Moreover, with the increase in the PEG concentration water contact angle showed a decreasing trend. From the results, it can be concluded that the inclusion of PEG decreased the hydrophobicity of

electrospun PLA/PEG samples since PEG is a hydrophilic polymer [111].

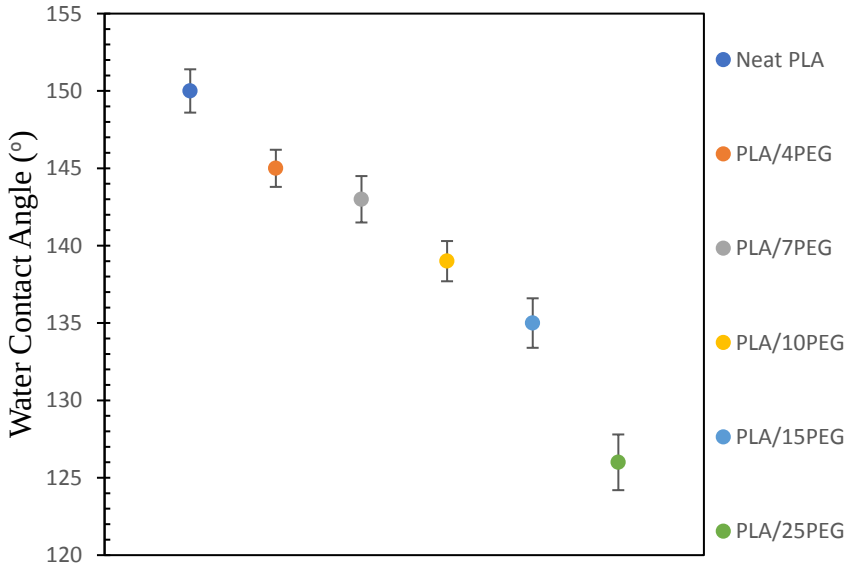

Figure 4.41 Contact angle measurements of electrospun PLA/PEG samples.

To study the effect of HNTs concentration on the wettability of nanofibrous PLA/HNT mats, water conduct angle measurements were performed with samples produced at different HNTs concentrations. As it is seen in Figure 4.42 the water contact angle of the nanofibrous samples have a decreasing trend with the increase in HNTs concentration. Therefore, it can be concluded that the hydrophobicity of electrospun samples was affected by HNTs concentration. This effect can be explained by the capillary action of HNTs and hence their good wettability behavior [114]. Due to the hydophilic groups (Al-OH and Si-OH), HNTs contain on its surface beside the silica and alumina groups at the crystal edges, the hydrogen bonds are easily able to form between HNTs and water [115]. When the standard deviation values were considered for the electrospinning of PLA/HNT, it can be seen that carrying out the second solution preparation method at the HNTs concentration of 0.5 wt.% resulted in slightly lower water contact angle values with the ones generated with the electrospinning solution prepared by the first method. Similarly, applying different solution preparation methods exhibited slightly lower wettability

and water contact angle values of the PLA/HNT nanofibrous samples at the HNTs concentration of 3 wt.% as expected due to the hyrophilic nature of HNTs.

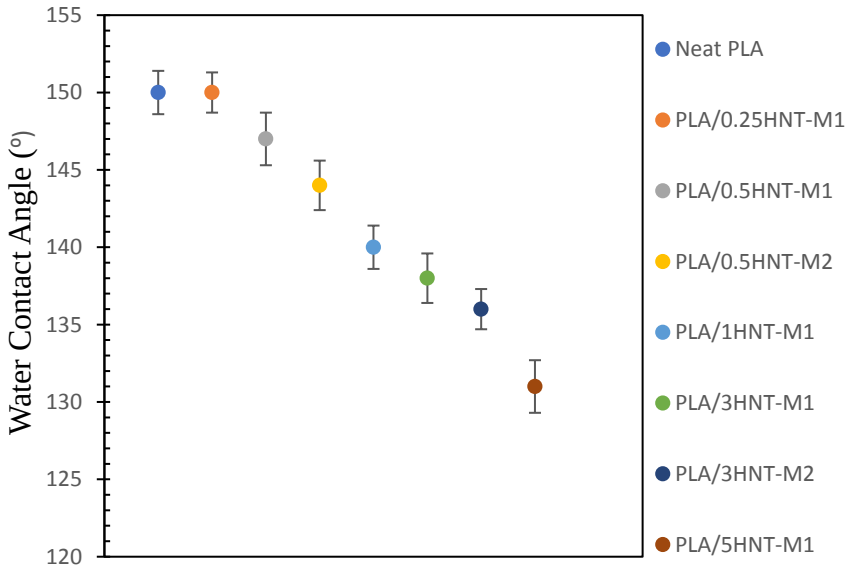

Figure 4.42 Contact angle measurements of electrospun PLA/HNT samples.

For the investigation of the impact of PEG and HNTs inclusion as well as polymer solution preparation methods on the wettability of nanofibrous PLA/PEG/HNT mats, water contact angle measurements were carried out with PLA/PEG/HNT samples produced with different solution preparation methods. As it was given in Figure 4.43 the water contact angle of the nanofibrous samples have a decreasing trend with the PEG and HNTs addition. Therefore, as expected, it can be seen that the hydrophobic behavior of electrospun samples was affected by PEG and HNTs in the system. Furthermore, as the standard deviation values are taken into account, it can be concluded that applying different polymer solution preparation methods did not have an important influence on the water contact angle values of electrospun PLA/PEG/HNT samples.

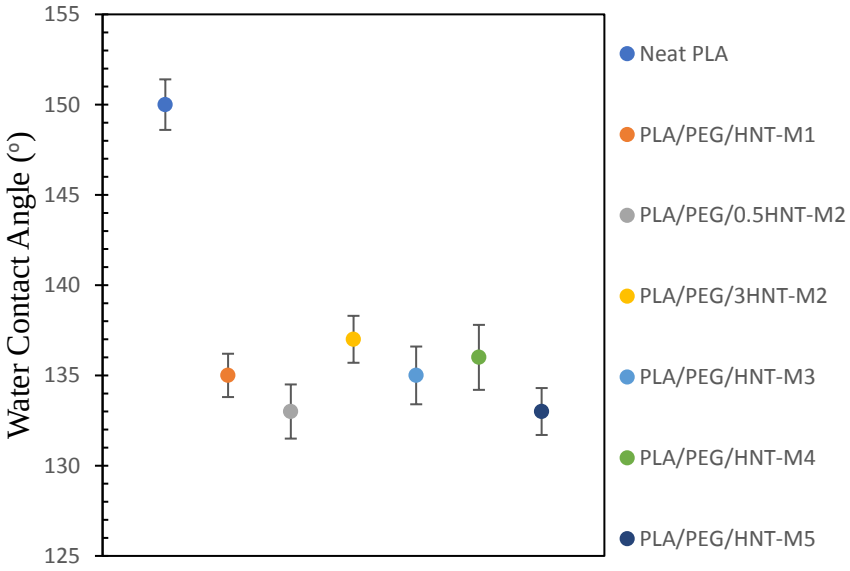

Figure 4.43: Contact angle measurements of electrospun PLA/PEG/HNT samples.

CHAPTER 5

CONCLUSIONS

The following results were obtained when all of the performed experiments within the thesis scope were reviewed:

1. Neat PLA, PLA/PEG, PLA/HNT, and PLA/PEG/HNT nanofibers were successfully generated by electrospinning method.
2. Optimization of process parameters such as solution feed rate, tip-to collector distance and applied voltage were successfully investigated. The optimum conditions for the electrospinning of fibrous neat PLA mats were determined as 1 ml/h of solution feed rate, 20 cm of tip-to-collector distance and 20 kV of applied voltage.
3. The influence of solution concentration and solvent ratio on the fiber morphology were also examined. It was found that at low solution concentrations, beaded morphologies were obtained. Moreover, as the solution concentration increases, fibrous morphologies were observed. As a result, 13 wt.% PLA of solution concentration and binary solvent system of CHL and DMF in 80/20 ratio by volume was identified as the optimum solution parameters.
4. The optimum parameters determined for neat PLA fiber production were also successfully applied to fibrous PLA/PEG and PLA/HNT mat generation.
5. The suitable PEG and HNT concentrations were investigated for PLA/PEG and PLA/HNT fibers, respectively. With respect to the enhancement in the mechanical properties, 15 wt.% of PEG concentration and 0.5 wt.% of HNT concentration in PLA matrix were found to be the optimum values.
6. Throughout the production of PLA/PEG/HNT fibers, the impact of solution preparation methods was studied. According to the results, the second solution preparation method, in which ultrasonication of HNT particles, and addition of PLA and PEG to HNTs suspension were involved, was found to

be the better choice in terms of morphology, thermal and mechanical properties.

7. The WCA of neat electrospun PLA was measured as ~150°. This value decreased with the addition of PEG and HNTs due to their hydrophilic nature.

REFERENCES

[1] Ramakrishna, S., K. Fujihara, W.E. Teo, T.C. Lim, Z. Ma (2005). An introduction to electrospinning and nanofibers. Hackensack, NJ: World Scientific. doi:10.1142/5894

[2] Xue, J., Wu, T., Dai, Y., Xia, Y. (2019). Electrospinning and electrospun nanofibers: Methods, materials, and applications. Chemical Reviews, 119(8), 5298-5415.

[3] Bhardwaj, N., Kundu, S. C. (2010). Electrospinning: a fascinating fiber fabrication technique. Biotechnology advances, 28(3), 325-347.].

[4] Bohlmann, G. M. (2005). General characteristics, processability, industrial applications and market evolution of biodegradable polymers. Handbook of biodegradable polymers, 183-218.

[5] Liu, H. and Zhang, J. (2011). Research progress in toughening modification of poly (lactic acid). Journal of polymer science part B: Polymer Physics, 49(15), 1051-1083.

[6] Hartmann H., (1998). High molecular weight polylactic acid polymers. In Kaplan D.L. (Ed.). Biopolymers from Renewable Resources, Berlin, Germany: Springer-Verlag, 367-411.

[7] Kharas G. B., Sanchez-Riera F., Severson D.K., (1994). Polymers of Lactic Acid. In Mobley D.P. (Ed.), Plastics from Microbes, New York, United States: Hanser Publishers, 92-238.

[8] Witzke D. R., (1997). Introduction to Properties, Engineering, and Prospects of Polylactide Polymers, in Chemical Engineering. Michigan State University: East Lansing, Michigan. 32-72.

[9] Jamshidian, M., Tehrany, E. A., Imran, M., Jacquot, M., Desobry, S. (2010). Poly-Lactic Acid: Production, Applications, Nanocomposites, and Release Studies.

Comprehensive Reviews in Food Science and Food Safety, 9(5), 552– 571. doi:10.1111/j.1541-4337.2010.00126.x

[10] Auras, R., Lim, L.-T., Selke, S. E. ., Tsuji, H. (Eds.). (2010). Poly(lactic acid): Synthesis, Structures, Properties, Processing, and Application. New Jersey, United States of America: John Wiley & Sons, Inc.

[11] Hakkarainen M., Wistrand A. F. (2011). Update on Polylactide Based Materials. Shropshire, England: iSmithers Rapra Publishing (p.7).

[12] Lasprilla, A. J. R., Martinez, G. a R., Lunelli, B. H., Jardini, A. L., Filho, R. M. (2012). Poly-lactic acid synthesis for application in biomedical devices a review. Biotechnology Advances, 30(1), 321–8

[13] Moon, S. I., Kimura, Y. (2003). Melt polycondensation of L-lactic acid to poly(L-lactic acid) with Sn(II) catalysts combined with various metal alkoxides. Polymer International, 52(2), 299–303. doi:10.1002/pi.960

[14] Baiardo, M., Frisoni, G., Scandola, M., Rimelen, M., Lips, D., Ruffieux, K., Wintermantel, E. (2003). Thermal and mechanical properties of plasticized poly (L-lactic acid). Journal of Applied Polymer Science, 90(7), 1731-1738.

[15] Cavallaro, G., De Lisi, R., Lazzara, G., Milioto, S. (2013). Polyethylene glycol/clay nanotubes composites. Journal of thermal analysis and calorimetry, 112(1), 383-389.

[16] Thanakkasaranee, S. and Seo, J. (2019). Effect of halloysite nanotubes on shape stabilities of polyethylene glycol-based composite phase change materials. International Journal of Heat and Mass Transfer, 132, 154-161.

[17] Erpek, C. E. Y., Ozkoc, G., Yilmazer, U. (2016). Effects of halloysite nanotubes on the performance of plasticized poly (lactic acid)-based composites. Polymer Composites, 11(37), 3134-3148.

[18] Sharma, S., Singh, A. A., Majumdar, A., Butola, B. S. (2019). Tailoring the mechanical and thermal properties of polylactic acid-based bionanocomposite films

using halloysite nanotubes and polyethylene glycol by solvent casting process. Journal of materials science, 54(12), 8971-8983.

[19] Nikalje, A. P. (2015). Nanotechnology and its Applications in Medicine, 5, 1–3. https://doi.org/10.4172/2161

[20] Vilchez, A., Acevedo, F., Cea, M., Seeger, M., Navia, R. (2020). Applications of electrospun nanofibers with antioxidant properties: A review. Nanomaterials, 10(1), 175

[21] Agarwal, S., Burgard, M., Greiner, A., Wendorff, J. (2016). Electrospinning. In Electrospinning. de Gruyter.

[22] Alghoraibi, I., Alomari, S. (2018). Different methods for nanofiber design and fabrication. Handbook of nanofibers, 1-46.

[23] Tripatanasuwan, S., Zhong, Z., Reneker, D. H. (2007). Effect of evaporation and solidification of the charged jet in electrospinning of poly (ethylene oxide) aqueous solution. Polymer, 48(19), 5742-5746.

[24] Nezarati, R. M., Eifert, M. B., Cosgriff-Hernandez, E. (2013). Effects of humidity and solution viscosity on electrospun fiber morphology. Tissue Engineering Part C: Methods, 19(10), 810-819.

[25] Doshi, J., Reneker, D. H. (1995). Electrospinning process and applications of electrospun fibers. Journal of electrostatics, 35(2-3), 151-160.

[26] Haider, A., Haider, S., Kang, I. K. (2018). A comprehensive review summarizing the effect of electrospinning parameters and potential applications of nanofibers in biomedical and biotechnology. Arabian Journal of Chemistry, 11(8), 1165-1188.

[27] Ki, C. S., Baek, D. H., Gang, K. D., Lee, K. H., Um, I. C., Park, Y. H. (2005). Characterization of gelatin nanofiber prepared from gelatin–formic acid solution. Polymer, 46(14), 5094-5102

[28] Z. Li, C. Wang, One-Dimensional nanostructures, 2013. doi:10.1007/978-3-642-36427-3.

[29] Tan SH, Inai R, Kotaki M, Ramakrishna S. Systematic parameter study for ultra-fine fiber fabrication via electrospinning process. Polymer 2005b; 46:6128–34.

[30] Koski, A., Yim, K., Shivkumar, S. J. M. L. (2004). Effect of molecular weight on fibrous PVA produced by electrospinning. Materials Letters, 58(3-4), 493-497.

[31] Zong, X., Kim, K., Fang, D., Ran, S., Hsiao, B. S., Chu, B. (2002). Structure and process relationship of electrospun bioabsorbable nanofiber membranes. polymer, 43(16), 4403-4412.

[32] Yang, Q., Li, Z., Hong, Y., Zhao, Y., Qiu, S., Wang, C. E., Wei, Y. (2004). Influence of solvents on the formation of ultrathin uniform poly (vinyl pyrrolidone) nanofibers with electrospinning. Journal of Polymer Science Part B: Polymer Physics, 42(20), 3721-3726.

[33] Pant, H. R., Bajgai, M. P., Yi, C., Nirmala, R., Nam, K. T., Baek, W. I., Kim, H. Y. (2010). Effect of successive electrospinning and the strength of hydrogen bond on the morphology of electrospun nylon-6 nanofibers. Colloids and Surfaces A: Physicochemical and Engineering Aspects, 370(1-3), 87-94.

[34] Buchko, C. J., Chen, L. C., Shen, Y., Martin, D. C. (1999). Processing and microstructural characterization of porous biocompatible protein polymer thin films. Polymer, 40(26), 7397-7407.

[35] Deitzel, J. M., Kleinmeyer, J., Harris, D. E. A., Tan, N. B. (2001). The effect of processing variables on the morphology of electrospun nanofibers and textiles. Polymer, 42(1), 261-272.

[36] Yördem, O. S., Papila, M., Menceloğlu, Y. Z. (2008). Effects of electrospinning parameters on polyacrylonitrile nanofiber diameter: An investigation by response surface methodology. Materials & Design, 29(1), 34-44.]

[37] Mazoochi, T., Hamadanian, M., Ahmadi, M., Jabbari, V. (2012). Investigation on the morphological characteristics of nanofiberous membrane as electrospun in the different processing parameters. International Journal of Industrial Chemistry, 3(1), 1-8.]

[38] Zuo, W., Zhu, M., Yang, W., Yu, H., Chen, Y., Zhang, Y. (2005). Experimental study on relationship between jet instability and formation of beaded fibers during electrospinning. Polymer Engineering & Science, 45(5), 704-709.

[39] Casper, C. L., Stephens, J. S., Tassi, N. G., Chase, D. B., Rabolt, J. F. (2004). Controlling surface morphology of electrospun polystyrene fibers: effect of humidity and molecular weight in the electrospinning process. Macromolecules, 37(2), 573-578.

[40] Natarajan, L., New, J., Dasari, A., Yu, S., Manan, M. A. (2014). Surface morphology of electrospun PLA fibers: mechanisms of pore formation. RSC Advances, 4(83), 44082-44088.

[41] Wang, C., Chien, H. S., Hsu, C. H., Wang, Y. C., Wang, C. T., Lu, H. A. (2007). Electrospinning of polyacrylonitrile solutions at elevated temperatures. Macromolecules, 40(22), 7973-7983.

[42] De Vrieze, S., Van Camp, T., Nelvig, A., Hagström, B., Westbroek, P., De Clerck, K. (2009). The effect of temperature and humidity on electrospinning. Journal of Materials Science, 44(5), 1357-1362.

[43] Casasola, R., Thomas, N. L., Trybala, A., Georgiadou, S. (2014). Electrospun poly lactic acid (PLA) fibres: Effect of different solvent systems on fibre morphology and diameter. Polymer, 55(18), 4728-4737.

[44] Menczel, J. D., Prime, R. B. (Eds.). (2009). Thermal analysis of polymers: fundamentals and applications. John Wiley & Sons.

[45] Shah V., "Handbook of Plastics Testing Technology", John Wiley & Sons, Inc., New York, 1998.

[46] Scheirs J., “Compositional and Failure Analysis of Polymers”, John Wiley & Sons, Inc., New York, 2000.

[47] Ramdhanie, L.I.; Aubuchon, S.R.; Boland, E.D.; Knapp, D.C.; Barnes, C.P.; Simpson, D.G.; Wnek, G.E.; Bowlin, G.L. Thermal and mechanical characterization of electrospun blends of poly(lactic acid) and poly(glycolic acid). Polym. J. 2006, 38, 1137–1145.

[48] Zhao, S., Wu, X., Wang, L., Huang, Y. (2004). Electrospinning of ethyl–cyanoethyl cellulose/tetrahydrofuran solutions. Journal of Applied Polymer Science, 91(1), 242-246.

[49] Ero-Phillips, O., Jenkins, M., Stamboulis, A. (2012). Tailoring crystallinity of electrospun plla fibres by control of electrospinning parameters. Polymers, 4(3), 1331-1348.]

[50] Kim, J. I., Pant, H. R., Sim, H. J., Lee, K. M., Kim, C. S. (2014). Electrospun propolis/polyurethane composite nanofibers for biomedical applications. Materials Science and Engineering: C, 44, 52-57.]

[51] Lins, L. C., Wianny, F., Livi, S., Hidalgo, I. A., Dehay, C., Duchet-Rumeau, J., Gérard, J. F. (2016). Development of bioresorbable hydrophilic–hydrophobic electrospun scaffolds for neural tissue engineering. Biomacromolecules, 17(10), 3172-3187.

[52] Jeong, J. S., Moon, J. S., Jeon, S. Y., Park, J. H., Alegaonkar, P. S., Yoo, J. B. (2007). Mechanical properties of electrospun PVA/MWNTs composite nanofibers. Thin Solid Films, 515(12), 5136-5141.]

[53] Scaffaro, R., Lopresti, F. (2018). Properties-morphology relationships in electrospun mats based on polylactic acid and graphene nanoplatelets. Composites Part A: Applied Science and Manufacturing, 108, 23-29.

[54] Toncheva, A., Mincheva, R., Kancheva, M., Manolova, N., Rashkov, I., Dubois, P., Markova, N. (2016). Antibacterial PLA/PEG electrospun fibers:

Comparative study between grafting and blending PEG. European Polymer Journal, 75, 223-233.

[55] Apalangya, V. A., Rangari, V. K., Tiimob, B. J., Jeelani, S., Samuel, T. (2019). Eggshell based nano-engineered hydroxyapatite and poly (lactic) acid electrospun fibers as potential tissue scaffold. International journal of biomaterials, 2019.

[56] Cai, N., Dai, Q., Wang, Z., Luo, X., Xue, Y., Yu, F. (2014). Preparation and properties of nanodiamond/poly (lactic acid) composite nanofiber scaffolds. Fibers and Polymers, 15(12), 2544-2552.

[57] Lins, L. C., Wianny, F., Livi, S., Hidalgo, I. A., Dehay, C., Duchet-Rumeau, J., Gérard, J. F. (2016). Development of bioresorbable hydrophilic–hydrophobic electrospun scaffolds for neural tissue engineering. Biomacromolecules, 17(10), 3172-3187.

[59] Alharbi, H. F., Luqman, M., Fouad, H., Khalil, K. A., Alharthi, N. H. (2018). Viscoelastic behavior of core-shell structured nanofibers of PLA and PVA produced by coaxial electrospinning. Polymer Testing, 67, 136-143.

[60] Chan C-M., Polymer Surface Modification and Characterization, Hanser Publishers, Munich, Viana, New York, 1993.

[61] Tulli, D., Janner, D., Pruneri, V. (2011). Room temperature direct bonding of LiNbO3 crystal layers and its application to high-voltage optical sensing. Journal of Micromechanics and Microengineering, 21(8), 085025.

[62] van der Straeten, K., Sparla, J., Olowinsky, A., Gillner, A. (2019). Influence of self-organizing microstructures on the wettability of molten plastic on steel for hybrid plastic-metal joints. Welding in the World, 63(5), 1431-1441.

[63] Sarmiento, P. M., Lopez, L. M., Sarmiento, A. P., Fajardo, J. I. (2012, November). Efficiency of the low-pressure cold plasma in the cleaning of steel sheet

for subsequent covering. In 2012 VI Andean Region International Conference (pp. 115-118). IEEE.

[64] "ASTM D7490-08, Standard Test Method for Measurement of the Surface Tension of Solid Coatings, Substrates and Pigments using Contact Angle Measurements," 2008

[65] Ma, M., Gupta, M., Li, Z., Zhai, L., Gleason, K. K., Cohen, R. E., Rutledge, G. C. (2007). Decorated electrospun fibers exhibiting superhydrophobicity. Advanced Materials, 19(2), 255-259.

[66] Singh, A., Steely, L., Allcock, H. R. (2005). Poly [bis (2, 2, 2-trifluoroethoxy) phosphazene] superhydrophobic nanofibers. Langmuir, 21(25), 11604-11607.

[67] Kang, M., Jung, R., Kim, H. S., Jin, H. J. (2008). Preparation of superhydrophobic polystyrene membranes by electrospinning. Colloids and Surfaces A: Physicochemical and Engineering Aspects, 313, 411-414.

[68] Scaffaro, R., Lopresti, F., Sutera, A., Botta, L., Fontana, R. M., Gallo, G. (2017). Plasma modified PLA electrospun membranes for actinorhodin production intensification in Streptomyces coelicolor immobilized-cell cultivations. Colloids and Surfaces B: Biointerfaces, 157, 233-241.

[69] Sahay, R., Kumar, P. S., Sridhar, R., Sundaramurthy, J., Venugopal, J., Mhaisalkar, S. G., Ramakrishna, S. (2012). Electrospun composite nanofibers and their multifaceted applications. Journal of Materials Chemistry, 22(26), 12953-12971.

[70] Dong, Y., Marshall, J., Haroosh, H. J., Mohammadzadehmoghadam, S., Liu, D., Qi, X., Lau, K. T. (2015). Polylactic acid (PLA)/halloysite nanotube (HNT) composite mats: influence of HNT content and modification. Composites Part A: Applied Science and Manufacturing, 76, 28-36.

[71] Marsi, T. C., Ricci, R., Toniato, T. V., Vasconcellos, L. M., Elias, C. D. M. V., Silva, A. D., ... Lobo, A. O. (2019). Electrospun nanofibrous poly (Lactic

Acid)/Titanium dioxide nanocomposite membranes for cutaneous scar minimization. Frontiers in Bioengineering and Biotechnology, 7, 421.

[72] Touny, A. H., Lawrence, J. G., Jones, A. D., Bhaduri, S. B. (2010). Effect of electrospinning parameters on the characterization of PLA/HNT nanocomposite fibers. Journal of Materials Research, 25(5), 857-865.

[73] Magiera, A., Markowski, J., Pilch, J., Blazewicz, S. (2018). Degradation behavior of electrospun PLA and PLA/CNT nanofibres in aqueous environment. Journal of Nanomaterials, 2018.

[74] Ozdemir, E., and Hacaloglu, J. (2018). Thermal degradation of Polylactide/Poly (ethylene glycol) fibers and composite fibers involving organoclay. Journal of Analytical and Applied Pyrolysis, 129, 181-188.

[75] Liu, L., Ren, Y., Li, Y., Liang, Y. (2013). Effects of hard and soft components on the structure formation, crystallization behavior and mechanical properties of electrospun poly (L-lactic acid) nanofibers. Polymer, 54(19), 5250-5256.

[76] Haroosh, H. J., Dong, Y., Chaudhary, D. S., Ingram, G. D., Yusa, S. I. (2013). Electrospun PLA: PCL composites embedded with unmodified and 3-aminopropyltriethoxysilane (ASP) modified halloysite nanotubes (HNT). Applied Physics A, 110(2), 433-442.

[77] Yang, C., Chen, S., Wang, J., Zhu, T., Xu, G., Chen, Z., ... Li, W. (2016). A facile electrospinning method to fabricate polylactide/graphene/MWCNTs nanofiber membrane for tissues scaffold. Applied Surface Science, 362, 163-168.

[78] Açık, E. (2014). Poly(Lactic Acid) Based Nanocomposites: Mechanical, Thermal And Rheological Properties And Morphology (thesis).

[79] NaturePlast, "NaturePlast Natural Evolution of Plastics," [Online]. Available: http://www.natureplast.eu. [Accessed 1 09 2021].

[80] Merck, “PEG 6000, Molecular Biology Grade [PDF]. (2017, February 06). Merck.,” Saf. Data Sheet, no. 1907, pp. 1–13, 2015.

[81] Halloysite Nanoclay (CAS 1332-58-7), Product specification, Sigma-Aldrich," Build. Res. Inf., vol. 21, no. 1, pp. 21–22, 1993.

[82] Electrospinning equipments: Nanofiber Machines: Inovenso. RSS. (1970, September 3). Retrieved October 10, 2021, from https://www.inovenso.com/.

[83] Oyama, H. T. (2009). Super-tough poly (lactic acid) materials: Reactive blending with ethylene copolymer. Polymer, 50(3), 747-751.

[84] Habibi, S., Saket, M., Nazockdast, H., Hajinasrollah, K. (2019). Fabrication and characterization of exfoliated chitosan–gelatin–montmorillonite nanocomposite nanofibers. The Journal of The Textile Institute, 110(11), 1672-1677.

[85] Rezaei, B., Ghani, M., Askari, M., Shoushtari, A. M., Malek, R. M. A. (2016). Fabrication of thermal intelligent core/shell nanofibers by the solution coaxial electrospinning process. Advances in Polymer Technology, 35(1).

[86] Saehana, S., Iskandar, F., Abdullah, M. (2013). Optimization of electrospinning parameter by employing genetic algorithm in order to produce desired nanofiber diameter. International Journal of Materials and Metallurgical Engineering, 7(1), 86-91.

[87] Li, L., Wu, Z., Jiang, S., Zhang, S., Lu, S., Chen, W., Zhu, M. (2015). Effect of halloysite nanotubes on thermal and flame retardant properties of polyamide 6/melamine cyanurate composites. Polymer Composites, 36

[88] Smallwood, I. (2012). Handbook of organic solvent properties. Butterworth-Heinemann.

[89] Zeng, J., Haoqing, H., Schaper, A., Wendorff, J. H., Greiner, A. (2003). Poly-L-lactide nanofibers by electrospinning–Influence of solution viscosity and electrical conductivity on fiber diameter and fiber morphology. e-Polymers, 3(1).

[90] Wunderlich, B. (2005). Thermal analysis of polymeric materials. Springer Science & Business Media.]

[91] Inai, R.; Kotaki, M.; Ramakrishna, S. Structure and properties of electrospun plla single nanofibres. Nanotechnology 2005, 16, 208–213.

[92] Bognitzki, M.; Czado, W.; Frese, T.; Schaper, A.; Hellwig, M.; Steinhart, M.; Greiner, A.; Wendorff, J.H. Nanostructured fibers via electrospinning. Adv. Mater. 2001, 13, 70–72.

[93] Jiyong, H., Yinda, Z., Hele, Z., Yuanyuan, G., Xudong, Y. (2017). Mixed effect of main electrospinning parameters on the β-phase crystallinity of electrospun PVDF nanofibers. Smart Materials and Structures, 26(8), 085019.

[94] Tsuji, H. and Ikada, Y. (1995). Properties and morphologies of poly (L-lactide): 1. Annealing condition effects on properties and morphologies of poly (L-lactide). Polymer, 36(14), 2709-2716.

[95] Carrizales, C., Pelfrey, S., Rincon, R., Eubanks, T. M., Kuang, A., McClure, M. J., ... Macossay, J. (2008). Thermal and mechanical properties of electrospun PMMA, PVC, Nylon 6, and Nylon 6, 6. Polymers for Advanced Technologies, 19(2), 124-130.].

[96] Tarus, B., Fadel, N., Al-Oufy, A., El-Messiry, M. (2016). Effect of polymer concentration on the morphology and mechanical characteristics of electrospun cellulose acetate and poly (vinyl chloride) nanofiber mats. Alexandria Engineering Journal, 55(3), 2975-2984.

[97] Tan, E. P. S., Ng, S. Y., Lim, C. T. (2005). Tensile testing of a single ultrafine polymeric fiber. Biomaterials, 26(13), 1453-1456.

[98] Shi, Q., Zhou, C., Yue, Y., Guo, W., Wu, Y., Wu, Q. (2012). Mechanical properties and in vitro degradation of electrospun bio-nanocomposite mats from PLA and cellulose nanocrystals. Carbohydrate Polymers, 90(1), 301-308.

[99] Maleki, H., Gharehaghaji, A. A., Moroni, L., Dijkstra, P. J. (2013). Influence of the solvent type on the morphology and mechanical properties of electrospun PLLA yarns. Biofabrication, 5(3), 035014.]

[100] Cai, N., Dai, Q., Wang, Z., Luo, X., Xue, Y., Yu, F. (2015). Toughening of electrospun poly (L-lactic acid) nanofiber scaffolds with unidirectionally aligned halloysite nanotubes. Journal of Materials Science, 50(3), 1435-1445.

[101] Nazari, T., Garmabi, H. (2014). Polylactic acid/polyethylene glycol blend fibres prepared via melt electrospinning: effect of polyethylene glycol content. Micro & Nano Letters, 9(10), 686-690.

[102] Morimune, S., Kotera, M., Nishino, T., Goto, K., Hata, K. (2011). Poly (vinyl alcohol) nanocomposites with nanodiamond. Macromolecules, 44(11), 4415-4421.

[103] Zhuang, W., Liu, J., Zhang, J. H., Hu, B. X., Shen, J. (2009). Preparation, characterization, and properties of TiO2/PLA nanocomposites by in situ polymerization. Polymer Composites, 30(8), 1074-1080.

[104] Yang, X., Li, L., Shang, S., Tao, X. M. (2010). Synthesis and characterization of layer-aligned poly (vinyl alcohol)/graphene nanocomposites. Polymer, 51(15), 3431-3435.

[105] Wang, Z., Cai, N., Zhao, D., Xu, J., Dai, Q., Xue, Y., Yu, F. (2013). Mechanical reinforcement of electrospun water-soluble polymer nanofibers using nanodiamonds. Polymer composites, 34(10), 1735-1744.

[106] Kim, J. Y., Park, H. S., Kim, S. H. (2006). Unique nucleation of multi-walled carbon nanotube and poly (ethylene 2, 6-naphthalate) nanocomposites during non-isothermal crystallization. Polymer, 47(4), 1379-1389.

[107] Pasbakhsh, P., Ismail, H., Fauzi, M. A., Bakar, A. A. (2010). EPDM/modified halloysite nanocomposites. Applied Clay Science, 48(3), 405-413.

[108] Liu, M., Guo, B., Du, M., Jia, D. (2007). Drying induced aggregation of halloysite nanotubes in polyvinyl alcohol/halloysite nanotubes solution and its effect on properties of composite film. Applied Physics A, 88(2), 391-395.

[109] Prashantha, K., Lacrampe, M. F., Krawczak, P. (2011). Processing and characterization of halloysite nanotubes filled polypropylene nanocomposites based

on a masterbatch route: effect of halloysites treatment on structural and mechanical properties. Express Polymer Letters, 5(4).

[110] Kim, I. H., Jeong, Y. G. (2010). Polylactide/exfoliated graphite nanocomposites with enhanced thermal stability, mechanical modulus, and electrical conductivity. Journal of Polymer Science Part B: Polymer Physics, 48(8), 850-858.

[111] Wang, B. Y., Fu, S. Z., Ni, P. Y., Peng, J. R., Zheng, L., Luo, F., Qian, Z. Y. (2012). Electrospun polylactide/poly (ethylene glycol) hybrid fibrous scaffolds for tissue engineering. Journal of Biomedical Materials Research Part A, 100(2), 441-449.

[112] Schadler, L. S., Giannaris, S. A., Ajayan, P. M. (1998). Load transfer in carbon nanotube epoxy composites. Applied physics letters, 73(26), 3842-3844.

[113] Tang, Y., Ye, L., Zhang, Z., Friedrich, K. (2013). Interlaminar fracture toughness and CAI strength of fibre-reinforced composites with nanoparticles–A review. Composites Science and Technology, 86, 26-37.

[114] Abdullayev, E., Price, R., Shchukin, D., Lvov, Y. (2009). Halloysite tubes as nanocontainers for anticorrosion coating with benzotriazole. ACS applied materials & Interfaces, 1(7), 1437-1443.

[115] Rawtani, D., Agrawal, Y. K. (2012). Multifarious applications of halloysite nanotubes: a review. Reviews on Advanced Materials Science, 30(3), 282-295.

[116] Lins, L. C., Wianny, F., Livi, S., Hidalgo, I. A., Dehay, C., Duchet-Rumeau, J., Gérard, J. F. (2016). Development of bioresorbable hydrophilic–hydrophobic electrospun scaffolds for neural tissue engineering. Biomacromolecules, 17(10), 3172-3187.

[117] Pillin, I., Montrelay, N., & Grohens, Y. (2006). Thermo-mechanical characterization of plasticized PLA: Is the miscibility the only significant factor?. Polymer, 47(13), 4676-4682.

[118] Nasirian, D., Salahshoori, I., Sadeghi, M., Rashidi, N., Hassanzadeganroudsari, M. (2020). Investigation of the gas permeability properties from polysulfone/polyethylene glycol composite membrane. Polymer Bulletin, 77(10), 5529-5552.

APPENDICES

A. REPRESENTATIVE STRESS-STRAIN CURVES OF THE GENERATED NANOFIBROUS SAMPLES

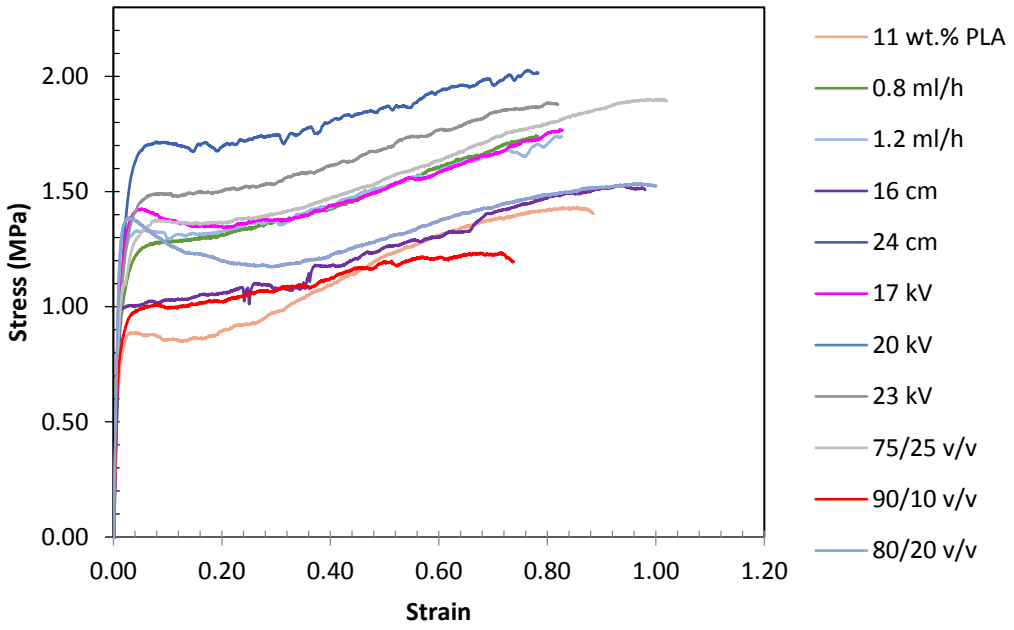

Figure A.1 Representative Stress-Strain Curves of Electrospun Neat PLA Samples for Parameter Studies.

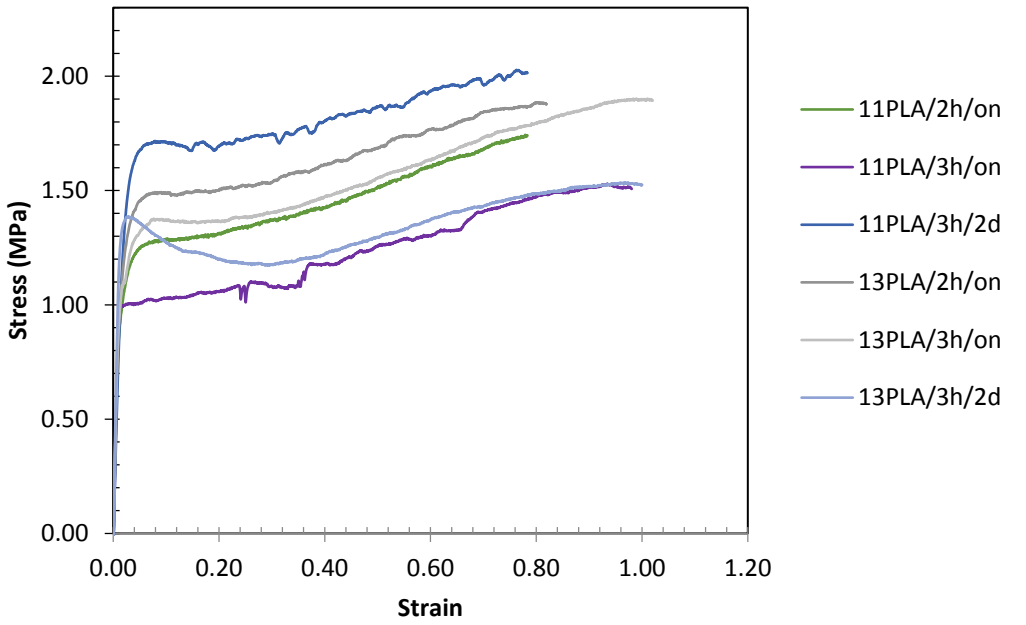

Figure A.2 Representative Stress-Strain Curves of Electrospun Neat PLA Samples for ED and SDD Studies.

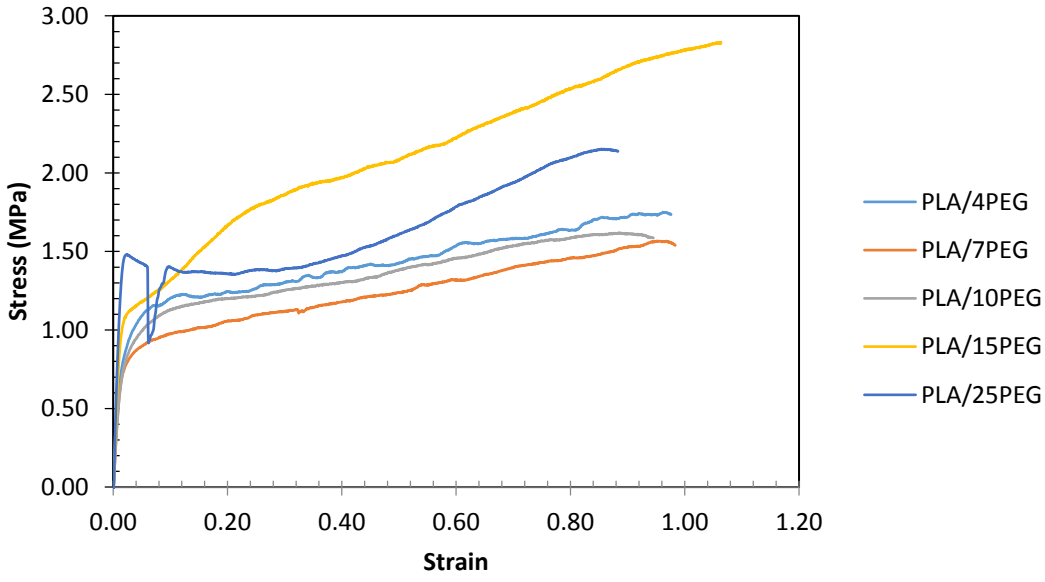

Figure A.3 Representative Stress-Strain Curves of Electrospun PLA/PEG Samples.

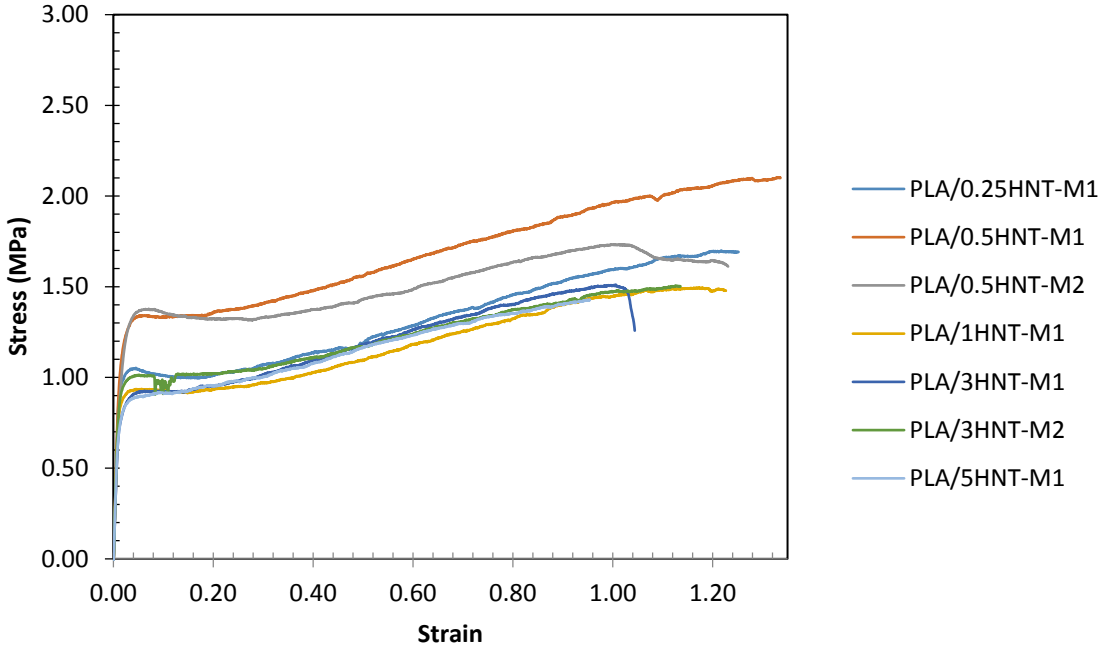

Figure A.4 Representative Stress-Strain Curves of Electrospun PLA/HNT Samples.

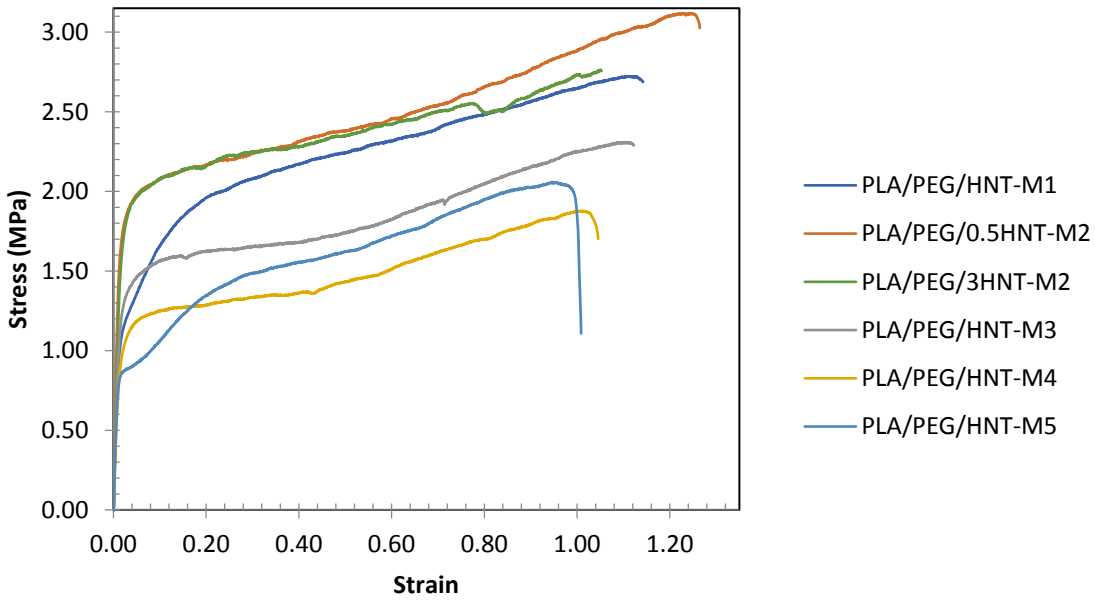

Figure A.5 Representative Stress-Strain Curves of Electrospun PLA/PEG/HNT Samples.

B. RAW DATA OF TENSILE TEST RESULTS

Table B.1 Tensile Test Data of Electrospun Neat PLA for Parameter Studies.

Sample	Tensile Strength (MPa)	Tensile Modulus (MPa)	Elongation at Break (%)
11 wt.%	1.39 ± 0.37	90.11 ± 3.66	77.50 ± 7.84
13 wt.%	1.60 ± 0.21	90.40 ± 1.42	96.05 ± 11.78
0.8 ml/h	1.70 ± 0.07	91.63 ± 1.12	77.29 ± 3.49
1 ml/h	1.60 ± 0.21	90.40 ± 1.42	96.05 ± 11.78
1.2 ml/h	1.66 ± 0.49	85.10 ± 4.92	92.86 ± 18.05
16 cm	1.59 ± 0.23	96.88 ± 1.16	71.17 ± 20.62
20 cm	1.60 ± 0.21	90.40 ± 1.42	96.05 ± 11.78
24 cm	1.73 ± 0.39	94.17 ± 5.64	73.28 ± 5.87
17kV	1.70 ± 0.46	95.11 ± 2.57	77.89 ± 4.09
20 kV	1.60 ± 0.21	90.40 ± 1.42	96.05 ± 11.78
23kV	1.74 ± 0.21	91.85 ± 0.78	81.45 ± 7.76
75/25 v/v	1.97 ± 0.10	96.32 ± 2.42	94.26 ± 11.86
80/20 v/v	1.60 ± 0.21	90.40 ± 1.42	96.05 ± 11.78
90/10 v/v	1.24 ± 0.37	94.70 ± 0.44	80.13 ± 21.14

Table B.2 Tensile Test Data of Electrospun Neat PLA for ED and SDD Studies.

Sample	Tensile Strength (MPa)	Tensile Modulus (MPa)	Elongation at Break (%)
11PLA/2h/on	1.69 ± 0.18	94.30 ± 2.44	79.66 ± 9.55
11PLA/3h/on	1.59 ± 0.27	90.11 ± 4.66	77.50 ± 7.84
11PLA/3h/2d	1.71 ± 0.27	91.96 ± 2.11	81.11 ± 9.09
13PLA/2h/on	1.60 ± 0.21	86.11 ± 4.55	92.94 ± 4.03
13PLA/3h/on	1.74 ± 0.24	89.51 ± 3.94	94.43 ± 10.64
13PLA/3h/2d	1.53 ± 0.35	90.40 ± 1.42	96.05 ± 11.78

Table B.3 Tensile Test Data of Electrospun PLA/PEG and PLA/HNT Samples.

Sample	Tensile Strength (MPa)	Tensile Modulus (MPa)	Elongation at Break (%)
Neat PLA Fibers	1.60 ± 0.21	90.40 ± 1.42	96.05 ± 11.78
PLA/4PEG	1.71 ± 0.20	64.94 ± 2.60	97.24 ± 1.93
PLA/7PEG	1.59 ± 0.10	56.53 ± 1.48	97.80 ± 2.59
PLA/10PEG	1.64 ± 0.15	50.80 ± 0.59	93.12 ± 7.06
PLA/15PEG	2.86 ± 0.13	95.28 ± 8.78	110.50 ± 4.71
PLA/25PEG	2.19 ± 0.17	97.12 ± 0.63	86.90 ± 5.37
PLA/0.25HNT-M1	1.77 ± 0.13	91.28 ± 1.67	124.01 ± 2.61
PLA/0.5HNT-M1	2.16 ± 0.41	93.72 ± 0.87	126.63 ± 13.92
PLA/0.5HNT-M2	1.81 ± 0.34	84.13 ± 3.57	122.58 ± 3.36
PLA/1HNT-M1	1.71 ± 0.24	81.44 ± 0.80	122.65 ± 9.47
PLA/3HNT-M1	1.67 ± 0.25	77.25 ± 3.46	103.09 ± 7.56
PLA/3HNT-M2	1.50 ± 0.20	81.24 ± 4.52	107.35 ± 4.62
PLA/5HNT-M1	1.44 ± 0.17	83.29 ± 1.69	94.50 ± 3.45

Table B.4 Tensile Test Data of Electrospun PLA/PEG/HNT Samples.

Sample	Tensile Strength (MPa)	Tensile Modulus (MPa)	Elongation at Break (%)
Neat PLA Fibers	1.60 ± 0.21	90.40 ± 1.42	96.05 ± 11.78
PLA/PEG/HNT-M1	2.69 ± 0.10	102.66 ± 4.33	120.94 ± 8.10
PLA/PEG/0.5HNT-M2	3.12 ± 0.33	115.04 ± 2.41	122.54 ± 10.17
PLA/PEG/3HNT-M2	2.72 ± 0.21	110.03 ± 1.42	107.35 ± 11.78
PLA/PEG/HNT-M3	2.32 ± 0.17	99.62 ± 0.68	117.16 ± 5.51
PLA/PEG/HNT-M4	1.88 ± 0.18	79.21 ± 1.50	103.89 ± 5.25
PLA/PEG/HNT-M5	2.09 ± 0.20	84.80 ± 10.10	103.39 ± 6.45

C. CONTACT ANGLE MEASUREMENTS

Table C.1 Contact Angle Data of Electrospun Neat PLA for Parameter Studies.

Sample	WCA, °
11 wt.%	152 ± 1.1
13 wt.%	150 ± 1.4
0.8 ml/h	149 ± 1.7
1 ml/h	150 ± 1.4
1.2 ml/h	150 ± 2.6
16 cm	150 ± 2.0
20 cm	150 ± 1.4
24 cm	148 ± 1.5
17kV	150 ± 1.3
20 kV	150 ± 1.4
23kV	146 ± 2.8
75/25 v/v	149 ± 1.2
80/20 v/v	150 ± 1.4
90/10 v/v	152 ± 1.3
PLA Film	140 ± 2.0

Table C.2 Contact Angle Data of Electrospun PLA/PEG and PLA/HNT Samples

Sample	WCA, °
Neat PLA Fibers	150 ± 1.4
PLA/4PEG	145 ± 1.2
PLA/7PEG	143 ± 1.5
PLA/10PEG	139 ± 1.3
PLA/15PEG	135 ± 1.6
PLA/25PEG	126 ± 1.8
PLA/0.25HNT-M1	150 ± 1.3
PLA/0.5HNT-M1	147 ± 1.7
PLA/0.5HNT-M2	144 ± 1.6
PLA/1HNT-M1	140 ± 1.4
PLA/3HNT-M1	138 ± 1.6
PLA/3HNT-M2	136 ± 1.3
PLA/5HNT-M1	131 ± 1.7

Table C.3 Contact Angle Data of Electrospun PLA/PEG/HNT Samples.

Sample	WCA, °
Neat PLA Fibers	150 ± 1.4
PLA/PEG/HNT-M1	135 ± 1.2
PLA/PEG/0.5HNT-M2	133 ± 1.5
PLA/PEG/3HNT-M2	137 ± 1.3
PLA/PEG/HNT-M3	135 ± 1.6
PLA/PEG/HNT-M4	136 ± 1.8
PLA/PEG/HNT-M5	133 ± 1.3